Fritz Laboratory Reports

Civil and Environmental Engineering

1971

Ultimate strength of single-span, rectangular steel box girders, PhD. dissertation, 1971

Joseph A. Corrado

ULTIMATE STRENGTH OF SINGLE-SPAN, RECTANGULAR STEEL BOX GIRDERS

by

Joseph A. Corrado

A Dissertation

Presented to the Graduate Faculty

of Lehigh University

in Candidacy for the Degree of

Doctor of Philosophy

in

Civil Engineering

Lehigh University

1971

Approved and recommended for acceptance as a dissertation in partial fulfillment of the requirements for the degree of Doctor of Philosophy.

Sept. 23, 1971
(date)

Dr. Ben T. Yen
Professor in Charge

Accepted: _Sept 23, 1971_
(date)

Special committee directing
the doctoral work of Mr.
Joseph A. Corrado

Dr. Celal N. Kostem, Chairman

Dr. Alexis Ostapenko

Dr. Russell E. Benner

Dr. David A. VanHorn

ACKNOWLEDGMENTS

This dissertation is partly based on a research project, "Strength of Rectangular Composite Box Girders", presently being conducted at the Fritz Engineering Laboratory, Department of Civil Engineering, Lehigh University, Bethlehem, Pennsylvania. Dr. Lynn S. Beedle is Director of the Laboratory and Dr. David A. VanHorn is Chairman of the Civil Engineering Department. The project is being sponsored by the Pennsylvania Department of Transportation.

The author is deeply indebted to Dr. B. T. Yen, thesis supervisor, for his continued guidance, encouragement and cooperation. The interest and guidance of the candidate's special committee, comprised of Prof. C. Kostem, Chairman and Professors A. Ostapenko, R. Benner, and D. A. VanHorn, is gratefully acknowledged.

Many thanks are due the author's associates in Fritz Laboratory, particularly Dr. Roger G. Slutter, Chairman of the Operations Division, Mr. Kenneth Harpel, Laboratory Superintendent, and Mr. Charles Hittinger, Laboratory Foreman who fabricated the delicate test specimens.

Appreciation must also be extended to Mr. Jack Gera and his staff for the preparation of the drawings and to Mr. Richard Sopko for the photographs. Special thanks are extended to Mrs. Dorothy Fielding and Mrs. Jane Lenner for typing the manuscript.

TABLE OF CONTENTS

TABLE OF CONTENTS (continued)

LIST OF FIGURES

LIST OF FIGURES (continued)

LIST OF TABLES

ABSTRACT

This dissertation presents the results of a combined experi-
mental and analytical study on the ultimate strength of single-span
rectangular steel box girders.

The experimental phase involved the testing of two, slender-
web, steel model box girders under various combinations of bending,
shear and torsion. The specimens had been designed to simulate typical
box girder members. When subjected to shear and bending only, the
specimen exhibited a behavior quite similar to that of slender web
plate girders under similar loading conditions. The addition of
torsion had a significant effect on the behavior and ultimate strength
of the specimens. Under both conditions of loading the specimens
displayed definite stress redistribution capabilities and considerable
postbuckling strength. Failure modes were characterized by tension
field yielding of the webs followed by failure of the flanges.

By making use of results from the model tests and from previous
research on plate girders an analytical method is formulated for
evaluating the ultimate strength of single-span, rectangular steel box
girders subjected to either shear and bending or shear, bending and
torsion. The method assumes that deformation of the cross-section and
buckling of the compression flange will not occur. These assumptions
are valid for the type of box girder being considered. In the
development it is shown that the twisting moment is predominantly

supported through St. Venant torsion. Effects of warping torsion are found to be insignificant.

Equations are derived and defined for computing the ultimate strength under various loading conditions. Good agreement between the experimental results and analytical predictions was obtained.

1. INTRODUCTION

Extensive applications of closed thin-walled sections as load-carrying structural elements have occurred in both the aircraft and structural fields. Examples of these include the wing or fuselage of an aircraft and large tubular members of a building or a bridge truss. It is only recently, however, that the thin-walled steel box girder has gained considerable popularity for use as a main load carrying member in bridge structures. This can be attributed to an increased awareness of the structural efficiency, financial savings and pleasing aesthetic appearance which can be achieved with such a configuration.[1]

For bridge structures, steel box girders are usually fabricated using relatively thin webs and bottom flange plates in combination with a composite slab or orthotropic steel deck. Both transverse and longitudinal stiffeners are often used to stiffen the slender webs and bottom flange. The cross section of a box girder bridge may take on any one of several possible configurations containing one or more box girder cells. Figure 1.1 illustrates a few of the many possible configurations.

The two major classes of loading for bridge box girders are dead load and live load. As indicated in Fig. 1.2a, the former produces a wide area, near-uniform distribution of load. The live load shown in Fig. 1.2b often consists of non-uniformly distributed, localized

forces such as wheel loads. Both classes of loading can be decomposed into the two components presented in Fig. 1.3. By restraining the deck against vertical movement at the web-deck junctions, stresses due to plate action of the deck can be evaluated. This is referred to as a deck plate analysis. The other component of loading involves the application, at the web-deck junctions, of the equilibrants of the restraining forces obtained from the deck plate analysis. It is this component which produces bending and twisting of the box girder and is of prime interest when considering the ultimate strength of the member.

Most presently available methods of analysis for box girders are restricted to the linear, prebuckling range. Of these, the prismatic folded plate theory of Goldberg and Leve[2] offers the most accurate method of analysis. It considers the box girder to be made up of an assemblage of plates. Classical plate theory is used to describe the inplane and out-of-plane plate deformations. The analysis is limited to straight, prismatic box girders composed of isotropic plate elements, with no interior diaphragms and with neither cross-sectional deformations nor axial stresses at the ends of the constituent plates.

A number of other linear, prebuckling methods of analysis for box girders are based on thin-walled beam theory.[3] The box girder is treated as an assemblage of plates which bend as one-way slabs between the longitudinal edges or joints. Longitudinal stresses are assumed to vary linearly between the longitudinal joints. Wright,

Abdel-Samad and Robinson[4] have made use of thin-walled beam theory

to formulate an analogy between an elastic box girder and a beam on

an elastic foundation. This technique has been used to evaluate

stresses resulting from deformation of the cross section.

Another analytical technique which has been applied to box

girders as well as many other structural problems is the finite element

method. Scordelis[5,6] has effectively used this to analyze continuous

reinforced concrete box girders with rigid interior diaphragms.

Malcom and Redwood[7] have utilized it to study shear lag effects in

stiffened box girders. However, to date, no attempt has been made to

apply this technique to the ultimate strength evaluation of box gird-

ers.

One of the few studies which focused on the ultimate strength

of box girders was completed by Parr[8] in 1968. His work was re-

stricted to box shapes having very stocky web plates and subjected

to only flexural loads. Torsional loads were not considered and

post-buckling behavior was not of concern in this study.

A thin-walled box girder is in many respects very similar to

a plate girder. The slender webs of both are required to carry

practically all of the vertical shear while the flanges resist most

of the bending moment. For a long time the strength of plate girders

was believed to be limited by the theoretical, buckling strength of

the web. In the last decade, research[9,10,11] on plate girders has

indicated that the load carrying capacity is not limited by web

buckling but by the capability for stress redistribution among the

component parts of the girder. It is anticipated that a thin-walled

box girder also has considerable post-buckling strength and therefore its maximum load carrying capacity is much larger than the theoretical web buckling load.

The purpose of this study was to evaluate through use of model tests the postbuckling behavior, modes of failure and load carrying capacity of single-span, rectangular steel box girders. Intended was the development of a workable analytical method for estimating the ultimate strength of such box girders. The study also had as one of its goals the acquisition of information which would provide guidance for planning and conducting future theoretical and experimental research on the ultimate strength of box girders.

Specific objectives included:

1. Design and fabricate two model test specimens to simulate typical single-span, steel, rectangular box girders.

2. Determine the effects of transverse stiffener spacing, diaphragms or x-bracing, and loading conditions (different combinations of bending, shear and torsion) on the behavior, modes of failure and load carrying capacity of the model specimens.

3. Measure deflections and strains of each specimen up to the ultimate load.

4. Develop an analytical procedure for estimating the ultimate strength of single-span, steel, rectangular box girders.

5. Compare experimental results with corresponding analytically computed values.

2. TESTS OF MODEL BOX GIRDERS

2.1 Description of Test Specimens and Setup

2.1.1 Design Considerations

The first consideration for the design of the test speci-
mens was based on the procurement of a qualitative evaluation of
the post-buckling behavior and failure mechanisms for single-span
box girders subjected to shear, bending and torsion. Initiation of
failure in the web plates was of prime interest and governed, to a
large degree, the design of the relative dimensions of the component
parts of the specimens.

A rectangular cross section was chosen because it is one
of the most commonly used in box girder bridges. The selection of
the depth and width of the box was somewhat arbitrary although
several items were considered before a final choice was made. These
included: (1) providing an opening large enough to make possible
internal positioning of the X-bracing and tightening of the mechanical
alignment fasteners during fabrication, (2) thickness of readily
available sheet steel, (3) depth to width ratio of the box,
(4) slenderness ratio of the webs, (5) connection of webs to flanges,
and (6) the length of the specimens. The length was primarily governed
by the clear span available in the testing machine, although fabri-
cation and lateral distortions of the web plates caused during fabri-
cation were also considered.

The slenderness ratio (depth/thickness) and transverse stiffener spacing for the web plates were selected based on current AASHO specifications[1,2] for plate girders.

Design considerations for the top flange concentrated on simulation of the relative stiffness of a concrete deck and elimination of premature failure, that is, failure of the flange before one or more of the web panels failed. Because only single-span members were being investigated, yielding was the governing criterion for design of the bottom flange.

The design of the X-bracing was based on one prime objective. That was to make it strong enough to maintain the shape of the cross section for the entire range of loading. Connection of the bracing to the wall plates could be achieved through welding or use of mechanical fasteners.

One final design item involved the connection between the flanges and the web plates. It was necessary that these joints be continuous and have shear and tensile strengths strong enough to resist the ordinary shear forces resulting from bending and torsion and also tensile forces resulting from anticipated tension field action of the web plates. To achieve such a joint, a careful investigation of several different joining materials was undertaken.

2.1.2 Details and Properties of Test Specimens

Two specimens having a vertical axis of symmetry were fabricated from sheet steel and are shown in Figs. 2.1 and 2.2. The

specimens were formed by connecting the two flat flange plates to the two webs which had previously been bent into channel shapes. The flanges of the web channels facilitated the longitudinal connections. Holes had previously been drilled in the flanges and webs to accommodate fasteners which securely positioned the plate components during fabrication.

As was previously mentioned, careful consideration was given to a possible connecting medium. It was felt that the tensile forces which had to be carried by the joint would be the most critical, and therefore a series of tensile tests were performed using several different joints. Figure 2.3 shows the test configuration and results. Although the brazed and silver solder joints exhibited the greatest strength, neither of these was finally selected because the required heat inputs produced intolerable web and flange distortions. The 50-50 solder (50% Tin, 50% Lead) was used and produced satisfactory joints with only small amounts of web distortions.

Specimen M1 (Fig. 2.1) consisted of a box section 3 inches deep by 4 inches wide and had a span length of 24 inches. The nominal slenderness ratio for the webs was 192. Transverse stiffeners attached to the exterior surface divided the webs into panels having length-to-depth ratios (aspect ratio) ranging from 1.0 to 1.67. Solder, the same as that used for the longitudinal web-to-flange joints, was used to attach all transverse stiffeners. The top flange having a width of 7 inches and 5/64-inch thickness had been sized to simulate the deck of a composite box girder bridge. X-bracing was provided at the

loading and support points for the purpose of distributing the concentrated loads and maintaining the shape of the cross section. Intermediate bracing was provided at one additional location.

Specimen M2 (Fig. 2.2) had a configuration very similar to that of M1. The major differences were in the width of the top flange and the elimination of both the transverse stiffeners on the bottom flange and the intermediate X-bracing.

The component plate dimensions and material properties are listed in Table 1. Material properties were obtained from standard tensile specimens (ASTM E8) which had been cut from the original plates in the direction parallel to the longitudinal axis of the specimens. Table 2 presents the pertinent geometric properties for each specimen.

2.1.3 Instrumentation and Test Setup

Instrumentation

Instrumentation for both specimens consisted of dial gages, electrical-resistance strain gages and an extensometer. A total of seven 0.001 inch dial gages, arranged as shown in Figs. 2.4 and 2.5, were utilized to monitor the vertical and rotational displacement of each specimen. Possible support settlement and rigid body rotation dictated the employment of the end support gages.

Figures 2.6 and 2.7 show the strain gage layout for specimens M1 and M2, respectively. The three-element rectangular rosettes were mounted in back-to-back pairs at the center of pre-selected web

panels on both sides of the box. Orientation of these had the diagonal gage of the rosette aligned with the approximate direction of the tension diagonal of the panel. Back-to-back gages were needed so that stresses resulting from inplane bending and shear could be isolated from the out-of-plane bending stresses. Several linear gages were also mounted on specimen M1 to check the normal stress distribution (σ_z) over the cross section.

For identification purposes each panel, which consisted of two webs and two flanges, was assigned a number as indicated in Figs. 2.1 and 2.2. In addition, one vertical side of the cross section was designated "north" and the other "south" in order to identify the two webs of a given panel. Thus, the web designations 1S and 1N refer to the south and north side webs of panel 1, respectively.

Because the behavior of the web panels was of prime interest, it was thought that supplementary data could be obtained quite easily by measuring strains mechanically along the diagonals of the panel. Several difficulties were encountered with this technique but by and large it proved to be a useful device for checking web diagonal deformations. Figure 2.8 illustrates the basic application of this method.

A brittle whitewash coating was applied to M2 in an attempt to produce visual signs of yielding. This also proved to be valuable in the photographic documentation of the behavior of the specimen. Whitewash was not utilized on M1.

Test Setup

Specimens M1 and M2 were tested as simply supported members in a mechanical, screw type testing machine[*]. Load was applied mechanically through the center of the movable head to a spreader bar which distributed the load to the specimen (Fig. 2.9). By carefully varying the longitudinal and transverse position of the specimen with respect to the center of the movable head, various combinations of bending and torsion could be produced. Sketches of the loading configuration and corresponding shear, bending moment and twisting moment diagrams for M1 and M2 are indicated in Figs. 2.10 and 2.11, respectively.

A 1/2-inch diameter rod and 1/2-inch square bar were used as supports at opposite ends of each member. Hold-downs were also provided at each end to prevent possible lifting on one side due to torsion. These can be seen at the base of the bearing stiffeners in Fig. 2.9.

2.2 Testing of Specimens

2.2.1 Specimen M1

Testing of this specimen was initiated with applications of a series of symmetrical loads (no torsion) to check out the overall behavior of the member and the repeatability of test data. Two identical test sequences were performed in which the specimen was

---

[*]120,000 pound capacity "torque bar" Tinius Olsen Testing Machine.

loaded in 200 pound increments up to 1000 pounds; the upper load level being within the linear-elastic range. A full set of deflection and strain readings were obtained for each increment of load.

For all tests the strain rate in terms of free travel of the testing machine's movable crosshead was approximately 0.025 inches per minute. The actual travel speed under load was somewhat less than this. Data readings were initiated almost immediately after a given load level had been attained. Some drop in load occurred during the period of time in which data readings were being taken. In the linear-elastic range these load drops were small (20-40 pounds). However, they were as large as 250 pounds in the inelastic range. A drop in load took place, in most cases, over a period of 20 to 25 minutes while the vertical deflections remained perfectly stable. Such behavior was unexpected, especially in the linear-elastic range. Because of the qualitative nature of the study, it was not given serious consideration during testing of the specimens.

During the second symmetrical load sequence "canning" of web panel 2 on the south side of the cross section (abrupt change in out-of-plane deformation pattern) was observed at a load of approximately 950 pounds. This was not totally unexpected for such thin webs and testing was continued. A comparison of the test data from the two series of loads indicated that repeatability was achieved.

After the symmetric load tests were completed and the data reviewed, the specimen was carefully repositioned and unsymmetrical

loading initiated. For specimen M1 the loading condition can be seen in Fig. 2.10. With the load at midspan and directly over the north web, each half-span was subjected to identical bending, shear and torsion. Load was applied and data recorded at each 200 pound increment up to 1375 pounds when buckling of the web and transverse stiffener occurred directly under the load point. The specimen was unloaded and repairs effected by straightening and strengthening the loading stiffener. Testing was resumed and at 1200 pounds considerable additional local buckling of the web was noticed at the same locations although no evidence of stiffener buckling could be seen. Further inspection uncovered tearing of the upper portion of the solder joint connecting the loading stiffener to the web. Prior to this, bulging of the web along the tension diagonals of web panels 1N, 2N, 4N and 6N was clearly observed.

Repairs this time included straightening of the buckled web on the north side and the attachment of a heavy angle stiffener to each web at the load point location. The eccentricity was shifted to the south side to help avoid future possible premature failures. Prior to what turned out to be the final test of specimen M1, load was cycled several times between 0 and 1000 pounds.

Final testing proceeded without incident up to 1200 pounds. Full sets of deflection, strain and web diagonal measurements were recorded for each 200 pound increment. At 1400 pounds the first definite signs of tension diagonal web bulging appeared in panel 6S. Loading continued and at 1500 pounds tension field action was very

prominent in web panels 1S and 6S which had aspect ratios of 1.67

and 1.5, respectively. No visual evidence of tension field action

could be detected in the corresponding web panels on the north side.

It is significant to point out again that the load for this test was

directly above the web on the south side (eccentricity of 2 inches).

Upon further loading to 1600 pounds, a sharp cracking noise was heard

and a portion of the top flange near the centerline of the specimen

started to distort downwards on the south side. Large distortions

of the cross section were beginning to take place. Later inspection

indicated that failure of the midspan X-bracing was the cause of the

cracking noise. The load was very unstable at this point yet addi-

tional load could be supported. Pulling up of the bottom flange

and pulling down of the top flange at the tension diagonal corners

of web panels 1S and 6S started to occur at 1650 pounds. At 1750

pounds web bulging had occurred along the tension diagonals of 2S

and 4S in addition to failure of the X-bracing at the east end. A

maximum load of 1800 pounds was attained before excessive deflections

and cross-sectional deformation prohibited further loading. Even

at the maximum load no signs of web bulging could be detected on the

north side. Figures 2.12(a) and (b) clearly show the permanent de-

formations as viewed from the north and south sides. Bulging of the

web along the tension diagonals is obvious on the south side but not

on the north side. A closer look at the permanent web and flange

deformations on the south side is given in Figs. 2.13(a), (b) and (c).

Finally, a view from each end of the specimen, Figs. 2.14(a) and (b),

illustrates some of the cross-sectional distortions which took place.

2.2.2 <u>Specimen M2</u>

2.2.2.1 <u>Unsymmetrical Loading</u>

The descriptive terms symmetrical and unsymmetrical refer
to the position of the load with respect to the shear center which
theoretically lies on the vertical centroidal axis of the cross sec-
tion. Therefore, an unsymmetrical load will subject the member to
torsion in addition to bending, whereas symmetrical loads produce
only bending.

Prior to starting the unsymmetrical load test, a series of
symmetric loads were applied to check the specimen and test setup.
The procedure followed was similar to that used for specimen M1.
Following this, testing under the loading condition indicated in
Fig. 2.11(a) was begun with an eccentricity of 1-inch to the north
side. Load was applied in 200 pound increments up to 800 pounds and
thereafter in 100 pound increments. Vertical deflections, strains
and web diagonal measurements were recorded for each load increment.
The first significant observations involved bulging of the web along
the tension diagonal in panels 1N and 2N at about 1200 pounds. Further
loading produced additional bulging and at 1700 pounds flaking of the
whitewash along the tension diagonal of panel 2N had occurred. Similar
web deformations but to a lesser degree were observed in web panels
1S and 2S. None of the other web panels exhibited any signs of such
deformations at this load level. After a short pause in testing
during which time the load had been decreased to 400 pounds, loading
was resumed in 100 pound increments. A load of 1800 pounds produced
pulling up of the bottom flange at the lower tension field corner

of web panel 2N. Web bulging also had begun in web panel 5N. Visual inspection indicated that little or no cross-sectional deformations had occurred up to this point. Loading continued and caused additional bulging in web panel 2N while no further increases in similar web deformations of web panel 1N could be detected. At 1900 pounds, panel 2S also exhibited considerable web bulging along the tension diagonal. Shortly thereafter, the maximum load of 1930 pounds was attained. Some slight local buckling of the upper portion of the web adjacent to the loading stiffener in panel 3N was observed. Unloading followed and the resulting permanent web deformations are shown in Figs. 2.15(a) and (b).

2.2.2.2 Symmetrical Loading

Figure 2.16 shows the setup for the final test of specimen M2. It also points out the absence of damage of permanent deformations in panels 3, 4, 5 and 6 during the unsymmetrical test. For the shortened span this condition of loading (Fig. 2.11(b)) would subject the specimen to high flexural shear, a moderate amount of bending moment and no torsion. Failure was expected to occur in either panel 4 or 5.

The procedure followed was very similar to that employed in the previous tests. The first visual signs of tension field action showed up in both webs of panel 5 at 1700 pounds. Just prior to this, "canning" of web panel 5S had taken place. The lateral web deformations in these panels increased as loading continued but were not excessive even at 2400 pounds. The next increment of load produced the first noticeable signs of web bulging in panels 4S and 4N. At 2530 pounds flaking of the whitewash occurred along the tension diagonals of these

web panels. Additional loading caused the web deformation in both
sides of panels 4 and 5 to grow excessively. This was accompanied
by vertical deformations of the flanges over the length of these
panels. The maximum load that could be reached was 2650 pounds.
Flaking of the whitewash in both webs of panel 3 adjacent to the
transverse stiffener was observed at this load. The flaking formed
horizontal lines perpendicular to the transverse stiffener dividing
panels 3 and 4 (Figs. 2.17(a) and (b)). This type of behavior has
previously been experienced in the end post regions of plate gird-
ers.[14,15] Final deformation patterns are indicated in Figs. 2.17
and 2.18.

2.3 Description and Discussion of Test Results

2.3.1 Results of Symmetrical Load Test

Symmetrical loading would theoretically produce identical
shear and normal stresses in the webs of specimen M2. With the larger
of the two shear span-to-depth ratios being about 2.6 and the neutral
axis positioned approximately 1/4 the web depth from the compression
flange, shear was anticipated to govern the mode of failure. A plot
of the vertical shear stresses at the centerline of web panel 5
(Fig. 2.19) indicates quite closely the equivalence of stresses for
the webs. It also illustrates that good correlation with theoretical
values (computed using Eq. (3.13) of Chapter 3) was obtained for loads
less than that which produced significant out-of-plane web deformations.
Note that the stresses plotted in this figure have been obtained by
averaging the measured surface strains and are assumed to be uniform

through the thickness of the plate. This is also the case for all other stress plots unless noted otherwise.

Figure 2.20 illustrates the direction and magnitude of the principal stresses for panel 5 at three distinct load levels. The angle between the maximum principal stress and a horizontal axis is theoretically 45° for pure shear during the early stages of loading when the shear is carried through simple beam action. As the load increases and the shear exceeds the theoretical web buckling load, the principal stresses are gradually reoriented in the direction of the tension diagonal of the panel. Such a phenomenon was common in the other tests reported herein, and has previously been observed many times in shear and combined bending and shear tests of plate girders.[16]

The overall behavior of the specimen can best be described by referring to the load-deflection curve in Fig. 2.21. The response was essentially linear up to 2500 pounds. In the previous section it was noted that excessive web bulging and flaking of the whitewash occurred along the tension diagonals of web panels 4S and 4N at 2530 pounds. Strain readings indicated that yielding had initiated in both webs of panel 5 at 2550 pounds. With the webs yielding and able to carry little or no additional shear, the load-deflection curve became almost flat. A small amount of additional load was realized through the transverse shear strength of the flanges after the webs had failed. Evidence of this is indicated in Fig. 2.22 which shows a large increase in the top flange bending strains of panel 4

at 2500 pounds. This can be compared with the frame action contribution of plate girder flanges described by Chern and Ostapenko.[17] As depicted in Fig. 2.21, the maximum load of 2650 pounds was more than twice as large as the theoretical buckling loads for panels 4 and 5.

The data points marked with x's in the inelastic region of the load-deflection plot of Fig. 2.21 were recorded at the end of each data acquisition time interval. These lower load levels were a result of the load drops previously described in Section 2.2.1. A brief supplementary study, performed after testing had been completed, revealed that this type of behavior was due to a combination of the non-zero strain rate used during loading and relaxation of the solder joints. The limited scope of this supplementary study did not permit precise separation of the effects of strain rate and joint relaxation. However, it was evident that the effects of the non-zero strain rate were wiped out during the 20 to 30 minute period used for taking data readings and during which the deflection of the member was stable. This is analogous to the behavior associated with tensile coupon tests, in which the dynamic yield load decreases to the static yield load within a period of about five minutes.[18] Because of the inability to accurately separate the effects of joint relaxation and strain rate, it can only be reasoned that the statically applied loads, that is, those loads corresponding to a zero strain rate, lie between the upper (o) and lower (x) data points.

In conclusion, it is clear that the behavior and mode of failure (yielding along the web tension diagonals accompanied by deformation of the flanges) of symmetrically loaded box girders compare quite well with that of similarly loaded plate girders, providing premature failure of the compression flange is prevented.

2.3.2 Results of Unsymmetrical Load Tests

Under this loading configuration two tests were performed, one each on specimens M1 and M2. The results of specimen M2 are discussed first.

Figure 2.11(a) indicates the combination of shear, bending and torsion applied to this specimen. Due to the loading condition and geometry of the specimen, a shear type failure was again expected. Therefore, the vertical shear stress at the midpoint of the web would be a sensitive indicator of the behavior of the specimen. A theoretical evaluation of the shearing stresses resulting from flexure and St. Venant torsion indicated that these stresses would be largest in panels 1N and 2N. Evidence that this actually occurred during testing can be seen in Fig. 2.23. Correlation with the theoretical values described above is also evident.

A complete evaluation and understanding of the behavior of the specimen up to ultimate load requires a correlated review of the load-deformation and load-stress data. The load-deflection curve in Fig. 2.24 provides a logical starting point. From this it can be seen that the overall response was linear up to 1500 pounds. At this point the slope begins to change, and at 1700 pounds the slope has

decreased further but still is quite steep. It is at this load that

general yielding had been observed along the tension diagonal of

panel 2N. Figure 2.23 verifies this and also indicates that the

shear stress begins to decrease in web panel 1N and increase in

panels 1S and 2S upon the application of additional load. This im-

plies that a redistribution of the shear has taken place. Panel 2N

which has experienced general yielding could not carry any more shear

and therefore any additional flexural shear was carried by the web

on the south side. Failure of web panel 2N also affected the

torsional stiffness of the member as can be seen in Fig. 2.25. The

length of the member containing panel 2 (9-inch length to the left

of the load point) could no longer support its full share of the

twisting moment due to its decreased torsional stiffness, therefore,

a greater portion of the twisting moment had to be carried by the

section to the right of the loading point. This redistribution

phenomenon caused the shear stresses in this span to change. This

is clearly indicated in the shear stress plots for panel 5 in

Fig. 2.26. The change in the load versus shear stress curves can

be explained analytically by again simply considering the super-

position of the shear flow due to bending and St. Venant torsion.

For the given direction of torsion, these add on the north side and

subtract on the south side as shown in Fig. 2.27. It is important

to note that effects due to warping torsion and distortion of the

cross section have been considered. However, because of the rather

good correlation between the experimental stresses and those predicted

by considering only bending and St. Venant torsion, detailed consideration

of these factors is not deemed necessary for evaluation of the behavior of the specimen and the mode of failure.

Additional loading eventually caused general yielding along the tension diagonal of web panel 2S (Fig. 2.23) and an increased rate of deflection (Fig. 2.24). Prior to the attainment of the maximum load, flange deformations resembling the frame action described in the previous section occurred quite substantially on the north side of panel 2, but to a somewhat lesser degree on the south side of the same panel. The inability to develop further deformation of the flanges may have been affected by what was described in Section 2.2.2.1 as local buckling of the upper portion of the web in panel 3S, adjacent to the loading point.

Analogous to the results for symmetrical testing of M2, the data points denoted by circles and x's in the inelastic region of the load-deflection plot of Fig. 2.24, respectively, represent the upper and lower bounds of the static loads of the unsymmetrical load test of M2.

It is interesting to note that the load-rotation curve in Fig. 2.25 has not flattened out upon attainment of the maximum load. This infers that the torsional capacity of the member has not yet been exhausted and additional torsional moment could be supported by the undamaged portion to the right of the loading point.

A recapitulation of the pertinent events leading up to the ultimate load will help to clearly define the mode of failure for

specimen M2. Initial signs of failure showed up as tension diagonal yielding in the most critical web panel (2N), which is the panel having the most severe combination of stresses and geometry. Additional loading produced redistribution of the flexural shear to the other side of the box, that is, to web panel 2S. This obviously was accompanied by a redistribution of the normal bending stresses. The decreased torsional stiffness of the shear span containing panel 2N forced a redistribution of the twisting moment to the undamaged right shear span. The maximum load was reached when no additional flexural shear could be supported in panel 2. This took place after panel 2S had exhibited yielding along its tension diagonal and the flanges had been partially deformed due to frame action. Figure 2.15 portrays the failure mode configuration.

Keeping in mind the behavior and results of M2, attention is next focused on the results of specimen M1. In the final test of M1, the load was at midspan with an eccentricity of 2 inches to the south side. Under such loading conditions web panels on the south side were subjected to larger shear stresses than those on the north side, and therefore web failure would be expected to initiate on the south side of the cross section. Evidence that this actually occurred was reported in Section 2.2.1. The lower part of Fig. 2.28 clearly points out the difference in magnitude of the shear stresses on the north and south sides. The upper part of this figure shows that the relative magnitude of these stresses is reversed when the eccentricity is reversed. The distribution of shear

stresses prior to any web failure is quite similar to that obtained
for specimen M2 (refer to Fig. 2.23).

When web failures initiated on the south side, a redistri-
bution of the flexural shear to the north side was expected to occur.
Referring again to Fig. 2.28 it is seen that this was not the case. As
web panel 4S began to fail through yielding along its tension diagonal,
the shear stress in the corresponding web on the north side remained
relatively constant. Behavior of this type was also exhibited in
panels 1 and 6. This is unlike the behavior of specimen M2 which
demonstrated significant redistribution capability (Fig. 2.23).

The load-deflection and load-rotation curves of Figs. 2.29
and 2.30, respectively, indicate that little flexural or torsional
stiffness remained once web panels 1S and 6S had yielded. This is
also quite different than the behavior of M2 which possessed appreciable
torsional and flexural stiffness after panel 2N had yielded. Of course,
the lack of torsional stiffness in M1 could be expected because web
panel failures occurred almost simultaneously (1S and 6S) in each shear
span. (Recall that for M2 web failure occurred in only one of the
shear spans.) On the contrary, the absence of significant flexural
stiffness was not anticipated and must be attributed to the poor re-
distribution characteristics of the member. Failure of the midspan
X-bracing at approximately 1500 pounds and the resulting cross-sectional
deformation certainly had a major adverse effect on the ability to trans-
fer the load from the south web to the north web. Subsequent failure
of the X-bracing at the east end compounded the effect.

Thus, specimen M1 failed prematurely due to combined web panel yielding and excessive distortion of the cross section. It is clear that adequate diaphragms or X-bracing must be provided if the member is to provide full redistribution of the flexural shear and torsion and thus develop its true ultimate strength.

3. A METHOD FOR EVALUATING THE ULTIMATE STRENGTH

3.1 Introduction

The analytical method presented herein has been systematically developed for single-span, rectangular box girders subjected to bending and torsion by considering the following:

1) Stresses.

2) Behavior and strength of a box girder panel.

3) Behavior and strength of the overall member.

Simple thin-walled beam theory and past research on closed thin-walled members (Refs. 4, 19, 23) provide the necessary tools to estimate the stresses associated with a single-span, rectangular box girder in the elastic, prebuckling range. With the stresses known it is possible to predict the behavior and strength of a box girder panel utilizing some of the results from recent research on plate girders.[17,21] A panel of a box girder is a longitudinal segment of the member between the transverse web stiffeners. Finally, the overall behavior and strength of the box girders is analyzed by considering the member to be made up of a series of such panels.

3.2 Stresses in Box Girders

In order to develop a method which would not be unduly complex yet reliable for typical rectangular, box girder members, a number of assumptions affecting the stresses had to be made. These are listed on the following page:

1) Member is straight and prismatic.

2) Cross section is symmetrical about its vertical centroidal axis.

3) Transverse normal stresses in the planes of the flanges are negligible.

4) Stresses due to deformation of the cross section are negligible.

The first two assumptions place restrictions on the configuration of the member. They are not considered to be overly restrictive because many box girder designs would satisfy these assumptions. The third assumption neglects the stresses induced by partial fixity at the flange to web junctions in the direction of the flange's width. These stresses are normally small enough to render them negligible[19] and are not ordinarily considered in the analysis of box girders.

The final assumption implies that the shape of the cross section is sufficiently maintained such that stresses[4] resulting from cross-sectional deformations are small. This assumption is justified for two reasons: (1) maintenance of the shape of the cross section through proper design of diaphragms is necessary to derive maximum benefits from box girder designs based on ultimate strength, and (2) significant distortion of the cross section should be prevented to eliminate potential detrimental effects on the fatigue life of box girders.[4]

Application of an arbitrary transverse load to the deck

of a box girder causes the member to bend and twist. Assuming that

the principle of position is valid, stresses due to flexure and

torsion can be calculated separately and then combined to determine

the resultant member stresses.

3.2.1 Flexural Stresses

Transverse loading in the plane of symmetry of a box girder

produces normal and shearing stresses in the cross section which can

be closely approximated using the relationships from simple beam

theory. The normal stresses are given by

$$\sigma_B = \frac{M_B \, y}{I_x} \tag{3.1}$$

where y and I_x are based on the cross-sectional area. Figure 3.1(a)

illustrates the distribution of these stresses over the cross section

of a box girder. The neutral axis is located in the upper part of

the web, close to the top flange. This is typical for box girder

bridges having either a concrete or orthotropic steel deck and re-

sults in the larger portion of the web being in tension for single-

span members.

For closed, thin-walled sections loaded in a plane of sym-

metry, the flexural shear stresses can be evaluated from the expression,

$$\tau_B = \frac{V \, Q}{I_x \, t} \tag{3.2}$$

where $Q = \int_o^s y(s) t(s) ds$. Due to symmetry, τ_B and therefore Q are zero

at points where the flanges and vertical axis of symmetry intersect.

The shear stresses are assumed to be uniform across the thickness, t, of the wall plates and usually have a cross-sectional distribution similar to that indicated in Fig. 3.1(b) for the given loading. It is obvious from this sketch that the webs theoretically carry all of the vertical shear.

3.2.2 Torsional Stresses

In general, a box girder subjected to torsion will experience warping of its cross section as it twists. If warping is free to take place at every cross section along the length of the member, only shearing stresses due to St. Venant torsion develop. However, if warping is restrained at one or more cross sections, additional shear and normal stresses occur. When this takes place, the total applied twisting moment M_T is the sum of the warping contribution M_w and the St. Venant contribution M_{sv}, that is,

$$M_T = M_{sv} + M_w \qquad (3.3)$$

The governing differential equation for a member subjected to a concentrated torque is given by,

$$M_T = GK_T \frac{d\emptyset}{dz} - EI_\omega \frac{d^3\emptyset}{dz^3} \qquad (3.4)$$

where z = coordinate along the longitudinal axis

$\emptyset$ = angle of twist

G = shear modulus

K_T = torsion constant

E = modulus of elasticity

I_ω = warping moment of inertia

The general solution to this equation can be put in the form,[22]

$$\emptyset = C_1 + C_2 \cosh \lambda z + C_3 \sinh \lambda z + \frac{M_T z}{\lambda^2 EI_\omega} \qquad (3.5)$$

where $\lambda^2 = \frac{GK_T}{EI_\omega}$. The constants of integration C_1, C_2 and C_3 can be

determined from the applicable boundary conditions. Hence the angle

of twist is completely defined along the length of the member which

makes possible the evaluation of the torsional stresses from the

following expressions:[22]

$$\tau_{sv} = \frac{GK_T \emptyset'}{2 A_o t} \qquad (3.6)$$

$$\tau_w = - \frac{E \bar{S}_\omega \emptyset'''}{t} \qquad (3.7)$$

$$\sigma_w = E \omega_n \emptyset'' \qquad (3.8)$$

where $\bar{S}_\omega$ and ω_n are the warping statical moment and the normalized

unit warping, respectively. The terms K_T, I_ω, S_ω and ω_n are cross-

sectional properties which have been clearly defined for open thin-

walled sections.[23,24] The modified form of these for closed thin-

walled sections is given in Appendix A. A_o is the area enclosed by

the middle line of the wall plates.

The stresses defined by Eqs. (3.6) through (3.8) are dis-

tributed uniformly across the thickness of the box girder's wall

plates. Their distribution over a cross section of model specimen M1

is shown in Fig. 3.2. It is seen in Fig. 3.2(a) that the St. Venant

shear stresses are uniform over the width of a given wall plate

of constant thickness, whereas the shear and normal stresses due to warping exhibit (Figs. 3.2(b) and (c)) appreciable variation over the width. This is considered to be typical for a box girder member. More important is the distribution of these stresses along the length of the member. In order to provide some insight into this, a torsion analysis of model specimens M1 and M2 was performed using Eqs. (3.4) through (3.8). In the analysis it was assumed that warping was free to take place at the ends of the member. The results plotted in Figs. 3.3 and 3.4 show that the warping stresses are significant in localized regions adjacent to the point of restraint (loading point). These stresses decrease to practically zero at a relatively short distance from the restraint. However, the shear stresses due to St. Venant torsion, τ_{sv}, are prominent over almost the entire length of the member.

Another point to consider in attempting to establish the significance of the torsional stresses is the relative magnitude of these stresses with respect to the flexural stresses. Computations for specimens M1 and M2 indicated that the maximum normal stresses due to bending were 5 to 6 times larger than the maximum normal warping stresses. Web shear stresses due to flexure were from 2 to 3 times larger than the St. Venant shear stresses and from 1.25 to 2.5 times as large as the maximum shear stresses caused by warping.

Additional information on torsional stresses in box girders can be obtained by referring to some of the past literature on the subject. Results of experimental tests by Maggard and Parr[19] indicate that the warping stresses, σ_w and τ_w, in box-like,

thin-walled sections subjected to torsion, are negligible for loads within the linear, prebuckling range. In Ref. 24, Terrington states that stresses due to warping restraint are not present in closed, thin-walled sections to any measurable extent.

Taking into consideration the relative magnitude and distribution (both cross-sectional and longitudinal) of the torsional stresses and also the findings of previous studies, it was assumed that the effects of warping were insignificant and therefore would not be considered in the remaining development of the analytical method. It was thus implied that the twisting moment is carried by only St. Venant torsion and the resulting shear stresses can be computed from Bredt's formula, [25]

$$\tau_{sv} = \frac{M_T}{2A_o t} \tag{3.9}$$

3.2.3 Primary Stresses

The normal and shear stresses resulting from flexure and the shear stresses due to St. Venant torsion are hereafter referred to as the primary stresses. By making use of superposition, the shear effects due to flexure and torsion can be combined algebraically. An example of this is presented in Fig. 2.27. Of particular significance in this figure is the appreciable difference in the resultant shear flow for the two webs. This was found to play an important role in the development of panel failure mechanisms.

A summary of the primary stresses is given on the following page:

$$\sigma = \frac{M_B y}{I_x}$$

(3.10)

$$\tau = \frac{V Q}{I_x t} \pm \frac{M_T}{2A_o t}$$

(3.11)

3.3 Behavior and Strength of a Box Girder Panel

A box girder panel can be looked upon as being somewhat similar to that of a plate girder. In particular, the webs are analogous, having essentially the same geometry and boundary conditions. Also, both are subjected to linearly varying normal stresses and practically uniform shearing stresses over their depth. Therefore, it was expected that, like the slender web of a plate girder, box girders webs would exhibit significant post-buckling strength. Because of these similarities it was reasoned that strength formulas developed for unsymmetrical plate girder panels[26] could be applied with certain modifications to box girder panels.

In evaluating the behavior and strength of a box girder panel, two distinct loading conditions were considered. A symmetrical load which subjects the panel to shear and bending and an unsymmetrical or eccentric load which also imposes torsion on the panel. Examples of each are given in Fig. 3.5.

3.3.1 Symmetrical Load

For single-span box girders stress patterns similar to those shown in Fig. 3.1 develop as loading commences. The strength of a panel is governed by web failure, yielding of the tension flange, or failure

of the compression flange. Failure of the compression flange is restricted to either yielding of a steel plate or crushing of a concrete deck. Compression flange buckling has been excluded because it is not likely to occur with the large out-of-plane bending stiffness of a concrete or orthotropic steel deck.

A. Web Failure

When a panel is subjected to a symmetrical loading condition, the behavior of and stresses in the two webs are assumed to be identical. The panel strength, which is evaluated based on forces at the mid-length of the panel, is obtained as a sum of buckling (beam action), post-buckling (tension field action), and flange (frame action) contributions.

$$V_u = V_\tau + V_\sigma + V_f \qquad (3.12)$$

This approach is identical to that suggested by Chern and Ostapenko[21] for plate girders.

Prior to buckling the characteristic web stresses are given by the following relationships:

$$\tau = \frac{V}{2A_w} \qquad (3.13)$$

$$\sigma = \frac{V z_o y_c}{I_x} \qquad (3.14)$$

where V = panel shear

A_w = area of one web

z_o = distance from the end support of the girder to the mid-length of the panel

y_c = distance from the neutral axis to the extreme compression fiber of the web

equation (3.13) assumes that the flexural shear stress is distributed uniformly over the depth of the webs. This approximation has been successfully utilized in ultimate strength studies on plate girders[10,17], and because of similar shear stress distributions can also be applied to box girders. In Eq. (3.14) the moment, M_B, has been replaced by $V \cdot z_o$. This is possible for single-span members subjected to concentrated loads. Figure 3.6 depicts the assumed stress and boundary conditions for a typical web plate in a box girder subjected to symmetrical loading.

This combination of bending and shearing stresses is assumed to be limited by web buckling. The interaction equation defining this limit is given in Ref. 26 as,

$$\left(\frac{\tau_c}{\tau_{cr}}\right)^2 + \frac{1+R}{2}\left(\frac{\sigma_c}{\sigma_{cr}}\right) + \frac{1-R}{2}\left(\frac{\sigma_c}{\sigma_{cr}}\right)^2 = 1.0 \qquad (3.15)$$

Substitution of Eqs. (3.13) and (3.14) for τ_c and σ_c in the interaction equation results in the following expression for the beam action contribution, V_T.

$$V_T{}^2 \left[\frac{1}{(2A_w\tau_{cr})^2} + \frac{1-R}{2}\left(\frac{z_o y_c}{I_x \sigma_{cr}}\right)^2\right] + V_T\left[\frac{1+R}{2}\left(\frac{z_o y_c}{I_x \sigma_{cr}}\right)\right] - 1.0 = 0 \quad (3.16)$$

In the above equations,

τ_c = shear buckling stress of the web under combined shear and bending

σ_c = buckling stress at the extreme compression fiber

of the web under combined shear and bending

R = $-y_c/y_t$ (due to a lack of sufficient experimental

and theoretical data, conservatively use $R = -1.5$

for computed values less than -1.5)

y_t = distance from the neutral axis to the extreme

tension fiber of the web

y_c = distance from the neutral axis to the extreme com-

pression fiber of the web

τ_{cr} = web buckling stress under pure shear as defined in

Appendix B

σ_{cr} = web buckling stress under pure bending as defined

in Appendix B

From Ref. 26 the tension field action contribution is given
by one of the following expressions:

for $\lambda_v \leq 0.58$

$$V_\sigma = 0 \tag{3.17a}$$

for $0.58 < \lambda_v \leq \sqrt{2}$

$$V_\sigma = \frac{0.6\,\lambda_v - 0.348}{\sqrt{\alpha^2 + 1.6}}\,V_P \tag{3.17b}$$

for $\lambda_v > \sqrt{2}$

$$V_\sigma = \frac{0.9 - 0.787/\lambda_v^2}{\sqrt{\alpha^2 + 1.6}}\,V_P \tag{3.17c}$$

where λ_v = non-dimensional shear buckling parameter defined

in Appendix B

$V_p = 2 A_w \dfrac{\sigma_{yw}}{\sqrt{3}}$ = plastic shear force of two identical webs

$\alpha = a/b_w$ = web panel aspect ratio

For slender web box girders either Eq. (3.17b) or (3.17c) normally governs.

The frame action contribution of Eq. (3.12) represents the resistance of the flanges to the distortion of the web panel from a rectangle into a parallelogram. Its maximum contribution is reached when plastic hinges form across the effective width of the flanges as shown in Fig. 3.7. It is possible that for certain loading conditions and box girder designs only a portion of the full flange width would be effective. For the sake of simplicity the contribution of a portion of the web plates to the flanges and the effect of axial forces on the flange plastic moment are neglected. This does not appreciably influence the final result because the neglected effects are compensating and also because the flange contribution does not exceed 15% of the total strength for ordinary box girders. Therefore, the frame action shear is

$$V_f = \frac{2}{a} (m_c + m_t) \tag{3.18}$$

where m_c and m_t are the plastic moments of the compression and tension flanges, respectively, and "a" is the length of the panel. For a box girder with a concrete deck, m_c has to be modified accordingly.

B. Failure due to Yielding of Tension or Compression Flange

In this study, failure of the compression flange is restricted to either yielding or crushing of the top flange material. It had been assumed that compression flange buckling would not ordinarily occur in single-span box girder members. The panel's ultimate strength cannot exceed that which causes the compression flange stress, σ_{cf}, to be equal to the reference yield stress of the flange, $\sigma_{y(cf)}$. The most critical location is at the maximum moment end of the panel. In terms of the panel shear force, the ultimate strength is given by one of the following equations:

a. If Compression Flange Yields before Webs Buckle $(V_u < V_T)$

$$V_u = \frac{\sigma_{y(cf)} \, I_x}{(z_o + a/2) \, y_{cf}}$$

(3.19a)

where y_{cf} is the distance from the neutral axis to the centroid of the compression flange.

b. If Webs Buckle before Compression Flange Yields $(V_u > V_T)$

$$V_u = V_T + \frac{[\sigma_{y(cf)} - \sigma_{T(cf)}] \, A_{cf} \, d'}{(z_o + a/2)}$$

(3.19b)

where A_{cf} = effective area of the compression flange

d' = distance between the centroids of the tension and compression flange

$\sigma_{T(cf)}$ is the stress at the centroid of the compression flange due to the theoretical web buckling load, V_T. It can be computed from,

$$\sigma_{T(cf)} = \frac{V_T (z_o + a/2) \, y_{cf}}{I_x}$$

(3.20a)

Equation (3.19b) was derived assuming that the webs do not support any additional bending stress after buckling. This appears to be too conservative for box girder panels subjected to pure bending or a combination of large bending and a small amount of shear. Research on thin web plate girders[9] revealed that under such loading conditions the portion of the web plate in tension can support additional bending stresses after theoretical web buckling. In the case of single-span box girders such a situation is not likely to occur because, under loading conditions approaching pure bending and the neutral axis close to the compression flange, the load causing theoretical web buckling is nearly equal to or less than the ultimate load causing flange failure. Therefore, most of the strength is carried by beam action (the first term on the right hand side of Eq. (3.19b)) and the post-buckling strength defined by the other term of the same equation is small.

Similar expressions can be derived based on tension flange failure.

c. <u>If Tension Flange Yields before Webs Buckle</u> $(V_u < V_T)$

$$V_u = \frac{\sigma_{y(tf)} \, I_x}{(z_o + a/2) \, y_{tf}} \tag{3.21a}$$

where $\sigma_{y(tf)}$ = reference yield stress of the tension flange

y_{tf} = distance from the neutral axis to the centroid of the tension flange

d. <u>If Webs Buckle before Tension Flange Yields</u> $(V_u > V_T)$

$$V_u = V_T + \frac{[\sigma_{y(tf)} - \sigma_{T(tf)}] \, A_{tf} \, d'}{(z_o + a/2)} \tag{3.21b}$$

A_{tf} is the effective area of the tension flange and $\sigma_{T(tf)}$ is the stress at the centroid of the tension flange due to the theoretical web buckling load, V_T, and is given by,

$$\sigma_{T(tf)} = \frac{V_T\,(z_o + a/2)\,y_{tf}}{I_x} \tag{3.20b}$$

In summary, the ultimate strength of a box girder panel subjected to symmetrical loads is given by the smallest of the values computed from Eqs. (3.12), (3.19) and (3.21). Equation (3.12) defines the panel strength based on a web type failure. Panel failure resulting from compression or tension flange yielding is given by Eqs. (3.19) and (3.21), respectively. For convenience these are summarized in Appendix C.

3.3.2 Unsymmetrical Load

An unsymmetrical load on a box girder panel produces in addition to flexural shear and bending, torsion of the panel. As a result of the torsional component of loading, the webs on opposite sides of cross section are subjected to different stress states. Although the final failure mechanism is similar to one of those described for symmetrical loading, the development of the mechanism and the resulting ultimate strength are altered due to torsion.

The behavior and strength of the panel can be evaluated by analyzing the panel as it progresses through several distinct phases of loading. Web failure is considered first.

A. Web Failure

a. Phase 1 - Entire Cross Section is Effective

During this phase of loading the entire cross section effectively resists shear, bending and torsion. Stresses in the web are given by,

$$\sigma_{(1)} = \frac{M_1\, y_c}{I_x} = \frac{V_1\, z_o\, y_c}{I_x} \tag{3.22}$$

$$\tau_{(1)} = \frac{V_1}{2A_w} \pm \frac{V_1\, e}{2A_o\, t_w} \tag{3.23}$$

where e = eccentricity of the load with respect to the vertical, centroidal axis

A_o = area enclosed by the middle line of the wall plates

t_w = thickness of a web plate

The alternate signs for the second term of Eq. (3.23) indicate the addition of the flexural and torsional shear in one web (τ^p) and the subtraction of the same in the other web (τ^n). Phase 1 terminates when theoretical web buckling first occurs on the side where the shear stresses add. This is referred to as the positive side of the cross section and is identified by the superscript, p. The corresponding panel shear, V_1, is obtained by substituting expressions (3.22) and (3.23) into the interaction formula, Eq. (3.15), for σ_c and τ_c, respectively, and solving the resulting quadratic equation:

$$V_1^2 \left[\left(\frac{C_1}{\tau_{cr}}\right)^2 + \left(\frac{1-R}{2}\right)\left(\frac{C_2}{\sigma_{cr}}\right)^2 \right] + V_1 \left[\left(\frac{1+R}{2}\right)\left(\frac{C_2}{\sigma_{cr}}\right) \right] - 1.0 = 0 \tag{3.24}$$

where $C_1 = \left(\dfrac{1}{2A_w} + \dfrac{e}{2A_o t_w}\right)$

$C_2 = \dfrac{z_o\, y_c}{I_x}$

and R, τ_{cr} and σ_{cr} are as defined in the previous section for symmetrical loading.

b. Phase 2 - Web Buckled on Positive Side of the Cross Section

For this phase the bending stress in the web on the positive side of the cross section remains constant. Additional bending moment is carried by the two flanges and the web on the negative side constituting an effective cross section as shown in Fig. 3.8. Any additional bending is assumed to take place about a horizontal axis passing through the centroid of the remaining effective cross section. Distribution of the shear is assumed to be the same as for Phase 1 except that the mechanism for carrying the shear on the positive side has changed from beam action to tension field action. Expressed in terms of force, the shear carried by the positive web during Phase 2 is,

$$V_2{}^P = \frac{V_2}{2} + \frac{V_2\,eb}{2A_o} \tag{3.25}$$

where V_2 is the panel shear above V_1 and "b" is the depth of the web plate. The first term represents the flexural shear force and the second term defines the shear force resulting from torsion.

The web stresses on the negative side are described by formulas similar to those for Phase 1.

$$\sigma_{(2)}^n = \frac{V_2\,z_o\,y_c'}{I_x'} \tag{3.26}$$

$$\tau_{(2)}^n = V_2 \left[\frac{1}{2A_w} - \frac{e}{2A_o t_w} \right] \tag{3.27}$$

where y_c' and I_x' are properties of the effective cross section which consists of a single web and the two flanges.

The total stresses in the web on the negative side are obtained by adding the effects of Phases 1 and 2 as indicated below.

$$\sigma^n_{(1+2)} = \frac{V_1 z_o y_c}{I_x} + \frac{V_2 z_o y_c'}{I_x'} \qquad (3.28)$$

$$\tau^n_{(1+2)} = \left[V_1 + V_2 \right] \left[\frac{1}{2A_w} - \frac{e}{2A_o t_w} \right] \qquad (3.29)$$

Termination of Phase 2 is due to either buckling of the web on the negative side of the cross section or tension field yielding of the web on the positive side. The panel shear force, V_{2a}, causing the former to occur can be calculated from an expression similar to Eq. (3.24) by substituting the resultant stresses from Eqs. (3.28) and (3.29) into the interaction equation, Eq. (3.15).

$$V_{2a}^2 \left[(\frac{C_3}{\tau_{cr}})^2 + (\frac{1-R}{2}) (\frac{C_4}{\sigma_{cr}})^2 \right] + V_{2a} \left[2V_1 (\frac{C_3}{\tau_{cr}})^2 + (\frac{1+R}{2}) \frac{C_4}{\sigma_{cr}} + \right.$$

$$\left. \frac{(1-R) V_1 C_2 C_4}{\sigma_{cr}^2} \right] + \left[(\frac{V_1 C_3}{\tau_{cr}})^2 + (\frac{1+R}{2}) \frac{C_2}{\sigma_{cr}} + (\frac{1-R}{2}) (\frac{V_1 C_2}{\sigma_{cr}})^2 - 1.0 \right] = 0 \quad (3.30)$$

where

$$C_3 = (\frac{1}{2A_w} - \frac{e}{2A_o t_w})$$

$$C_4 = \frac{z_o y_c'}{I_x'}$$

In order to simplify the computation of V_{2a}, R can be taken as the average of the values computed for the cross section assumed to be effective against bending during Phases 1 and 2, that is,

$$R = -\frac{1}{2}\left[\,^y t/y_c + \,^{y'} t/y'_c\right] \quad \text{if } R > -1.50 \qquad (3.31)$$

The above approximation has little or no effect on the strength evaluation because the neutral axis shifts very little due to the elimination of one web. If the average value of R is algebraically less than -1.5, then a value of R = -1.5 is to be used in Eq. (3.30).

The panel shear, V_{2b}, which causes tension field yielding of the web on the positive side is obtained by making use of Eq. (3.25).

$$\frac{V_\sigma}{2} = \frac{V_{2b}}{2} + \frac{V_{2b}\,eb}{2A_o} \qquad (3.32a)$$

or

$$V_{2b} = V_\sigma/C_5 \qquad (3.32b)$$

where $C_5 = (1 + \,^{eb}/A_o)$. V_σ is defined by Eq. (17) and $V_\sigma/2$ is the tension field contribution of one web plate.

The smaller of V_{2a} and V_{2b} causes the termination of Phase 2. Depending on which of these controls, the behavior of the girder panel differs as additional load is applied.

c. **Phase 3a - Both Webs are Buckled**

This phase of loading will take effect if V_{2a} has caused the termination of Phase 2. During this phase any additional bending moment is supported only by the flanges (Fig. 3.8). Bending stresses in the webs remain constant while the shear forces are carried through tension field action. Phase 4a will commence when the web on the positive side is unable to support any additional shear force due

to tension field yielding. It is characterized by the following loading condition:

$$V_\sigma = (V_{2a} + V_{3a})\, C_5 \qquad (3.33a)$$

then,

$$V_{3a} = V_\sigma/C_5 - V_{2a} \qquad (3.33b)$$

Phase 3b - Web on Positive Side has Experienced Tension Field Yielding

It is not expected that this phase would occur very often for ordinary box girders. The eccentricity of the load has to be quite large to cause tension field yielding in one web before the other web buckles. However, for the sake of completeness it is considered.

When one web yields, it is unable to resist any additional flexural shear. As a result of this, the flexural shear is redistributed to the web on the opposite side of the cross section. This has an important effect on the ultimate strength of the member. If such redistribution does not take place, the strength of the member is significantly decreased. This point is made clear when the theoretical and experimental results are compared in the next chapter.

It is also necessary to consider the effects of any additional torsion on the stresses and behavior of a damaged panel. After one of the webs has yielded, the torsional stiffness of the panel decreases considerably because its remaining effective cross

section is no longer of a closed configuration. The mechanism for carrying any additional torque is altered. No doubt, the actual mechanism is quite complex and undefinable in simple terms, especially when the effects of adjacent panels are considered. In any event, theoretical computations for the model specimens indicate that a large percentage of the girder's strength will have been exhausted when yielding of the first web takes place. Also, any additional load produces flexural shear and bending stresses in the effectively open cross section which out-weigh the additional torsional stresses. For these reasons, the effects of any additional torque, on the behavior and strength of a panel having one or both of its webs rendered ineffective due to tension diagonal yielding, are assumed to be insignificant and thus ignored.

The bending stresses during Phase 3b are supported by the flanges and the remaining web. Buckling of the web on the negative side of the cross section terminates this phase of loading. The web stresses for Phase 3b are given by,

$$\sigma^n_{(3b)} = \frac{V_{3b} z_o y'_c}{I'_x} \tag{3.34}$$

$$\tau^n_{(3b)} = V_{3b}/A_w \tag{3.35}$$

Combining the web stresses for Phases 1, 2b and 3b results in the following:

$$\sigma^n_{(1+2b+3b)} = \frac{V_1 z_o y_c}{I_x} + \left[V_{2b} + V_{3b} \right] \left[\frac{z_o y'_c}{I'_x} \right] \tag{3.36}$$

$$\tau^n_{(1+2b+3b)} = \left[V_1 + V_{2b}\right]\left[\frac{1}{2A_w} - \frac{e}{2A_o t_w}\right] + \frac{V_{3b}}{A_w} \tag{3.37}$$

Substitution of Eqs. (3.36) and (3.37) into formula (3.15) results in the following expression for the panel shear force, V_{3b}.

$$V_{3b}^2\left[\frac{1}{(A_w \tau_{cr})^2} + (\frac{1-R}{2})(\frac{C_4}{\sigma_{cr}})^2\right] + V_{3b}\left[\frac{2\,C_7}{A_w \tau_{cr}} + (\frac{1+R}{2})\frac{C_4}{\sigma_{cr}} + \frac{(1-R)C_4}{\sigma_{cr}^2}\right]$$

$$+ \left[(\frac{C_7}{\tau_{cr}})^2 + (\frac{1+R}{2})\frac{C_6}{\sigma_{cr}} + (\frac{1-R}{2})(\frac{C_6}{\sigma_{cr}})^2 - 1.0\right] = 0 \tag{3.38}$$

In the above expression, R, is the larger of -1.5 or the value computed from Eq. (3.31) and,

$$C_6 = V_1\,C_2 + V_{2b}\,C_4$$

$$C_7 = C_3\,(V_1 + V_{2b})$$

d. Phase 4 - Web on Positive Side has Yielded, Web on Negative Side has Buckled

This phase of loading occurs regardless of whether Phase 3a or 3b preceded it. During this stage bending moment is supported only by the flanges. The web on the negative side carries all the additional flexural shear and the effects of any additional torque are assumed to be negligible. Termination of this phase occurs when tension field yielding of the negative side web initiates. If Phase 3a has preceded Phase 4, the characteristic panel shear force, V_{4a}, is given by,

$$V_{4a} = 1/2\left[V_\sigma - V_{3a}\,C_8\right] \tag{3.39}$$

with $C_8 = (1 - {}^{eb}/A_o)$. However, if Phase 4 was preceded by Phase 3b, then,

$$V_{4b} = \frac{V_\sigma}{2} \qquad (3.40)$$

where again $\frac{V_\sigma}{2}$ is the tension field contribution of one web.

e. <u>Phase 5 - Both Webs have Yielded</u>

Only the flanges are effective during the fifth and final phase of loading. The additional panel shear is supoorted through frame action of the flanges. Similar to the case of symmetrical loading it can be calculated from,

$$V_5 = V_f = \frac{2}{a} (m_c + m_t) \qquad (3.41)$$

Figure 3.8 summarizes the cross-sectional characteristics for each phase of loading. The solid lines represent that part of the cross section which is effective.

f. <u>Ultimate Panel Strength</u>

The strength of a panel due to a web type failure in terms of the panel shear force is the summation of the appropriate contributions from each phase of loading. Depending on the panel geometry and loading conditions it is determined from either,

$$V_u = V_1 + V_{2a} + V_{3a} + V_{4a} + V_5 \qquad (3.42a)$$

or

$$V_u = V_1 + V_{2b} + V_{3b} + V_{4b} + V_5 \qquad (3.42b)$$

B. <u>Failure due to Yielding of Tension or Compression Flange</u>

It is also possible for a box girder panel under unsymmetrical loading to fail by yielding of either of the flanges. Like the case of symmetrical loading the strength of the panel cannot exceed that which causes the compression flange stress, σ_{cf}, to be equal to the reference yield stress, $\sigma_{y(cf)}$. This condition can be checked for one of the two possible mechanisms of failure previously described. The effect of shear stresses on compression flange yielding has been ignored because they are normally quite small due to the relatively large thickness of the deck. However, in some cases it may be necessary to consider the shear stresses in addition to using a different failure criterion.

a. <u>Phases 1-2a-3a-4a-5 Mechanism</u>

$$\left| \sigma_{y(cf)} \right| \geq \left| \frac{-V_1 (z_o + a/2) y_{cf}}{I_x} - \frac{V_{2a} (z_o + a/2) y'_{cf}}{I'_x} \right.$$
$$\left. - \frac{(z_o + a/2)}{A_{cf} d'} (V_{3a} + V_{4a} + V_5) \right| \qquad (3.43)$$

b. <u>Phases 1-2b-3b-4b-5 Mechanism</u>

$$\left| \sigma_{y(cf)} \right| \geq \left| \frac{-V_1 (z_o + a/2) y_{cf}}{I_x} - \frac{(z_o + a/2) y'_{cf}}{I'_x} (V_{2b} + V_{3b}) \right.$$
$$\left. - \frac{(z_o + a/2)}{A_{cf} d'} (V_{4b} + V_5) \right| \qquad (3.44)$$

Calculation of the flange stress at the end of each loading phase provides a progressive check for this possible failure mode.

If the previous condition (Eq. (3.43) or (3.44)) is not satisfied at the end of one of the loading phases, it is a simple matter to compute the panel shear force during that phase which causes compression flange yielding. The summation of that shear force and the panel shear forces calculated for all proceeding phases determines the strength of the girder panel. For example, assume that when applying Eq. (3.43) the yield stress, $\sigma_{y(cf)}$, is exceeded at the end of Phase 4a. Then the shear force at which flange yielding initiates during Phase 4a is given by,

$$V_{4a} = \frac{A_{cf}d'}{(z_o + a/2)} \left[\sigma_{y(cf)} - (z_o + a/2) \left(\frac{V_1 y_{cf}}{I_x} + \frac{V_{2a} y'_{cf}}{I'_x} + \frac{V_{3a}}{A_{cf}d'} \right) \right] \quad (3.45)$$

The corresponding panel strength is,

$$V_u = V_1 + V_{2a} + V_{3a} + V_{4a} \quad (3.46)$$

where V_{4a} comes from Eq. (3.45).

Of course, it is also necessary to check failure of the tension flange. Yielding of the flange material is again the governing criterion. For the case of unsymmetrical loading, shear stresses due to St. Venant torsion could have a significant effect on tension flange yielding and therefore are included in the yield condition. Applying von Mises's yield criterion to the tension flange stress state illustrated in Fig. 3.9 results in the following,

$$\sigma_z^2 + 3\tau_{xz}^2 - \sigma_{y(tf)}^2 \leq 0 \quad (3.47)$$

where

$$\sigma_z = \sigma_{tf} = \frac{V_1(z_o + a/2)y_{tf}}{I_x} + \frac{V_{2a}(z_o + a/2)y'_{tf}}{I'_x}$$

$$+ \frac{(z_o + a/2)}{A_{tf}d'}(V_{3a} + V_{4a} + V_5)$$

(3.48)

and

$$\tau_{xz} = \frac{e}{2A_o t_{tf}}\left[V_1 + V_{2a} + V_{3a}\right]$$

(3.49)

if Phases 1-2a-3a-4a-5 develop. If the other phases of loading take precedent then,

$$\sigma_z = \sigma_{tf} = \frac{V_1(z_o + a/2)y_{tf}}{I_x} + \frac{(z_o + a/2)y'_{tf}}{I'_x}(V_{2b} + V_{3b})$$

$$+ \frac{(z_o + a/2)}{A_{tf}d'}(V_{4b} + V_5)$$

(3.50)

and

$$\tau_{xz} = \frac{e}{2A_o t_{tf}}\left[V_1 + V_{2b}\right]$$

(3.51)

The yield condition (Eq. (3.47)) can be checked at the end of each loading phase and the corresponding ultimate strength evaluated if tension flange yielding occurs.

Equations (3.49) and (3.51) contain shear stress terms associated with St. Venant torsion of the closed section. For reasons previously discussed, torsional shear stresses occurring after one or both of the webs of a panel fail are not included.

Appendix D contains a summary of the ultimate strength equations for unsymmetrical loading.

Thus, the ultimate strength of a box girder panel has been defined for both symmetrical and unsymmetrical loading conditions. In the next section this is utilized to evaluate the ultimate strength of a single-span box girder member.

3.4 Behavior and Strength of a Single-Span Box Girder

The ultimate strength of a box girder member is directly dependent upon the strength of its component panels. A single-span box girder which is statically determinate for flexural loads reaches its ultimate shear or bending capacity when at least one of its panels develops a failure mechanism. For the entire member, the statical redundancy of the torsional force makes it quite possible that the member's torsional capacity is not reached at the same load which produces failure of a panel. This implies that a redistribution of the torsional moment takes place in box girders.

3.4.1 Ultimate Strength under Symmetrical Loading

Theoretically, there is no torsion associated with this loading condition. The ultimate strength is reached when the weakest constituent panel (or panels) reaches its maximum capacity as defined by the smallest of the values computed from Eqs. (3.12), (3.19) and (3.21). Relationships between the ultimate panel strength, V_u, and the member strength, P_u, can be obtained from the corresponding shear diagram.

3.4.2 Ultimate Strength under Unsymmetrical Loading

When the loading conditions and panel geometries are such that initial web failure due to tension field yielding occurs first

in only one of the shear spans (as, for example, in Fig. 3.10), the torsional stiffness of that shear span is decreased considerably relative to that of the other, undamaged, shear span. This results in a redistribution of any additional twisting moment.

It was mentioned earlier that when the web of a box girder panel fails, its effective cross section changes from that of a closed box to an open channel section. Keeping in mind that a shift of the shear center takes place when this occurs, it is shown in a separate study that any additional load theoretically produces an additional twisting moment in the undamaged shear span.[27] For the loading condition shown in Fig. 3.10, the additional twisting moment in the shear span to the right of the loading point is given by,

$$\Delta M_T = \Delta P \ (e + \frac{L_2}{L_1 + L_2} \cdot x_{s.c.})$$ (3.52)

where $x_{s.c.}$ is the distance from the shear center of the originally closed section to the shear center of the effective open section. This is portrayed in the lower ΔM_T diagram of Fig. 3.10. In other cases, redistribution of the twisting moment must be computed considering the particular geometric and loading configurations of the member.

It is important to point out that redistribution of the twisting moment does not affect the distribution of the shear and bending moment, however, it can have an effect on the ultimate strength of the member. Implementation of this effect into the

ultimate strength evaluation can be achieved by keeping an orderly ac-
counting of the characteristic panel loads defined in Section 3.3.2
and by relating the panel loads to the girder loads for each phase of
loading.

For the special case when the loading condition and geometric
properties are symmetrical about the longitudinal centerline of the
member, redistribution of the twisting moment does not occur and
the torsional strength is essentially exhausted when initial web
failure takes place. Although the member possesses additional shear
and bending capacity, for all practical purposes its ultimate strength
will have been reached at the occurrence of initial web failure. Again,
the strength of the member can be evaluated by relating the panel forces
to the externally applied loads.

4. COMPARISON OF EXPERIMENTAL AND ANALYTICAL
BEHAVIOR AND RESULTS

The purpose of this chapter is to discuss and compare the observed and predicted behavior, modes of failure and strength of single-span, rectangular box girders. Little emphasis is placed on the precise quantitative comparison of either stress magnitudes and distributions or deformations of a member. However, when possible, stresses and deformations are used to help describe the behavior of the member and provide qualitative correlation with the analytical method.

In conformance with previous descriptions of the experimental results and analytical predictions, the two conditions of loading, symmetrical and unsymmetrical, are treated spearately.

4.1 Symmetrical Loading

First to be considered is the behavior of the web plates of a box girder panel under symmetrical loading.

One of the main assumptions of the analytical method is that the two webs of a given box girder panel are subjected to the same stresses and behave identically. Figure 4.1 provides some experimental verification of this assumed behavior. Shear stresses were found to be essentially the same in both webs of panel 5, specimen M2, for practically the entire range of loading.

Figure 4.1 also shows that the theoretical web shear stresses predicted from Eq. (3.13) for the prebuckling range (beam action) of loading agree quite well with the measured values. Above the web buckling load the tension field action becomes prominent. The actual stress state in the web is quite complex and cannot be accurately estimated. However, the bulging of the web along the tension diagonal (Figs. 2.17 and 2.18) and the increase of the tensile stress in the same direction (Fig. 2.20) confirm the occurrence of tension field action as a part of the failure mechanism. This was as predicted in the analysis.

The analytical method also assumes that frame action of the flanges provides additional panel shear capacity after the tension field contribution has been exhausted. This undoubtedly can only occur if prior flange yielding, resulting from bending of the cross section, has not taken place. Evidence of frame action was obtained in the symmetric load test of specimen M2. Figure 2.22 shows that a sharp increase in the longitudinal bending strain in the top flange of panel 4 occurred at a load of 2500 pounds, just before the failure of the member. This is attributed to the marked increase in flange curvature as frame action begins to occur. The load at which such behavior initiated corresponded to that which caused the depletion of the tension field contribution of panel 4.

Thus, with the help of Fig. 4.1 it is obvious that one of the three assumed panel failure modes for symmetrical loading was demonstrated experimentally. The observed mode of failure

compared well with the analytically described web type failure. Deformations corresponding to the assumed tension field action and frame action of a panel are quite evident in Fig. 2.18. The photographs in this figure also provide proof that the webs of a particular panel behaved identically as predicted.

The test specimens were not intended for observation of failure due to tension or compression flange yielding. These modes of failure were considered to be uncomplicated and predictable from theory. For the purpose of this dissertation, experimental verification of these was not deemed to be necessary.

Up to this point it should be clear that the assumed behavior and modes of failure for a panel subjected to symmetrical loading have been satisfactorily verified. A further test of the validity of the analytical method lies in the accuracy of the ultimate strength computation.

In Section 2.3.1, it was stated that load drops experienced during testing were due to a combination of the non-zero strain rate used during testing and relaxation of the solder joints. It was reasoned that the true static load-carrying capacity lies between the upper (o) and lower (x) data points of Fig. 2.21. This resulted in an upper bound of 2650 pounds and a lower bound of approximately 2350 pounds for the experimental static strength, P_u^{exp}, of the member. Comparing these with the predicted strength, P_u, of 2360 pounds resulted in the theoretical value being approximately 12.3% smaller than the upper bound and about 0.4% larger than the

lower bound. The use of the static yield stress values (Table 1) in the theoretical computations meant that the predicted strength was computed assuming a zero strain rate.

It must be realized that in addition to the strain rate and relaxation of the solder joints during testing, other factors more than likely had effects on the measured and computed strengths. A brief review of some of the more important ones is in order.

One of these factors involves differences between the actual model dimensions and the nominal ones of Fig. 2.2. Actual geometric properties no doubt were influenced by the contribution of the large solder joints which were not considered in the computed values.

The assumptions made in the analysis also play a significant role. Some of the important ones have a direct bearing on the computation of the beam, tension field and frame action contributions to the ultimate strength. For instance, the assumed web boundary conditions of fixity along the flanges and simply supported along the transverse stiffeners directly influence the beam action contribution. Evaluation of the frame action contribution is affected by the omission of the axial forces in the flanges and an effective strip of the webs in the computation of the flange plastic moments. Also, there are several inherent assumptions which have been carried over from plate girder theory.[17,21,26] These involve approximations which surely affect the theoretical results.

In addition, residual stresses which were not considered could have had an effect on the difference between the analytical and experimental strengths.

In order to present further correlation between the experimental and theoretical results, attention is given to a comparison of the strength evaluations of M2 based on failure of either panel 4 or 5. According to the plate girder theory being utilized, these are the most critical panels because they are subjected to the largest shear and bending moments (Fig. 2.11) and also have the largest web plate aspect ratios. From the shear and moment diagrams of Fig. 2.11 it is noticed that the loading on panel 4 is slightly more severe than that of panel 5. However, the shear capacity of panel 5 is less than the shear capacity of panel 4 because panel 5 has a larger transverse stiffener spacing, thus a larger aspect ratio (a/b_w). The characteristic loads summarized in Table 3 bear this out. The final column of Table 3 indicates very little difference (60 pounds) in the theoretical ultimate strength, P_u, based on failure of either panel 4 or 5. Therefore, the experimentally observed simultaneous failure of panels 4 and 5, in the symmetrical load test of M2, was to be expected based on the analytical results.

Results in Table 3 also indicate once again that the ultimate panel shear, V_u, was not limited by the panel shear, V_{cr} or V_T, which causes theoretical web buckling. Sample computations for the individual strength contributions and the ultimate strength of the member are given in Appendix C.

4.2 Unsymmetrical Loading

A comparison of the observed and predicted behavior of a panel subjected to unsymmetrical load can be initiated by considering the five distinct load phases described in Section 3.3.2. The results from the unsymmetrical load test of M2 are used in the comparison.

In Chapter 2 it was revealed that the strength of specimen M2 was governed by failure of panel 2. This panel had been subjected to the most severe combination of shear, bending and torsion (Fig. 2.11) and had one of the largest web panel aspect ratios (Fig. 2.2). To aid in the comparison, a plot of the panel shear versus panel shear stress for both webs of panel 2 is presented in Fig. 4.2. Included in the figure are the theoretical boundaries of the various loading phases and the corresponding effective cross section (denoted by the solid lines) for shear loading.

Phase 1 of the analytical method assumes that the entire cross section is effective for shear, bending and torsion and stresses can be estimated using Eqs. (3.22) and (3.23). Correlation between the measured and predicted shear stresses does not appear to be very satisfactory (Fig. 4.2), but general agreement is exhibited. The strength contribution of this loading phase corresponds to the beam action contribution for the condition of symmetrical loading.

In Figure 4.2, termination of Phase 1, which is due to theoretical web buckling of 2N, is not characterized by any distinguishing variation in the experimental curves. The same is true for Phase 2 which is terminated by theoretical web buckling of panel 2S. Such

behavior was expected for these two phases because sudden buckling of a web does not ordinarily occur. Instead, out-of-plane web deformations begin at the commencement of loading due to the always present initial web imperfections. This results in a gradual transition from beam action to tension field action. Evidence of this has been clearly exhibited in past plate girder tests.[16] The observed similarity of behavior between plate and box girder webs assured the applicability of the analytical model for these early phases of box girder strength.

By the analytical method it was expected that termination of Phases 3a and 4 would be characterized by leveling off of the shear force-shear stress curves for 2N and 2S, respectively. This is because the assumed termination point of each of these phases was marked by tension diagonal yielding and no additional shear would be expected to be carried by the web. Tension field action did actually occur in both webs of panel 2 and the shear force-shear stress curves did level off as shown in Fig. 4.2, but at loads higher than predicted. The differences between the theoretical and experimental loads associated with the termination of Phases 3a and 4 are not considered to be significant. The actual condition of shear stress distribution in this intermediate phase of strength development is not known, and the experimental stresses are only for qualitative indication. Deemed more important is that the predicted loading phases and web failure mechanism did take place during testing.

Similar explanation can be applied to the shear stresses on the south side of panel 2 during the last phase of loading.

Phase 5 of the analytical method represents the condition that both webs have yielded and the additional shear strength of the box girder panel is contributed by the flanges. Differences in predicted and measured values of shear stresses and panel strength not withstanding, Fig. 4.2 confirms that, after yielding of the webs the panel sustained some additional load before failure.

In reality, transverse deformation of the flanges, thus frame action, begins to occur first on the side of the cross section which experienced initial web failure at the load producing such failure. The deformations progress across the width of the flanges to the opposite side of the cross section until the other web fails. The capacity of the panel is reached when the flanges cannot sustain anymore load. This suggests that frame action of the flanges actually begins to occur before the last web fails. By the time both webs have yielded some of the frame action conbribution has been spent. This helps to explain the rather small difference between V_{max} and the load which produced web yielding in panel 2S (Fig. 4.2).

Further verification of the predicted panel behavior is provided by examining stresses in box girder panels. In the formulation of the analytical model it had been assumed that redistribution of the shear within a panel takes place when one of the webs fail due to yielding along the tension diagonal. Figure 2.23 shows a noticeable change in the slope of the load-stress curve for web panel 2S at the same load which produced yielding in panel 2N. This indicates

that tension diagonal yielding of web panel 2N caused a redistribution of any additional shear to panel 2S.

The analytical method also predicts redistribution of the torsional moment from one shear span to another. It is described in Section 3.4.2 that when initial web failure occurs in a panel, its torsional stiffness decreases greatly because its cross section has essentially been changed from a closed to an open configuration for any additional loads. As a result, the torsional stiffness of the corresponding shear span is decreased considerably. Therefore, any additional twisting moment is redistributed to the undamaged shear span. Test data revealed that such a phenomenon was exhibited in the testing of M2 and is depicted in the stress plots of Fig. 2.26. It is seen that at the load increment (from 1600 to 1700 pounds) which caused yielding in panel 2N, thus causing a decrease in the torsional stiffness of the shear span to the left of the concentrated torque, an abrupt change in the load-stress curves for panel 5, which was located to the right of the loading point, had occurred. The increase in the stress rate for the web on the north side and the decrease of the same for the web on the south side are due to the redistributed twisting moment. Such moment, with the direction indicated in the insert of Fig. 2.26, produces a corresponding increase and decrease in the shear stress in the north and south webs, respectively, as demonstrated in Fig. 2.27.

Attention is now directed to the mode of failure. The failure mechanism experienced during the unsymmetrical load test of M2 is portrayed in Fig. 2.15. The photographs show that failure was of the

web type, that is, tension diagonal yielding in both webs accompanied by transverse flange deformations. This is identical to one of the possible failure modes described in the analytical method for unsymmetrical loading.

Thus, the experimental behavior of model specimen M2 and its failure mode both correlated very well with the predictions by the analytical method. All that remains to be checked is the ultimate strength evaluation for specimen M2. The computed strength was 1810 pounds while the measured static strength as ascertained from Fig. 2.24 had an upper bound of 1930 pounds and a lower bound of about 1800 pounds. As a result, the experimental upper bound of the static strength was approximately 6.6% larger than the theoretical value while the lower bound was about 0.5% smaller than the theoretical strength. Again, it must be remembered that factors previously cited for the case of symmetrical loading obviously had some effects on either the experimental or analytical results. In addition, the omission of warping torsion and disregard of stresses due to deformation of the box girder cross section could also have had an effect.

Appendix E contains sample calculations of the ultimate strength evaluation for unsymmetrical loading.

Throughout the previous discussions no attempt was made to correlate the observed behavior of M1 with the theory. Failure of the X-bracing at the loading point (Fig. 2.1) at approximately 1500 pounds and a similar subsequent failure at the east support

permitted the cross section to deform and thus reduced the capability for shear redistribution within individual panels. That this was the condition can be derived from the lower portion of Fig. 2.28, where it is seen that the shear stress in the web on the north side remained practically unchanged even after the web on the opposite side had yielded. This is contrary to the behavior observed in panel 2 of specimen M2 (Fig. 2.23), where transfer of the shear to web 2S took place when panel 2N began to yield. Consequently, the predicted phases of loading were not carried through in the failure testing of model M1. Discrepancies between the experimental and theoretical results were to be expected.

As a result of the X-bracing failure, the maximum experimental load of M1 turned out to be approximately 23% lower than the calculated strength based on no cross-sectional deformations. This makes clear the importance of the X-bracing in the development of the ultimate strength of a box girder.

In order to provide further insight into the behavior of specimen M1, supplementary strength computations were made assuming that the full cross section was only effective up to 1500 pounds, the load at about which initial X-bracing failure occurred. Thereafter, it was assumed that only half of the cross section was effective, the side on which the load was applied. This assumption is thought to be reasonable because with the load directly above the web on the south side (Fig. 2.10) and the X-bracing at the loading point no longer effective, there was very little transfer of load to the north side. Appreciable differential bending between the two sides

of the cross section, as depicted in Figs. 4.3 and 2.12, indicates
that this type of behavior was evident in specimen M1. The lack of
shear redistribution which had been determined from strain readings
(Fig. 2.28) indicated the same.

Thus, it is assumed that any load above 1500 pounds was sup-
ported by essentially a plate girder consisting of the south side web
plate and flanges one-half as wide as the original flange plates.
The theoretical failure mechanism of a plate girder then corresponded
to that observed in the test (Figs. 2.12 and 2.13). This could be
described as a web type failure with yielding along the tension di-
agonal followed by transverse flange deformations. Such failure modes
have been well demonstrated before in plate girder tests.[14,17,21]

Based on the above assumptions, the theoretical strength of
M1 was computed to be approximately 1700 pounds. Comparing this to
the measured strength of 1800 pounds resulted in a difference of 6%.
The slight under estimate of the strength was better than expected
because of the conservative assumption regarding the behavior of the
member after X-bracing failure and because the measured strength was
an upper bound of the member's static load-carrying capacity. The
significant results are that the behavior of M1 under unsymmetrical
loading could be closely described and that the strength could be
reasonably approximated.

A summary of the measured and computed strengths and the
observed and predicted modes of failure are given in Table 4 for
all tests.

5. SUMMARY AND CONCLUSIONS

This dissertation presents the results of a combined experimental and theoretical study on the post-buckling behavior, modes of failure and ultimate strength of single-span, rectangular steel box girders subjected to either shear and bending or shear, bending and torsion. Buckling of the compression flange was not considered in the investigation because it was not expected to occur in an ordinary single-span box girder having a concrete or an orthotropic steel deck.

From the results of tests on two thin-web model box girders, the following conclusions were reached:

1. The load-carrying capacity of slender web box girders is not limited to the theoretical web buckling load.

2. A single-span, rectangular box girder subjected to high shear and a moderate amount of bending exhibits a behavior and failure mechanism resembling those of a similarly loaded plate girder.[14,15] Failure is due to simultaneously yielding along the tension diagonal of both webs of a given box girder panel followed by large vertical deformations of the flange.

3. Web failures occur first in those panels subjected to the most severe combination of shear and bending or shear, bending

and torsion. For panels subjected to identical loading, web failure occurs first in the panel having the largest web aspect ratio.

4. Torsional stresses in a rectangular box girder with negligible cross-sectional deformations and warping restraint can be fairly, closely estimated for the elastic, prebuckling range of loading considering only the effects of St. Venant torsion.

5. Torsional stresses can have an important effect on the behavior and load-carrying capacity of box girders.

6. A panel of a box girder subjected to shear, bending and torsion and properly braced to prevent deformation of the cross section can effectively redistribute shear stresses within the panel when one of the two webs fail by yielding.

7. Web failure in a box girder panel subjected to shear, bending and torsion occurs first on the side of the cross section where the flexural and torsional shear stresses add. Subsequent failure of the other web follows.

8. The shear or bending capacity of a single-span box girder is reached when one of its panels fails.

9. The torsional stiffness of a box girder panel is greatly reduced when the panel experiences initial web failure due to yielding along the tension diagonal. Redistribution of the torsional moment to the other side of the span away from the failed panel can take place.

10. Premature failure of diaphragms or X-bracing adversely affect the load-carrying capacity of box girders subjected to torsional loads.

11. Model specimens such as those utilized in this investigation are quite suitable for preliminary studies into the post-buckling behavior, failure modes and ultimate strength of steel box girders.

By utilizing the results from the model tests and some of the findings from previous research on plate girders,[17,21,26] an analytical method was developed for predicting the behavior and strength of single-span, rectangular steel box girders.

The method assumes that the shape of the cross section is essentially maintained and buckling of the compression flange does not occur. Stresses due to warping torsion were shown to have a negligible effect on the behavior and strength of the member. The ultimate strength of the box girder is reached when the first panel fails due to one of the following:

1. Yielding of the tension flange

2. Web type failure

3. Yielding or crushing of the compression flange

In accordance with the present state of the art for web plate analysis, the analytical method considers the shear strength of a web to consist of two contributions:

1. Beam action contribution

2. Tension field action contribution

The method of analysis presents two distinct sets of equations for estimating the ultimate strength of a box girder under symmetrical loading (shear and bending) and unsymmetrical loading (shear, bending and torsion).

A comparison of the experimental and theoretical results indicated that good correlation had been obtained for the overall behavior, modes of failure and ultimate strength of single-span, rectangular box girders. Therefore, it was concluded that a satisfactory, workable method had been developed for estimating the ultimate strength of such box girders.

To the best of the author's knowledge, the investigation described herein is the first to concern itself with the ultimate strength of slender web box girders subjected to shear, bending and torsion. A great deal of additional research is needed in this area. Some of the important topics which should be given attention are:

1. Refinement of the analytical method, described in this dissertation, based on the results of future, large scale experimental tests on box girders. Particular attention should be given to:

    a. Possible effects of warping torsion and cross-sectional deformations due to loading between diaphragm locations and different box girder designs.

    b. Modification of the strength equations obtained directly from plate girder theory for a more accurate application to box girders.

    c. Effects of shear lag on the behavior and strength of box girders.

    d. Precise and thorough experimental evaluation of stresses and deformations in box girders.

    e. Effects of a stud connected concrete deck on the behavior and strength of a composite box girder panel.

2. Post-buckling behavior and ultimate strength of single-cell box girders having non-rectangular cross sections.

3. Post-buckling behavior and ultimate strength of multi-cell box girders.

4. Post-buckling behavior and ultimate strength of curved box girders.

5. Effects of negative bending on the behavior and strength of box girders.

6. Development of a design procedure for box girders based on the ultimate strength concept.

6. APPENDICES

A. EXPRESSIONS FOR COMPUTING TORSIONAL PROPERTIES K_T, I_ω, $\bar{S}_\omega$ AND ω_n

FOR A CLOSED THIN WALLED CROSS-SECTION

Torsion Constant, K_T

$$K_T = \frac{4A_o^2}{\oint \frac{ds}{t(s)}} \tag{A-1}$$

where

A_o = area enclosed by the middle line of the walls

s = coordinate measured along the middle line of the walls

$t(s)$ = wall thickness

$\oint$ = defines integration around the entire length of the middle line

Normalized Unit Warping, ω_n

$$\omega_n = \frac{1}{A} \oint \bar{\omega}_o \, t(s) \, ds - \bar{\omega}_o \tag{A-2}$$

A is equal to the area of the cross-section and,

$$\bar{\omega}_o = \int_o^s \rho_o \, ds - \frac{2A_o}{\oint \frac{ds}{t(s)}} \int_o^s \frac{ds}{t(s)} \tag{A-3}$$

The integrals are performed for the cross-section which has been rendered open by an arbitrary cut. ρ_o is the perpendicular distance

from a tangent line passing through a general point $Q(s)$ to the torsion center. (Refer to Reference 22 for a more detailed explanation).

Warping Moment of Inertia, I_ω

$$I_\omega = \oint \omega_n^2 \, t(s) \, ds \qquad \text{(A-4)}$$

Warping Statical Moment, $\overline{S}_\omega$

$$\overline{S}_\omega = S_\omega - \frac{\oint S_\omega \dfrac{ds}{t(s)}}{\oint \dfrac{ds}{t(s)}} \qquad \text{(A-5)}$$

where

S_ω is the warping statical moment for an equivalent open cross-section and is given by,

$$S_\omega = \int_0^s \omega_n \, t(s) \, ds \qquad \text{(A-6)}$$

B. EXPRESSIONS FOR EVALUATING WEB BUCKLING UNDER PURE SHEAR AND PURE BENDING

The equations presented herein completely define τ_{cr} and σ_{cr} for a web plate fixed along the flange boundaries and pinned at the stiffeners. All were obtained directly from Reference 26.

WEB BUCKLING STRESS UNDER PURE SHEAR

The critical buckling stress, τ_{cr}, is given by one of the following equations:

for $\lambda_v \leq 0.58$ (strain-hardening range)

$$\tau_{cr} = [1 + 4.3 (0.58 - \lambda_v)^{1.56}] \tau_y \qquad (B-1a)$$

for $0.58 < \lambda_v < \sqrt{2}$ (elastic-plastic range)

$$\tau_{cr} = [1 - 0.615 (\lambda_v - 0.58)^{1.18}] \tau_y \qquad (B-1b)$$

for $\tau_v > \sqrt{2}$ (elastic range)

$$\tau_{cr} = \frac{1}{\lambda_v^2} \tau_y \qquad (B-1c)$$

where

$$\lambda_v = \frac{b}{t_w} \sqrt{\frac{12(1 - \mu^2) \sigma_{y(w)}}{\sqrt{3} \pi^2 E k_v}} \qquad (B-2)$$

$$\tau_y = \sigma_{y(w)}/\sqrt{3}$$

The plate buckling coefficient, k_v, is computed for the assumed boundary conditions from the following:

$$k_v = \frac{5.34}{\alpha^2} + \frac{6.55}{\alpha} - 13.71 + 14.10 \, \alpha \qquad (B-3a)$$

for $\alpha < 1.0$

or

$$k_v = 8.98 + \frac{6.18}{\alpha^2} - \frac{2.88}{\alpha^3} \qquad (B-3b)$$

for $\alpha \geq 1.0$

WEB BUCKLING STRESS UNDER PURE BENDING

The buckling stress under pure bending, σ_{cr}, is computed from the following equations which are analogous to Eqs. (B-1):

for $\lambda_b \leq 0.58$ (yielding)

$$\sigma_{cr} = \sigma_{y(w)} \qquad (B-4a)$$

for $0.58 < \lambda_b \leq \sqrt{2}$ (elastic-plastic range)

$$\sigma_{cr} = [1 - 0.615 \, (\lambda_b - 0.58)^{1.18}] \, \sigma_{y(w)} \quad (B-4b)$$

for $\lambda_b > \sqrt{2}$ (elastic range)

$$\sigma_{cr} = \frac{1}{\lambda_b^2} \, \sigma_{y(w)} \qquad (B-4c)$$

where,

$$\lambda_b = \frac{b}{t_w} \sqrt{\frac{12(1 - \mu^2) \, \sigma_{y(w)}}{\pi^2 \, E \, k_b}} = 1.314 \, \lambda_v \sqrt{\frac{k_v}{k_b}} \qquad (B-5)$$

By conservatively assuming $\alpha = \infty$, the plate buckling coefficient is obtained from,

$$k_b = 13.54 - 15.64R + 13.32R^2 + 3.38 \, R^3 \qquad (B-6)$$

C. <u>SUMMARY OF ULTIMATE STRENGTH EQUATIONS FOR SYMMETRICAL LOADING</u>

1. <u>Web Failure</u>

$$V_u = V_\tau + V_\sigma + V_f \tag{3.13}$$

a. <u>Beam Action Contribution, V_τ</u>

$$V_\tau{}^2 \left[\frac{1}{(2A_w \tau_{cr})^2} + (\frac{1-R}{2})(\frac{z_o \, y_c}{I_x \, \sigma_{cr}})^2 \right] + V_\tau \left[(\frac{1+R}{2})(\frac{z_o \, y_c}{I_x \, \sigma_{cr}}) \right] - 1.0 = 0 \tag{3.17}$$

b. <u>Tension Field Action Contribution, V_σ</u>

<u>for $\lambda_v \leq 0.58$</u>

$$V_\sigma = 0 \tag{3.18a}$$

<u>for $0.58 < \lambda_v \leq \sqrt{2}$</u>

$$V_\sigma = \frac{0.6 \, \lambda_v - 0.348}{\sqrt{\alpha^2 + 1.6}} \; V_p \tag{3.18b}$$

<u>for $\lambda_v > \sqrt{2}$</u>

$$V_\sigma = \frac{0.9 - 0.787/\lambda_v{}^2}{\sqrt{\alpha^2 + 1.6}} \; V_p \tag{3.18c}$$

c. <u>Frame Action Contribution, V_f</u>

$$V_f = \frac{2}{a} (m_c + M_t) \tag{3.19}$$

2. Flange Failure

    a. Compression Flange Yields before Webs Buckle ($V_u < V_\tau$)

$$V_u = \frac{\sigma_{y(cf)} \, I_x}{(z_o + a/2) \, y_{cf}}$$ (3.20a)

    b. Webs Buckle before Compression Flange Yields ($V_u > V_\tau$)

$$V_u = V_\tau + \frac{\left[\sigma_{y(cf)} - \sigma_{\tau(cf)}\right] A_{cf} \, d'}{(z_o + a/2)}$$ (3.20b)

    c. Tension Flange Yields before Webs Buckle ($V_u < V_\tau$)

$$V_u = \frac{\sigma_{y(tf)} \, I_x}{(z_o + a/2) \, y_{cf}}$$ (3.21a)

    d. Webs Buckle before Tension Flange Yields ($V_u > V_\tau$)

$$V_u = V_\tau + \frac{\left[\sigma_{y(tf)} - \sigma_{\tau \, tf)}\right] A_{tf} \, d'}{(z_o + a/2)}$$ (3.21b)

D. SUMMARY OF ULTIMATE STRENGTH EQUATIONS FOR UNSYMMETRICAL LOADING

1. Web Failure

    a. Phase 1 - Entire Cross Section is Effective

Termination of Phase 1 is due to buckling of the web on the positive side of the cross-section. The corresponding panel shear V_1 is computed from,

$$V_1 \left[(\frac{C_1}{\tau_{cr}})^2 + (\frac{1-R}{2})(\frac{C_2}{\sigma_{cr}})^2 \right] + V_1 \left[(\frac{1+R}{2})(\frac{C_2}{\sigma_{cr}}) \right] - 1.0 = 0$$ (3.24)

b. Phase 2 - Web Buckled on Positive Side of the Cross-Section

Termination of Phase 2 is due to either buckling of the web on the negative side of the cross-section or tension field yielding of the web on the positive side.

1. Buckling of the web on the negative side in terms of the panel shear, V_2 , is given by,

$$V_{2a}^2 \left[(\frac{C_3}{\tau_{cr}})^2 + (\frac{1-R}{2})(\frac{C_4}{\sigma_{cr}})^2 \right] + V_{2a} \left[2V_1(\frac{C_3}{\tau_{cr}})^2 + (\frac{1+R}{2})\frac{C_4}{\sigma_{cr}} + \frac{(1-R)V_1 C_2 C_4}{\sigma_{cr}^2} \right]$$

$$+ \left[(\frac{V_1 C_3}{\tau_{cr}})^2 + (\frac{1+R}{2})\frac{C_2}{\sigma_{cr}} + (\frac{1-R}{2})(\frac{V_1 C_2}{\sigma_{cr}})^2 - 1.0 \right] = 0 \qquad (3.30)$$

2. Yielding of the web on the positive side in terms of the panel shear, V_{2b}, is given by,

$$V_{2b} = \frac{V_\sigma}{C_5} \qquad (3.32b)$$

The smaller of V_{2a} and V_{2b} govern termination of Phase 2.

c. Phase 3a - Both Webs are Buckled

Termination of Phase 3a is due to yielding of the web on the positive side of the cross-section. The corresponding panel shear, V_{3a}, can be calculated from,

$$V_{3a} = \frac{V_\sigma}{C_5} - V_{2a} \qquad (3.33b)$$

d.   Phase 3b - Web on Positive Side has Experienced Tension

Field Yielding

Termination of Phase 3b is due to buckling of the web on the
negative side of the cross-section.   The panel shear, V_{3b}, is
obtained from,

$$V_{3b}^2 \left[\frac{1}{(A_w \tau_{cr})^2} + (\frac{1-R}{2})(\frac{C_4}{\sigma_{cr}})^2 \right] + V_{3b} \left[\frac{2C_7}{A_w \tau_{cr}^2} + (\frac{1+R}{2})(\frac{C_4}{\sigma_{cr}}) + \frac{(1-R)C_4}{\sigma_{cr}^2} \right]$$

$$+ \left[(\frac{C_7}{\tau_{cr}})^2 + (\frac{1+R}{2}) \frac{C_6}{\sigma_{cr}} + (\frac{1-R}{2})(\frac{C_6}{\sigma_{cr}})^2 - 1.0 \right] = 0 \quad (3.38)$$

e.   Phase 4 - Web on Positive Side has Yielded, Web on Negative

Side has Buckled

Termination of Phase 4 is due to yielding of the web on the
negative side of the cross-section.

1.   If Phase 3a preceded Phase 4,

$$V_{4a} = 1/2 \left[V_\sigma - V_{3a} C_8 \right] \quad (3.39)$$

2.   If Phase 3b preceded Phase 4,

$$V_{4b} = V_\sigma/2 \quad (3.40)$$

f.   Phase 5 - Both Webs have Yielded

Termination of Phase 5 causes failure of the panel.   The
panel shear, V_5, is given by,

$$V_5 = \frac{2}{a} (m_c + m_t) \quad (3.41)$$

g. <u>Ultimate Panel Strength under a Web Type Failure</u>

Depending on the formation of the previous phases the ultimate

panel shear strength is given by either,

$$V_u = V_1 + V_{2a} + V_{3a} + V_{4a} + V_5 \qquad (3.42a)$$

or

$$V_u = V_1 + V_{2b} + V_{3b} + V_{4b} + V_5 \qquad (3.42b)$$

2. <u>FAILURE DUE TO YIELDING OF TENSION OR COMPRESSION FLANGE</u>

This possible type of failure must be checked using the

equations which follow.

a. <u>Compression Flange Yielding</u>

1. Phase 1 - 2a - 3a - 4a - 5 mechanism

$$\left| \sigma_{y(cf)} \right| \geq \left| \frac{-V_o (z_o + a/2) y_{cf}}{I_x} - \frac{V_{2a}(z_o + a/2)}{I_x'} - \frac{(z_o + a/2)}{A_{cf} d'} (V_{3a} + V_{4a} + V_5) \right| \qquad (3.43)$$

2. Phase 1 - 2b - 3b - 4b - 5 mechanism

$$\left| \sigma_{y(cf)} \right| \geq \left| \frac{-V_1 (z_o + a/2) y_{cf}}{I_x} - \frac{(z_o + a/2) y_{cf}'}{I_x'}(V_{2b}+V_{3b}) - \frac{(z_o + a/2)}{A_{cf} d'} (V_{4b} + V_5) \right| \qquad (3.44)$$

b. <u>Tension Flange Yielding</u>

1. Phase 1 - 2a - 3a - 4a - 5 mechanism

$$\left[\frac{V_1\,(z_o+a/2)y_{tf}}{I_x} + \frac{V_{2a}\,(z_o+a/2)y'_{tf}}{I_x'} + \frac{(z_o+a/2)}{A_{tf}\,d'}(V_{3a}+V_{4a}+V_5)\right]^2$$

$$\left[+\,3\,\frac{e}{2A_o\,t_{tf}}\,(V_1 + V_{2a} + V_{3a})\right]^2 - \sigma^2_{y(tf)} \leq 0$$

2. Phase 1 - 2b - 3b - 4b - 5 mechanism

$$\left[\frac{V_1\,(z_o+a/2)y_{tf}}{I_x} + \frac{(z_o+a/2)y'_{tf}}{I_x'}(V_{2b} + V_{3b})+ \frac{(z_o+a/2)}{A_{tf}\,d'}(V_{4b}+V_5)\right]^2$$

$$+\,3\left[\frac{e}{2A_o\,t_{tf}}\,(V_1 + V_{2b})\right]^2 - \sigma^2_{y(tf)} \leq 0$$

E. <u>SAMPLE COMPUTATION OF ULTIMATE STRENGTH FOR SYMMETRICAL LOADING</u>

Computations are given below for the ultimate strength evaluation of specimen M2 based on failure of panel 4.

1. Loading condition
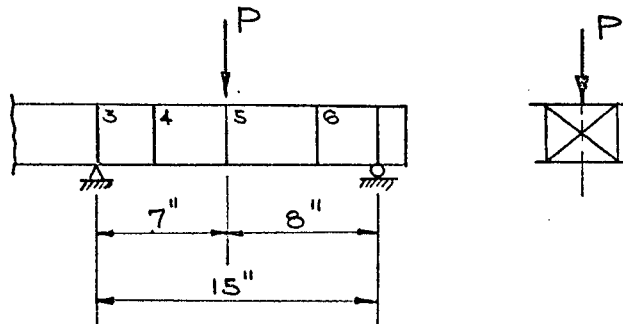
2. Cross-Sectional Properties

$$I_x = 1.095 \text{ in.}^4 \qquad\qquad y_{tf} = 2.1951 \text{ in.}$$

$$A_w = 0.0435 \text{ in.}^2 \qquad\qquad y_{cf} = 0.8584 \text{ in.}$$

$$y_t = 2.1804 \text{ in.} \qquad\qquad t_w = 0.0145 \text{ in.}$$

$$y_c = 0.8197 \text{ in.} \qquad\qquad t_{cf} = 0.0775 \text{ in.}$$

$$A_o = 12.21 \text{ in.}^2 \qquad\qquad t_{tf} = 0.0294 \text{ in.}$$

$$A_{tf} = 0.1396 \text{ in.}^2 \qquad\qquad d' = 3.0535 \text{ in.}$$

3. Material Properties

$$\sigma_{y(w)} = 30,500 \text{ psi} \qquad\qquad E = 29,600 \text{ ksi}$$

$$\sigma_{y(cf)} = 32,520 \text{ psi} \qquad\qquad \mu = 0.3$$

$$\sigma_{y(tf)} = 31,340 \text{ psi}$$

4. Web Panel Characteristics (Panel 4)

$$a = 4.0 \text{ in.} \qquad \alpha = 1.33 \qquad z_o = 5.0 \text{ in.}$$

$$b_w = 3.0 \text{ in.} \qquad \beta = 206$$

A. ULTIMATE STRENGTH BASED ON WEB FAILURE

1. Beam Action Contribution, V_T

Using Eq. (B-3b) compute the shear buckling coefficient, k_v.

$$k_v = 8.98 + \frac{6.18}{1.77} - \frac{2.88}{3.35} = 11.25$$

Then the buckling parameter λ_v is from Eq. (B-2)

$$\lambda_v = \beta \sqrt{\frac{12(1 - \mu^2)}{\sqrt{3} \, \pi^2 \, E} \frac{\sigma_{y(w)}}{k_v}} = 206 \sqrt{\frac{10.92}{506 \times 10^3} \cdot \frac{30.5}{11.25}} = 1.577$$

For $\lambda_v > \sqrt{2}$, the buckling stress under pure shear, τ_{cr}, is given by Eq. (B-1C).

$$\tau_{cr} = \frac{1}{\lambda_v^2} \tau_y = \frac{30,500}{1.732 \, (1.577)^2} = 7100 \text{ psi}$$

It is next necessary to calculate the buckling stress, σ_{cr}, for pure bending. First evaluate the buckling coefficient, k_b, from Eq. (B-6)

$$k_b = 13.54 - 15.64R + 13.32R^2 + 3.38R^3$$

Now $R = -y_t/y_c = -2.1804/0.8197 = -2.659$ which is less than -1.5 therefore use $R = -1.5$.

Therefore,

$$k_b = 13.54 - 15.64(-1.5) + (13.32)(2.25)$$
$$+ 3.38 \, (-3.375) = 55.62$$

From Eq. (B-5)

$$\lambda_b = 1.314 \, \lambda_v \sqrt{k_v/k_b} = 1.314 \, (1.577) \sqrt{\frac{11.25}{55.62}} = 0.930$$

With $0.58 < \lambda_b < \sqrt{2}$, σ_{cr} is calculated from Eq. (B-4b).

$$\sigma_{cr} = [1 - 0.615 \, (\lambda_b - 0.58)^{1.18}] \, \sigma_{y(w)}$$
$$= [1 - 0.615(0.930 - 0.58)^{1.18}](30,500) = 25,100 \text{ psi}$$

Summarizing then,

$$\tau_{cr} = 7100 \text{ psi and } \sigma_{cr} = 25,100 \text{ psi}$$

Next substitute all known terms into Eq. (3.17) to obtain the beam action contribution, V_τ.

$$\frac{1}{2A_w \tau_{cr}} = \frac{1}{0.087 (7.1)} = 1.619$$

$$\frac{z_o y_c}{I_x \sigma_{cr}} = \frac{5.0 (.8197)}{1.095(25.1)} = 0.149$$

$$V_\tau^2 [(1.619)^2 + 1.25(0.149)^2] + V_\tau [-0.25(0.149)] - 1.0 = 0$$

This yields the following,

$$V_\tau^2 - 0.0140 V - 0.378 = 0$$

Solving this results in,

$$\boxed{V_\tau = 621.5 \text{ lbs.}}$$

2. **Tension Field Action Contribution, V_σ**

For $\lambda_v > \sqrt{2}$, Eq. (3.18c) defines the tension field action contribution, V_σ.

$$V_\sigma = \frac{0.9 - 0.787/\lambda_v^2}{\sqrt{\alpha^2 + 1.6}} V_P$$

$$V_p = \frac{2A_w \sigma_{y(w)}}{\sqrt{3}} = \frac{0.087 (30,500)}{1.732} = 1534 \text{ lbs.}$$

Then,

$$V_\sigma = \frac{0.9 - 0.317}{\sqrt{1.77 + 1.6}} (1534) = 487 \text{ lbs.}$$

$$\boxed{V_\sigma = 487 \text{ lbs.}}$$

3. **Frame Action Contribution, V_f**

Using Eq. (3.19),

$$V_f = \frac{2}{a}(m_c + m_t) = \frac{2}{4}\left[\frac{(5.5)(0.0775)^2(32,520)}{4}\right.$$

$$\left. + \frac{(4.75)(0.0294)^2(31,340)}{4}\right] = 150 \text{ lbs.}$$

$$\boxed{V_f = 150 \text{ lbs.}}$$

Then the ultimate strength based on web failure of panel 4 is,

$$V_u = 621.5 + 487 + 150 = 1258 \text{ lbs.}$$

$$\boxed{V_u = 1258 \text{ lbs.}} \qquad \text{Based on Web Failure}$$

It is also necessary to check yielding of the flanges.

B. **ULTIMATE STRENGTH BASED ON FLANGE YIELDING**

Only the tension flange is checked because it is the more critical. Yielding is checked at the maximum moment end of panel 4 using Eqs. (3.21). From Eq. (3.21a),

$$V_u = \frac{\sigma_{y(tf)} I_x}{(z_o + a/2) y_{tf}} = \frac{31,340 \ (1.095)}{7.0 \ (2.1951)} = 2230 \text{ lbs.}$$

This indicates that the web buckles before the tension flange yields because $V_u > V_\sigma$, therefore Eq. (3.21b) must be used. Using Eq. (3.21c) first,

$$\sigma_{T(tf)} = \frac{V_T \ (z_o + a/2) y_{tf}}{I_x} = \frac{621.5(7.0)(2.1951)}{1.095} = 8720 \text{ psi}$$

Then substituting into Eq. (3.21b),

$$V_u = 621.5 + \frac{(31,340 - 8720)(0.1396)(3.0535)}{7}$$

$$= 621.5 + 1378 = 2000 \text{ lbs.}$$

$$\boxed{V_u = 2000 \text{ lbs.}}$$

Based on Tension
Flange Yielding

Comparing the ultimate strength values computed based on web failure and tension flange yielding, it is obvious that the former controls. Relating the panel shear to the load, P, produces the following:

$$P_u = \frac{15}{8} V_u = \frac{15}{8} (1258) = 2359 \text{ lbs.}$$

Similar computations are made for the other panels. The minimum value for P_u defines the ultimate strength of the member.

F. SAMPLE COMPUTATION OF ULTIMATE STRENGTH FOR UNSYMMETRICAL LOADING

Computations are given below for the ultimate strength evaluation of Specimen M2 based on failure of panel 2.

GIVEN:

1. Loading Condition
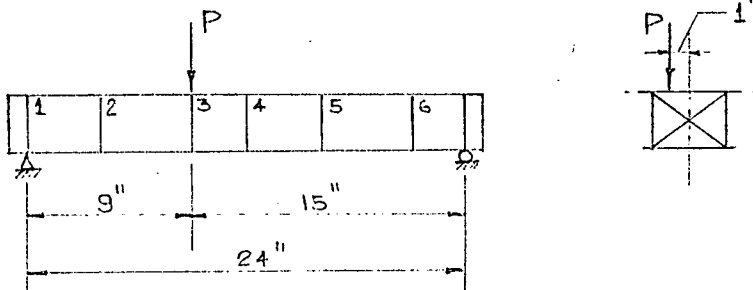
2. Cross-Section Properties (as given in Appendix E)

3. Material Properties (as given in Appendix E)

4. Web Panel Characteristics (Panel 2)

$a = 5.0$ in. $\alpha = 1.67$ $z_o = 6.5$ in.

$b_w = 3.0$ in. $\beta = 206$

A. Ultimate Strength based on Web Failure

a. Phase 1

Having previously calculated τ_{cr} and σ_{cr} from expressions given in Appendix B, compute V_1 from equation (3.24)

$$C_1 = \frac{1}{2A_w} + \frac{e}{2A_c t_w} = \frac{1}{0.0870} + \frac{1}{0.354} = 14.32$$

$$C_2 = \frac{z_o y_c}{I_x} = \frac{6.5 (0.8197)}{1.095} = 4.86$$

$$R = -\frac{y_t}{y_c} = -\frac{2.1804}{0.8197} = -2.66, \text{ therefore use } R = -1.5$$

Substituting into Eq. (3.24) results in,

$$V_1^2 \left[(\frac{14.32}{6.686})^2 + 1.25 \; (\frac{4.86}{25.1})^2 \right] + V_1 \left[-0.25 \; (\frac{4.86}{25.1}) \right] - 1.0 = 0$$

Solving for V_1 yields,

$$V_1 = \frac{+ \; 0.0104 \pm \sqrt{.0001 + .8628}}{2}$$

$$V_1 = 0.470$$

Therefore,

$$\boxed{V_1 = 470 \text{ lbs.}}$$

b. Phase 2

First compute from Eq. 3.30 the panel shear which causes
buckling of the web on the north side of the cross-section.
In order to make use of this equation the new cross-sectional
properties had to be determined for the effective cross-
section consisting of two flanges and the remaining unbuckled
web. These were calculated to be,

$$I_x' = 1.038 \text{ in.}^4, \qquad y_c' = 0.7710 \text{ in.}, \qquad y_t' = 2.2290 \text{ in.}$$

$$y_{cf}' = 0.8097 \text{ in.}, \qquad y_{tf}' = 2.2437 \text{ in.}$$

$$C_3 = \frac{1}{2A_w} - \frac{e}{2A_o\,t_w} = 11.494 - 2.825 = 8.669$$

$$C_4 = \frac{z_o\,y_c'}{I_x'} = \frac{0.7710\ (6.5)}{1.038} = 4.828$$

Substituting into equation (3.30) results in,

$$V_{2a}^2 \left\{ \left(\frac{8.669}{6.686}\right)^2 + 1.25\left(\frac{4.828}{25.1}\right)^2 \right\} + V_{2a} \left\{ 2(0.470)\left(\frac{8.669}{6.686}\right)^2 \right.$$

$$\left. - 0.25\left(\frac{4.828}{25.1}\right) + \frac{2.5(0.470)(4.86)(4.828)}{(25.1)^2} \right\}$$

$$+ \left\{ \left[\frac{(0.470)(8.669)}{6.686}\right]^2 - \frac{0.25(4.86)}{25.1} \right.$$

$$\left. + 1.25\left[\frac{(0.470)(4.86)}{25.1}\right]^2 - 1.0 \right\} = 0$$

Solving for V_{2a} yields,

$$V_{2a} = \frac{-\ 0.912 \pm \sqrt{0.832 + 1.544}}{2}$$

$$V_{2a} = 0.3145$$

Therefore,

$$\boxed{V_{2a} = 314.5\ \text{lbs.}}$$

Now compute from Eq. (3.32b) the panel shear, V_{2b}.

$$V_{2b} = V_o/C_5$$

From expressions given in Appendix B, V_σ was computed to be,

$$V_\sigma = 440.8 \text{ lbs.}$$

$$C_5 = 1 + \frac{eb}{A_o} = 1 + \frac{3}{12.21} = 1.245$$

Then,

$$V_{2b} = \frac{440.8}{1.245} = 360$$

$$\boxed{V_{2b} = 360 \text{ lbs.}}$$

From the above results it has been found that V_{2a} is less than V_{2b} and therefore governs the termination of Phase 2, which is caused by buckling of the web on the negative side.

c. Phase 3a

Evaluation of the panel shear V_{3a} is obtained using equation (3.33b).

$$V_{3a} = \frac{V_\sigma}{C_5} - V_{2a} = \frac{440.8}{1.245} - 314.5$$

$$\boxed{V_{3a} = 45.5 \text{ lb.}}$$

The end of Phase 3a was due to yielding of the web on the positive side of the cross-section. In accordance with the analytical method, the torsional stiffness of the shear span to the left of the concentrated load has thus been decreased appreciably. The full amount of any additional torsion is thus carried by the other shear span. This must be taken into account when checking panel failures on the right side of the loading point.

d. Phase 4

Evaluation of the panel shear V_4 causing termination of Phase 4 can be obtained from Eq. (3.39).

$$V_{4a} = 1/2 \left[V_\sigma - V_{3a} \, c_8 \right]$$

$$c_8 = 1 - \frac{eb}{A_o} = 1 - 0.245 = 0.755$$

Then,

$$V_{4a} = 1/2 \left[440.8 - 34.3 \right] = 183.0$$

$$\boxed{V_{4a} = 183.0 \text{ lbs.}}$$

e. Phase 5

Using equation (3.41) the frame action contribution of the flanges can be evaluated.

$$V_5 = \frac{2}{a}(m_c + m_t) = \frac{2}{5}\left[\frac{b_{cf}\,t_{cf}^2}{4}\sigma_{y(cf)} + \frac{b_{tf}\,t_{tf}^2}{4}\sigma_{y(tf)}\right]$$

$$= 1/10\,[(5.5)(0.0775)^2(32.52) + (4.75)(0.0294)^2(31.34)]$$

$$V_5 = 1/10\,(1.201)$$

$$\boxed{V_5 = 120.1 \text{ lbs.}}$$

Then the ultimate strength of panel 2 based on web failure

is,

$$V_u = V_1 + V_{2a} + V_{3a} + V_{4a} + V_5$$

$$= 470.0 + 314.5 + 45.5 + 183 + 120$$

$$\boxed{V_u = 1133 \text{ lbs.}}$$

It is also necessary to check yielding of the flanges.

B. <u>Failure Due to Yielding of Tension or Compression Flange</u>

Only the tension flange is checked because it is obviously the more critical. Yielding is checked at the maximum moment end of panel 2 using Eqs. (3.47), (3.48) and (3.49). From equation (3.48),

$$\sigma_z = \sigma_{tf} = \frac{470(9.0)(2.1951)}{1.095} + \frac{314.5(9.0)(2.2437)}{1.038}$$

$$+ \frac{9.0}{(0.1396)(3.0534)}\,[45.5 + 183 + 120] = 8480 + 6120 + 7360$$

$$\sigma_z = 21,960 \text{ psi}$$

Making use of Eq. (3.49) yields the following,

$$\tau_{xz} = \frac{1}{24.42\ (0.0294)}\ [470.0 + 314.5 + 45.5]$$

$$\tau_{xz} = 1160\ psi$$

Substituting into equation (3.47) the computed values for σ_z and τ_{xz} and the tension flange yield stress, $\sigma_{y(tf)}$, results in the following:

$$(21.96)^2 + 3\ (1.16)^2 - (31.34)^2 \leq 0$$

$$482.2 + 4.0 - 982.1 < 0$$

The above inequality indicates that yielding of the tension flange does not occur under the loads which produced web failure in panel 2. Hence web failure controls the strength of panel 2 which was calculated to be,

$$\boxed{V_u = 1133\ lbs.}$$

By relating the panel shear to the applied load, P, the ultimate strength of the member based on failure of panel 2 can be determined.

$$P_u = 24/15\ V_u = 24/15\ (1133)$$

$$\boxed{P_u = 1813\ lbs.}$$

Similar computations are made for the other panels. The
minimum value for P_u defines the ultimate strength of the member.

7. NOMENCLATURE

A   area of cross section

A_{cf} effective area of compression flange

A_{tf} effective area of tension flange

A_o area enclosed by middle lines of the wall plates

A_w area of each web plate

C_1 $(\dfrac{1}{2A_w} + \dfrac{e}{2A_o t_w})$

C_2 $(z_o y_c / I_x)$

C_3 $(\dfrac{1}{2A_w} - \dfrac{e}{2A_o t_w})$

C_4 $(z_o y_c{}' / I_x')$

C_5 $(1 + eb/A_o)$

C_6 $V_1 C_2 + V_{2b} C_4$

C_7 $C_3 (V_1 + V_{2b})$

C_8 $(1 - eb/A_o)$

E   Young's modulus

G   shear modulus

I_x moment of inertia of original cross section

I_x' moment of inertia of reduced cross section

I_ω warping moment of inertia

K_T	torsion constant
L	span length of a box girder
M_B	bending moment
M_T	twisting moment
M_{SV}	twisting moment resulting from pure torsion
M_W	twisting moment resulting from warping torsion
P	load
P_{max}	maximum load (experimental)
P_u^{exp}	static load-carrying capacity (experimental)
P_u	ultimate load (theoretical)
Q	statical area moment
R	ratio of $-y_t, (y_t')$ to $y_c(y_c')$
$\bar{S}_\omega$	statical warping moment
V	shear force on a box girder panel
V_τ	beam action contribution to ultimate panel shear force
V_σ	tension field action contribution to ultimate panel shear force
V_f	frame action contribution to ultimate panel shear force
V_u	ultimate panel shear force
a	length of a web panel
b	depth or width of a web panel
d'	distance between centroids of flanges
e	eccentricity of load w.r.t. the vertical, centroidal axis
q	shear flow

q_b	shear flow due to flexure
q_{sv}	shear flow due to St. Venant torsion
s	coordinate measured along middle line of the cross section
$t(s)$	varying thickness of a wall plate
t_{cf}	thickness of compression flange
t_{tf}	thickness of tension flange
t_w	thickness of web
x	coordinate measured in the direction of the horizontal centroidal axis
x_{sc}	distance from shear center of original closed section to shear center of effective open section
y	coordinate measured in the direction of the vertical centroidal axis
y_c, y_c'	distance from N.A. to extreme compression fiber of the web
y_t, y_t'	distance from N.A. to extreme tension fiber of the web
y_{cf}, y_{cf}'	distance from N.A. to centroid of compression flange
y_{tf}, y_{tf}'	distance from N.A. to centroid of tension flange
z	coordinate measured from end support in the direction of the member's longitudinal axis
z_o	distance from end support to mid-length of a panel

α	aspect ratio of web plate (a/b_w)
β	slenderness ratio of web plate (b_w/t_w)
λ_b	non-dimensional buckling parameter for bending
λ_v	non-dimensional buckling parameter for shear
μ	Poisson's ratio

σ_B normal stress due to bending

σ_c web buckling stress at extreme compression fiber under combined shear and bending

σ_{cr} web buckling stress under pure bending

σ_w normal stress due to warping rorsion

$\sigma_{y(cf)}$ yield stress of compression flange

$\sigma_{y(tf)}$ yield stress of tension flange

$\sigma_{y(w)}$ yield stress of web

σ_z normal stress in direction of z-axis

τ_B shear stress due to bending

τ_c shear buckling stress of web under combined shear and bending

τ_{cr} buckling stress of web under pure shear

τ_{sv} shear stress due to St. Venant torsion

τ_w shear stress due to warping torsion

τ_y yield stress in shear

ϕ angle of twist

ω_n unit normalized warping

TABLE 1   PLATE DIMENSIONS AND PROPERTIES

Specimens M1 & M2	Width (inches)	Thickness (inches)	Static Yield Stress[2] (ksi)	Ultimate Stress (ksi)	Elongation in 2 inches (%)
Top Flange	7 (5-1/2)[1]	5/64	32.52	47.38	38.2
Webs	3	1/64	30.40	43.36	30.5
Bottom Flange	4-3/4	1/32	31.34	45.59	44.8

[1] 7" for M1; 5-1/2" for M2

[2] Yield stress corresponding to zero strain rate

TABLE 2   GEOMETRIC PROPERTIES

Specimen No.	b_w/t_w	a/b_w	Cross Sectional Properties			
			A (in.^{2})	I_x (in.^{4})	K_T (in.^{4})	I_ω (in.^{6})
M1	192	1.0 - 1.67	0.769	1.168	0.980	0.577
M2	192	1.0 - 1.67	0.653	1.095	0.980	0.512

TABLE 3   THEORETICAL PANEL STRENGTH (M2 - SYM. LOAD)

Panel	Beam Action Contribution V_τ (lbs)	Tension Field Contribution V_σ (lbs)	Frame Action Contribution V_f (lbs)	Ultimate Panel Strength V_u (lbs)	Ultimate Member Strength P_u (lbs)
4	621	487	150	1258	2360
5	574	436	120	1130	2420

TABLE 4   COMPARISON OF EXPERIMENTAL AND THEORETICAL RESULTS

Test Specimen	Observed Failure Mode	Predicted Failure Mode	Measured Strength P_u^{exp} (lbs)	Computed Strength P_u (lbs)	$\dfrac{P_u - P_u^{exp}}{P_u}$ (%)
M1 (Unsym. Load)	Web Failure on S.S. of Panels 1 & 6	Web Failure of Panel 1	1800[1]	2340 (1700)[2]	23.1 -(5.9)
M2 (Sym. Load)	Web Failure of Panels 4 & 5	Web Failure of Panel 4	2650[3] (2350)[4]	2360	-12.3 (0.4)
M2 (Unsym. Load)	Web Failure of Panel 2	Web Failure of Panel 2	1930[3] (1800)[4]	1810	-6.6 (0.5)

[1] Not the true load-carrying capacity due to premature failure of x-bracing

[2] Approximate strength assuming only one-half of the cross-section is effective after the x-bracing fails

[3] Upper bound

[4] Lower bound
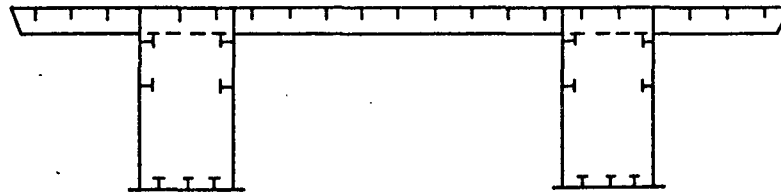
TWIN BOX GIRDERS WITH AN ORTHOTROPIC
STEEL DECK
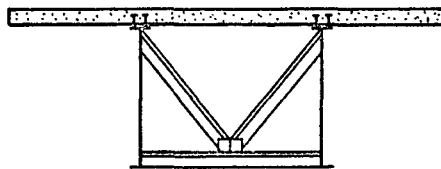
COMPOSITE BOX GIRDER

MULTICELL BOX GIRDER

Fig. 1.1   Cross-Sectional Configurations
for Box Girder Bridges
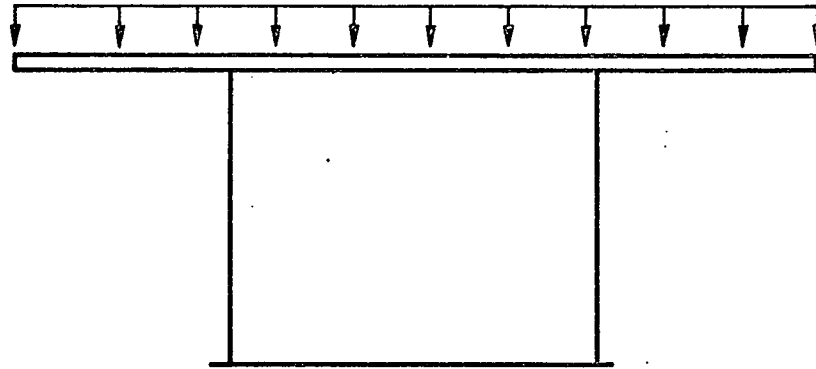
(a) Dead Load
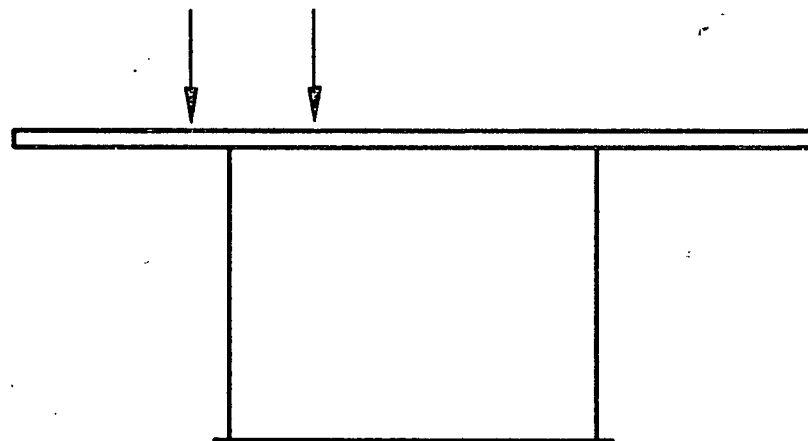
(b) Live Load

Fig. 1.2   Major Classes of Loading
for Box Girder Bridges
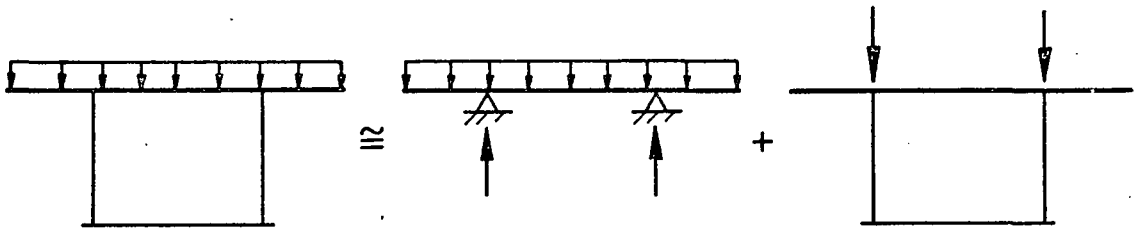
DECOMPOSITION OF DEAD LOAD
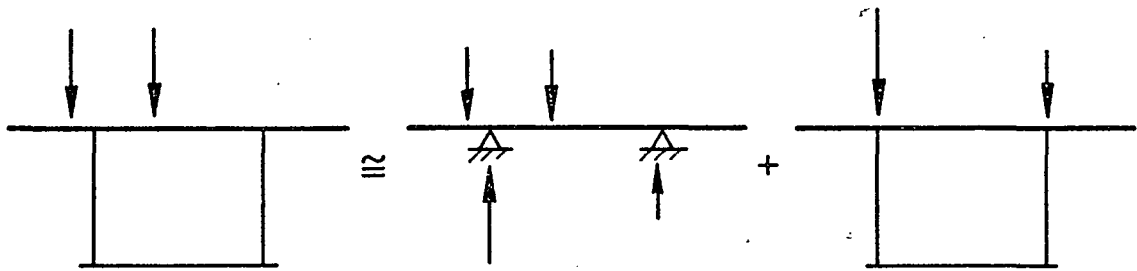
DECOMPOSITION OF LIVE LOAD

Fig. 1.3   Decomposition of Major Classes of Loading

Fig. 2.1   Dimensions and Geometry of Specimen M1

Note: X = Location of X - Bracing
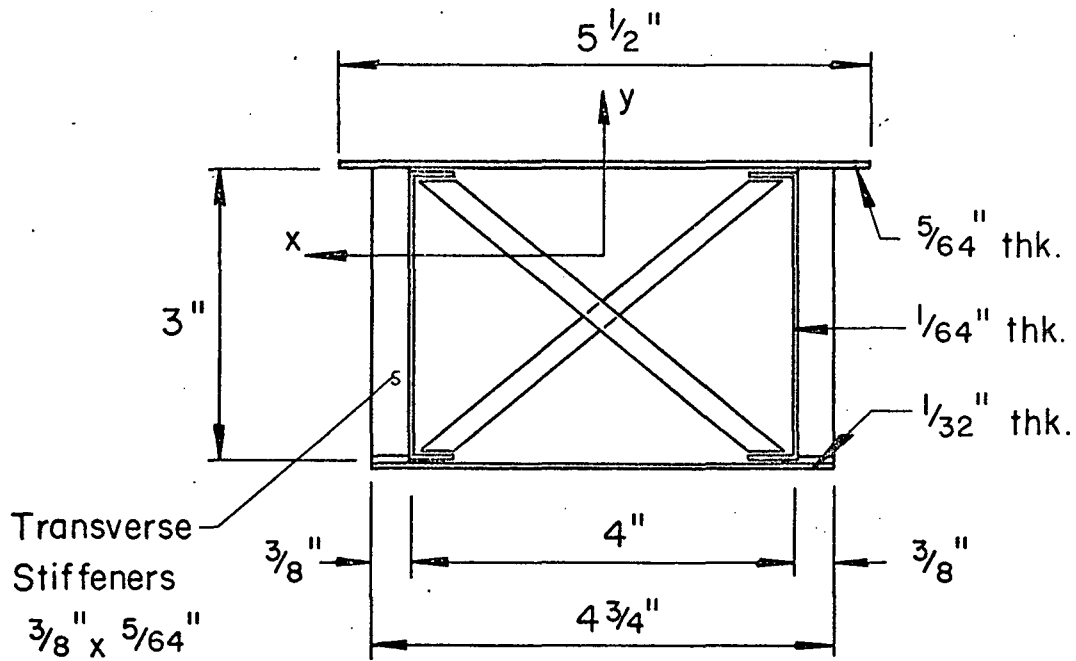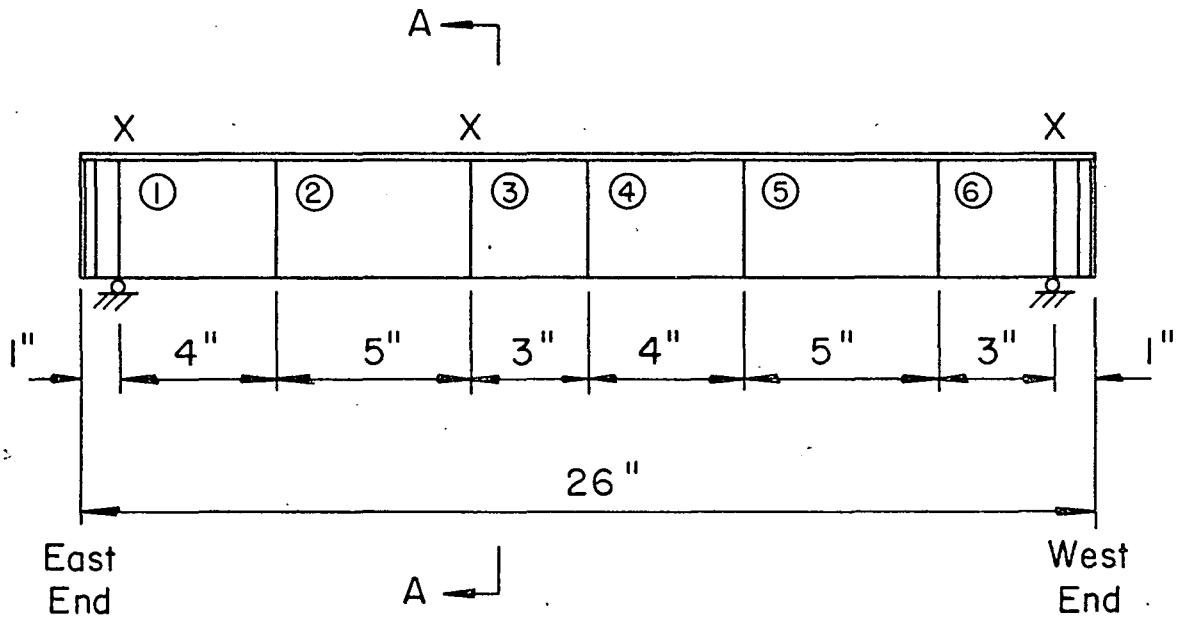
Fig. 2.2   Dimensions and Geometry of Specimen M2

I" x 3/16"

Joint
Material

I" x 1/64"

3/8"
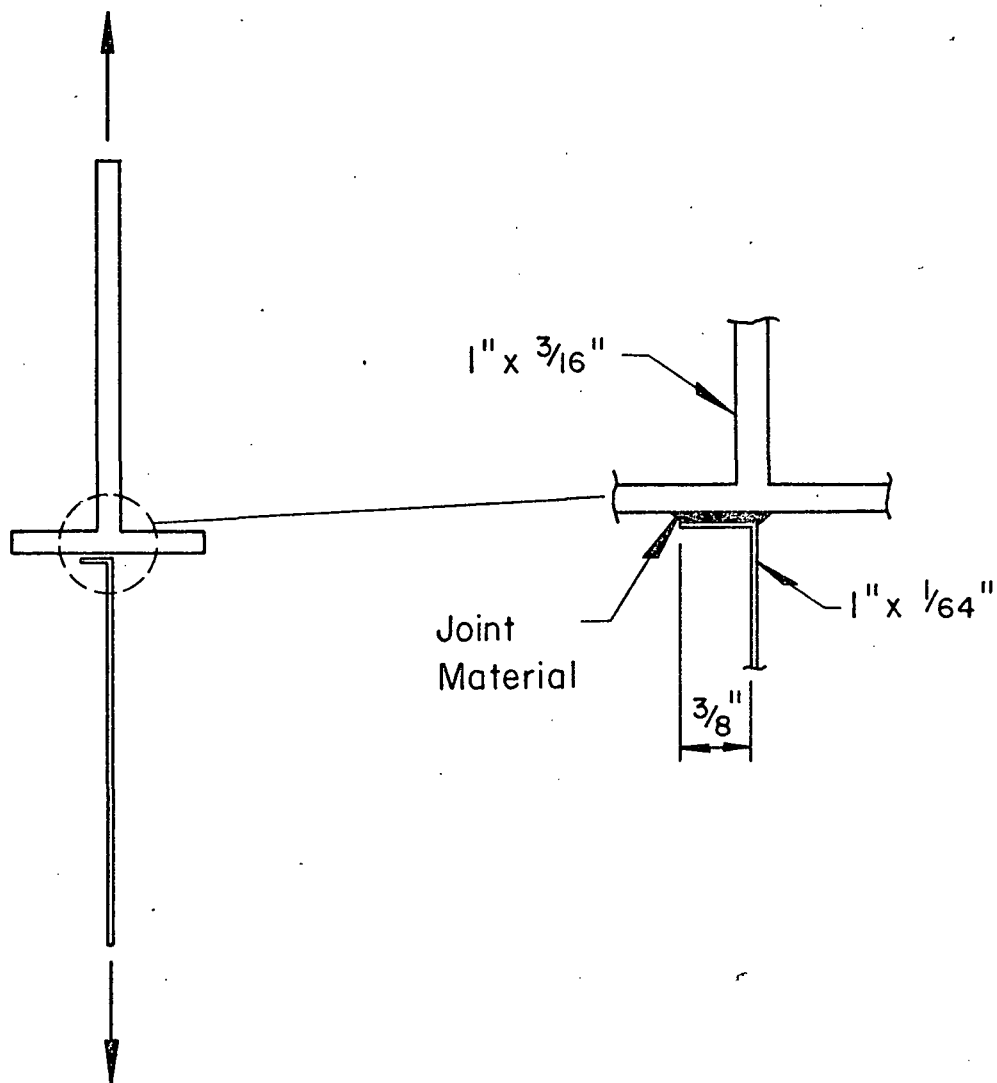
TEST RESULTS

Type Joint	Max. Load (lbs)	Location of Fracture
Silver Solder	657;753	1/64" thk. Material
Brazed	716;752	1/64" thk. Material
50-50 Solder	570;555	Joint
Epoxy "A"	151;215	Joint
Epoxy "B"	110;125	Joint

Fig. 2.3   Test Joint Configuration and Results

9" (Sym. Abt. ℄)

℄

MIDSPAN DIAL GAGES

9" (Sym. Abt. ℄)

℄

END SUPPORT DIAL GAGES
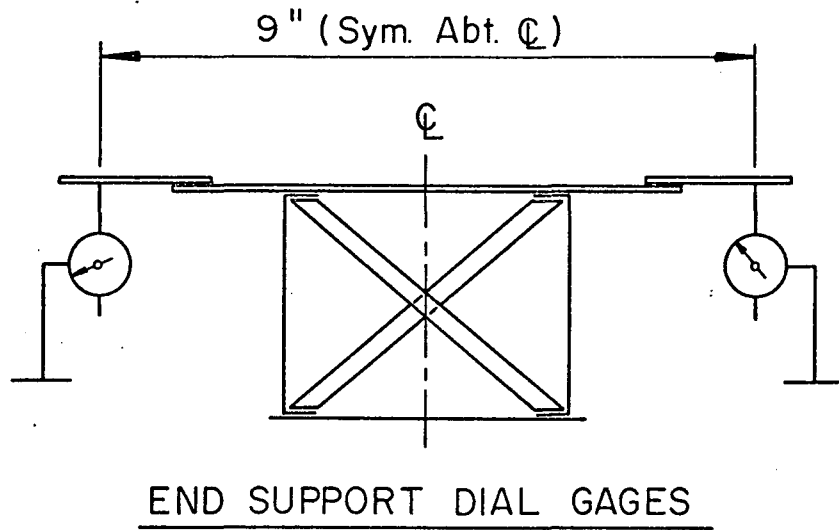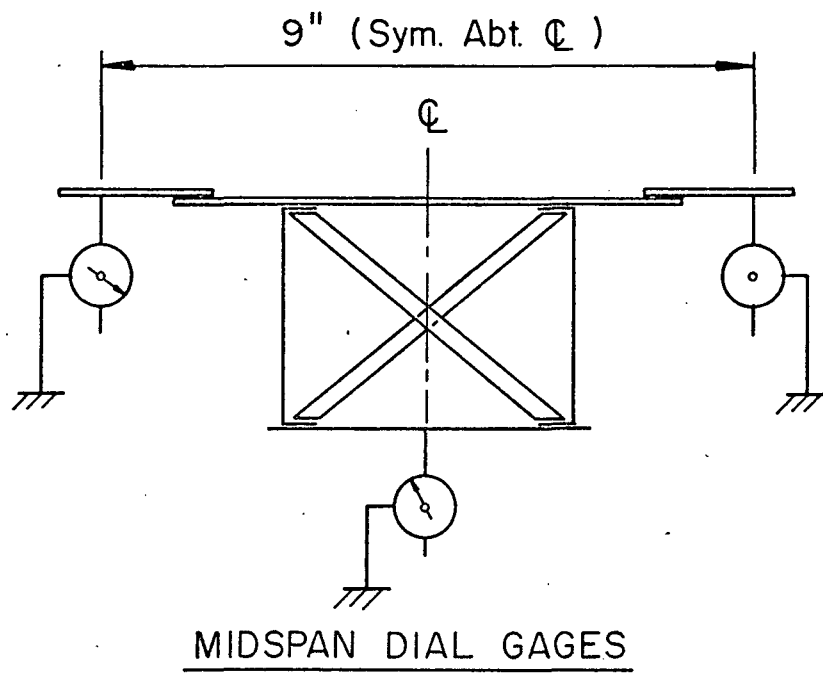
Fig. 2.4   Dial Gage Arrangement - Specimen M1

7" (Sym. Abt. ℭ)

MIDSPAN DIAL GAGES

7" (Unsym. Load Test)

9" (Sym. Load Test)

END SUPPORT DIAL GAGES
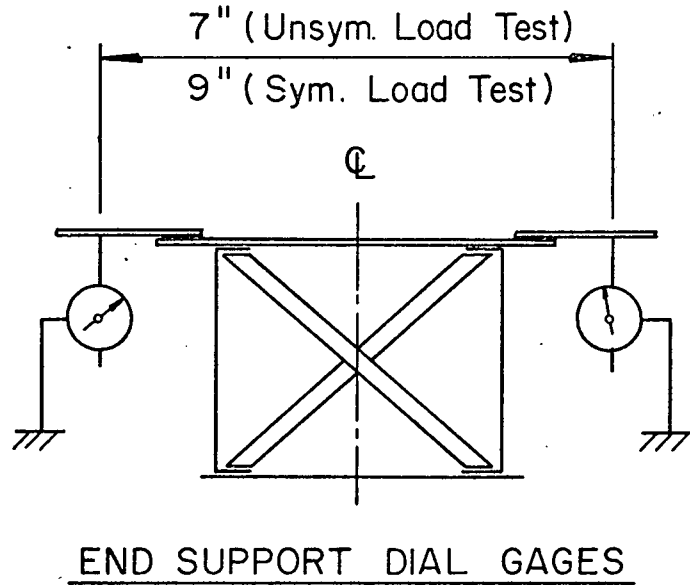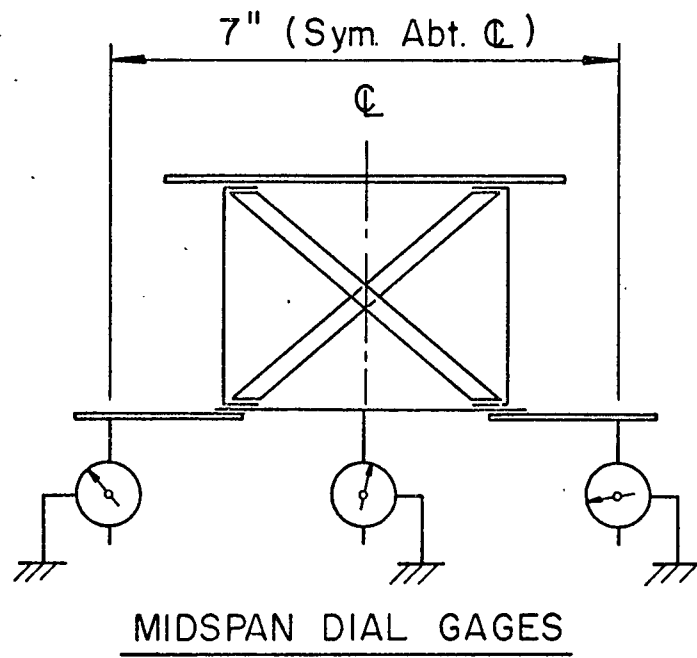
Fig. 2.5   Dial Gage Arrangement - Specimen M2
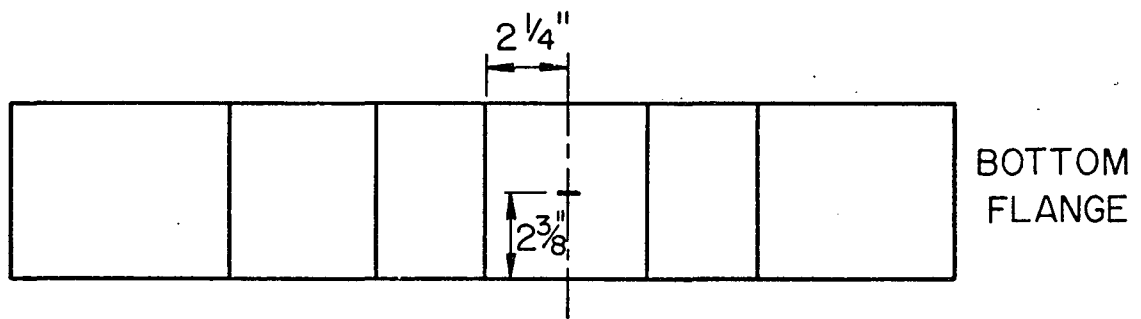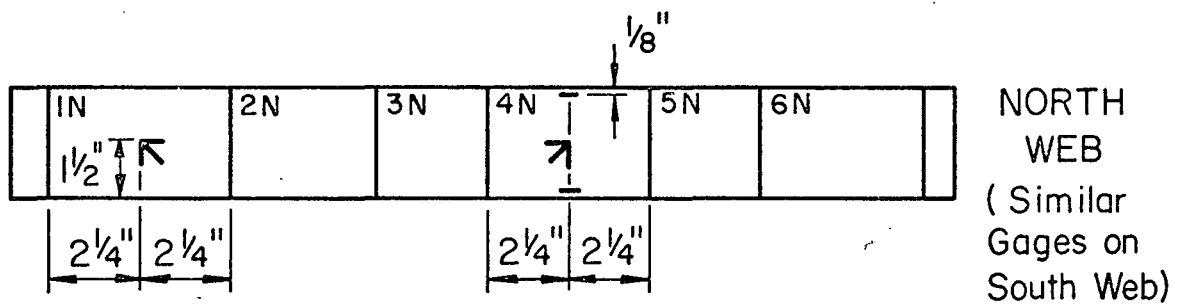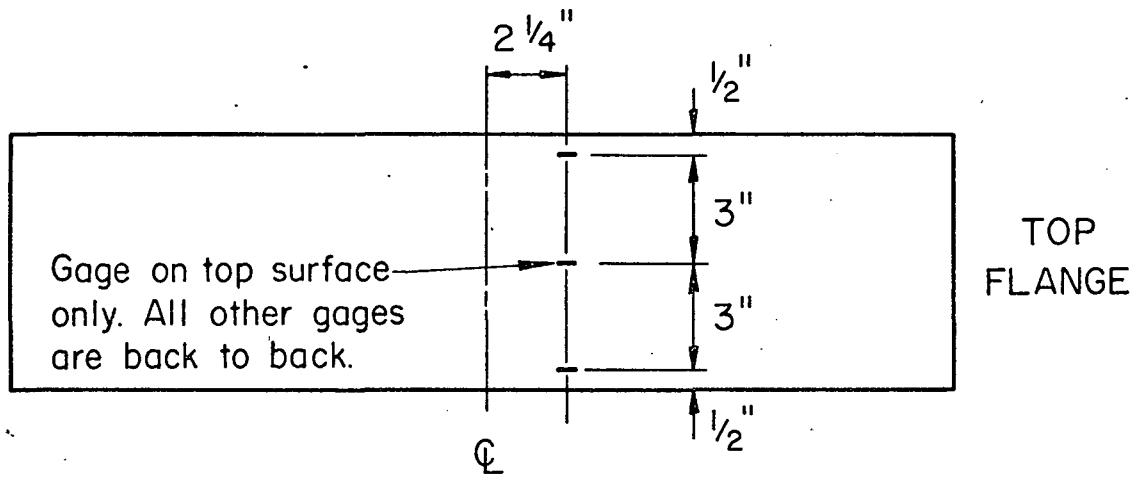
Fig. 2.6   Strain Gage Layout - Specimen M1
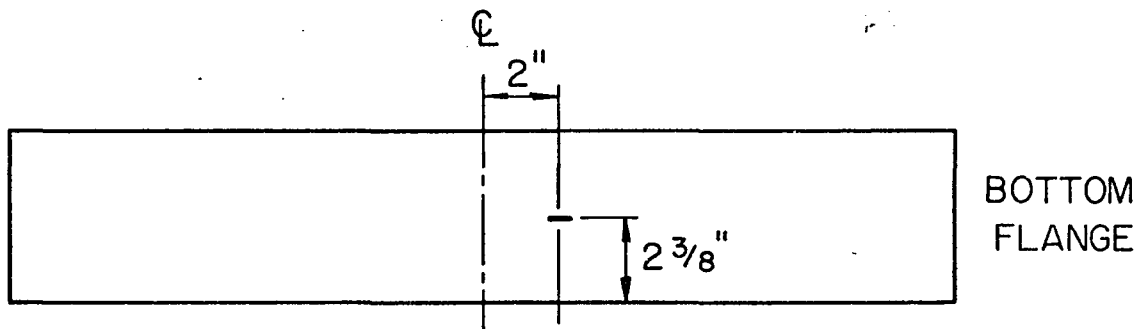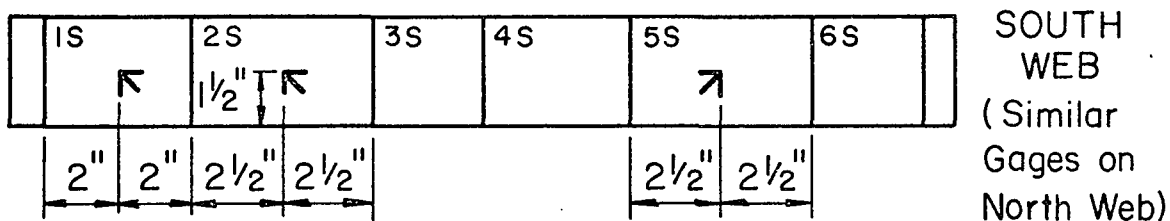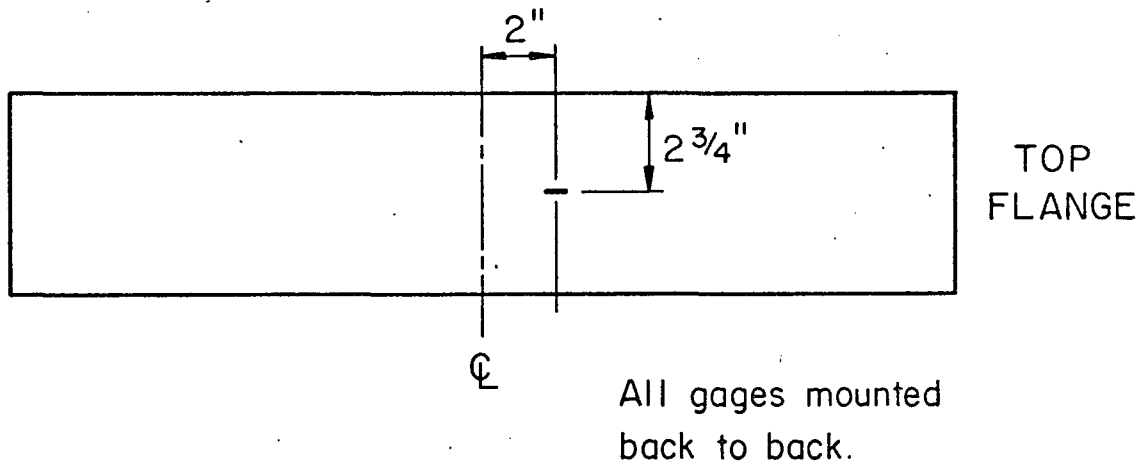
Fig. 2.7   Strain Gage Layout - Specimen M2

All measurements made with a Huggenberger
extensometer to the nearest 0.001 mm.

UNLOADED WEB PANEL

Steel Ball Epoxied
to Web Surface

V

L_f

V

LOADED WEB PANEL

$$\text{Diagonal Strain} = \frac{L_f - L_i}{L_i}$$
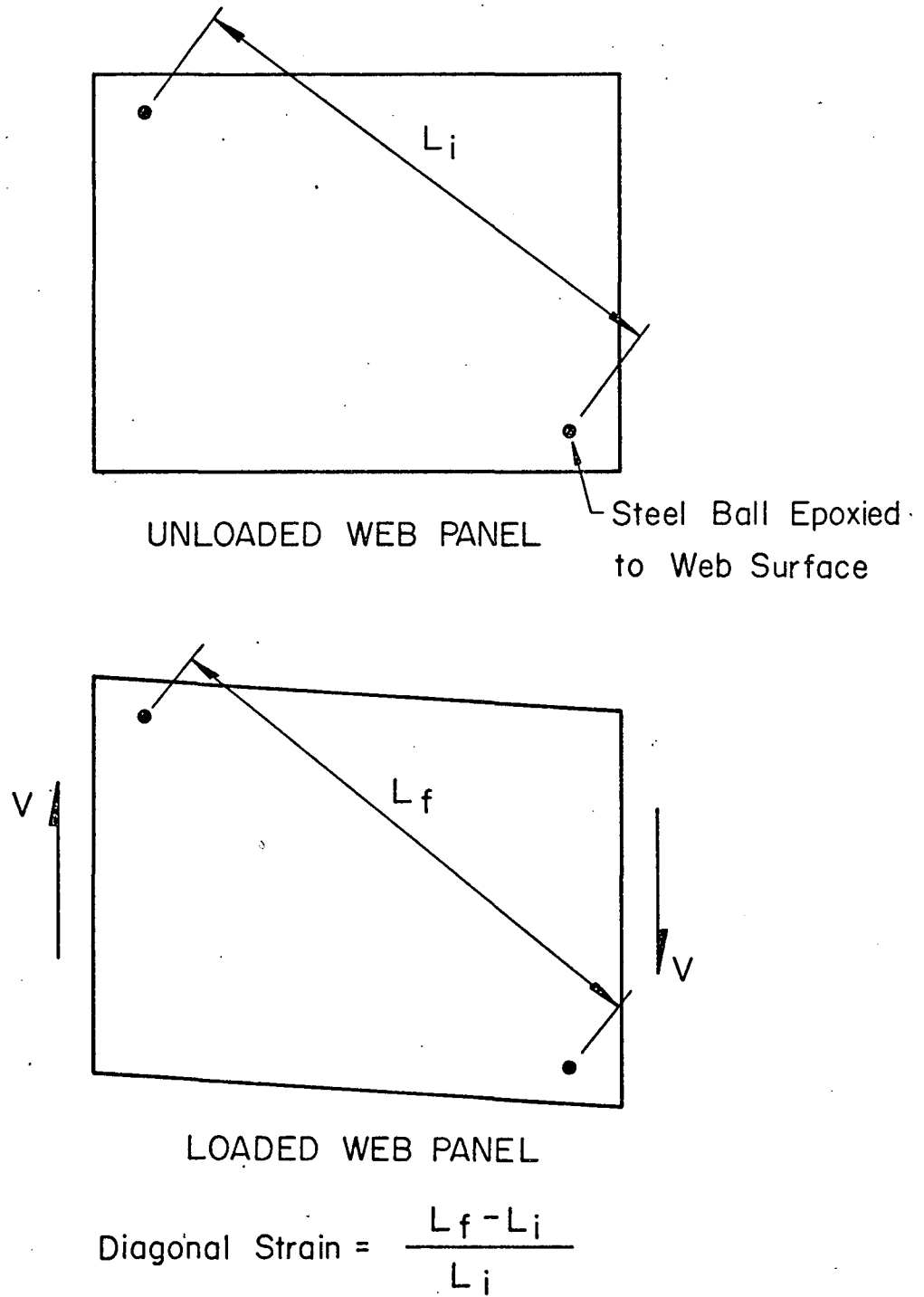
Fig. 2.8   Mechanical Measurement of Web Diagonal Strains
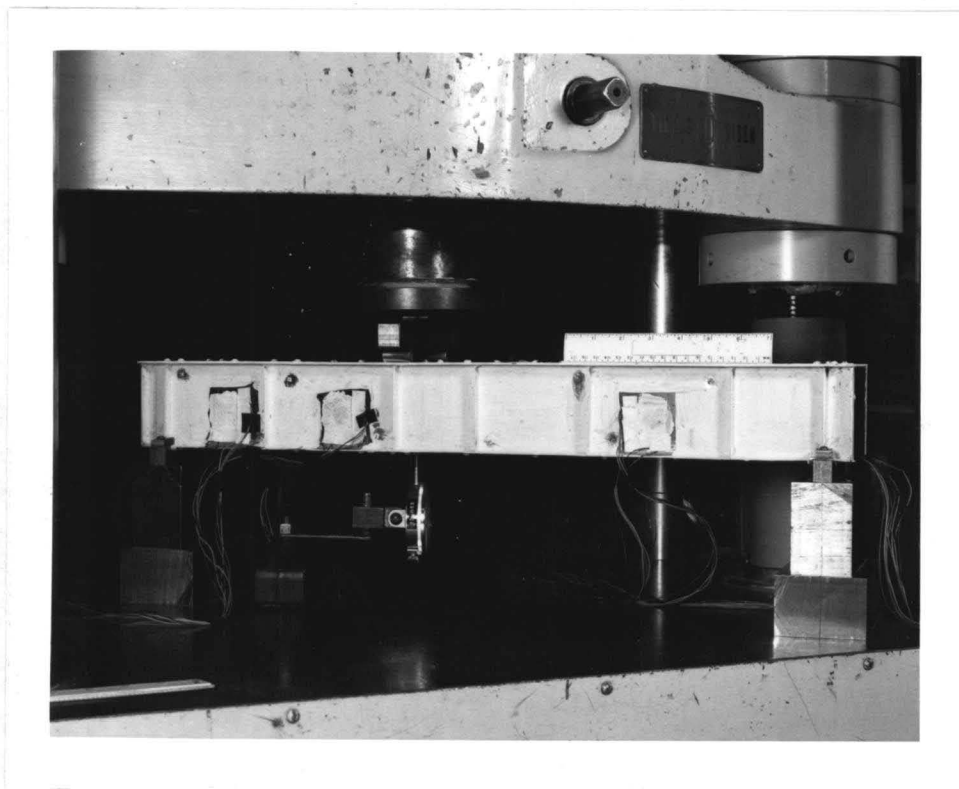
Fig. 2.9   TYPICAL TEST SETUP
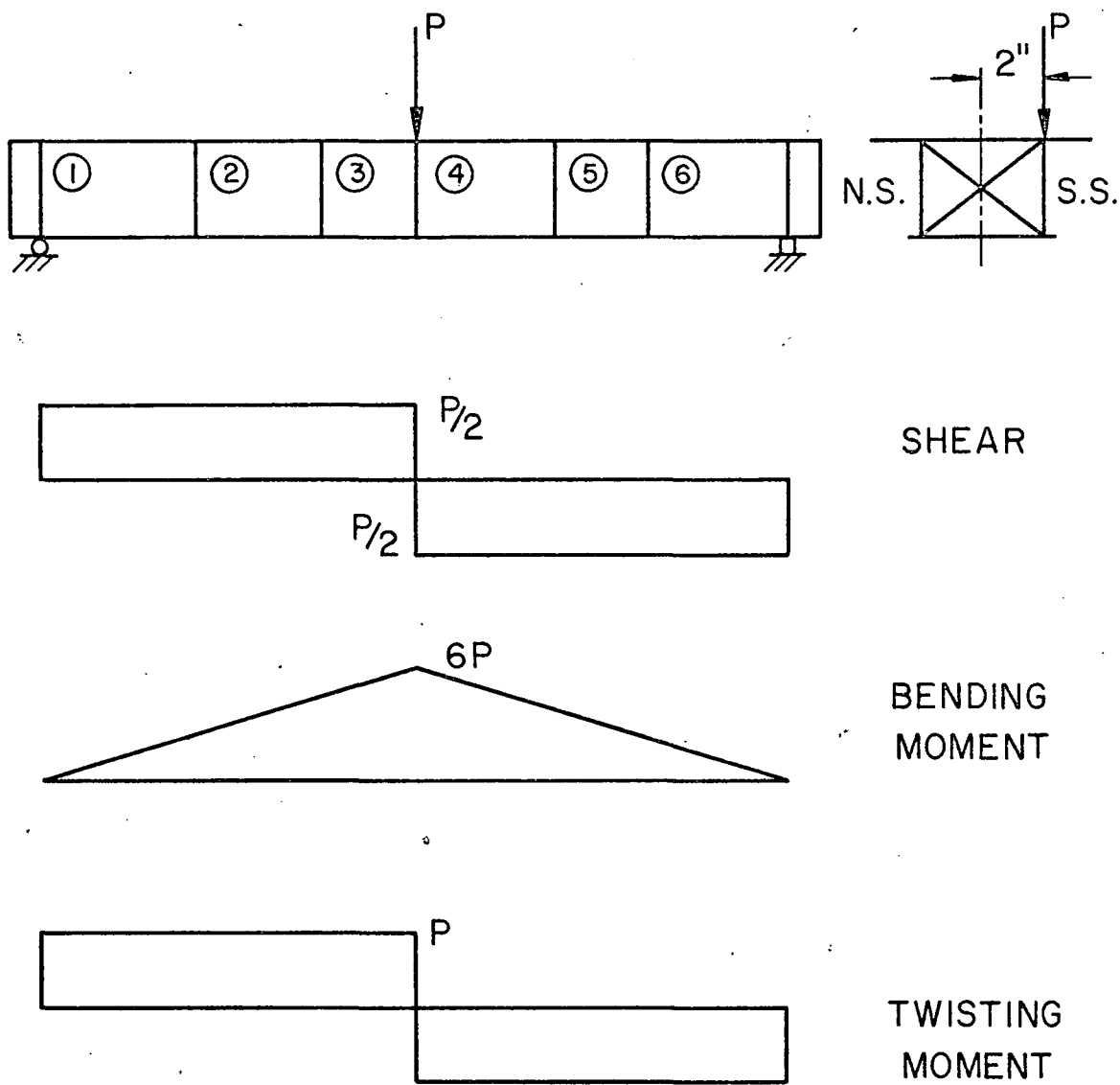
Fig. 2.10 Loading Condition - Specimen M1

Unsymmetrical Load

P

① ② ③ ④ ⑤ ⑥

P |← I" →|

N.S.   S.S.

℄

$5P/8$

SHEAR

$3P/8$

$45P/8$

BENDING
MOMENT

$5P/8$

TWISTING
MOMENT

$3P/8$ (a)

Symmetrical Load

P

① ② ③ ④ ⑤ ⑥

P

℄

$8P/15$

SHEAR

$7P/15$

$56P/15$
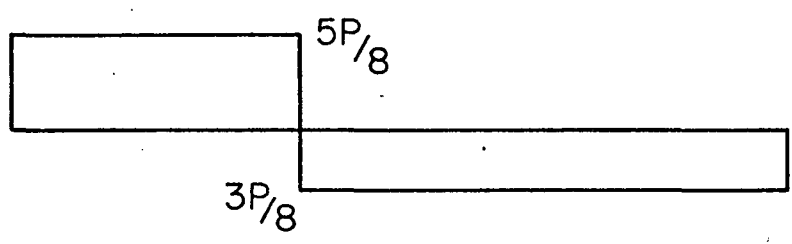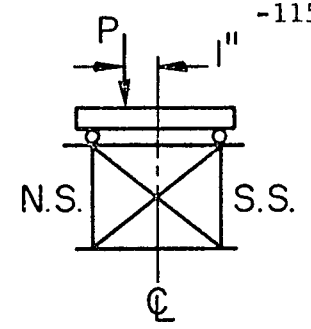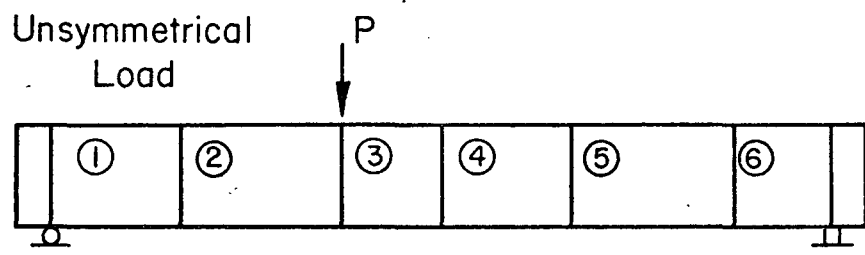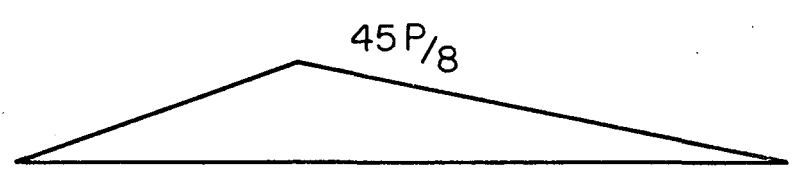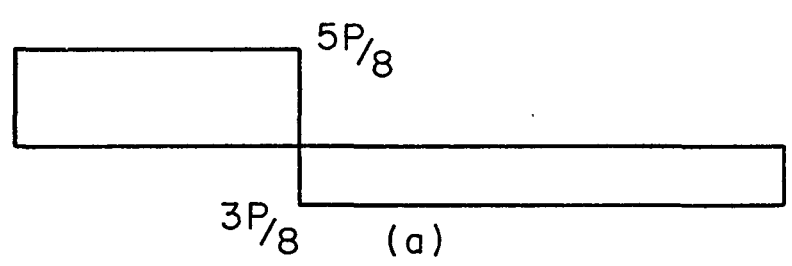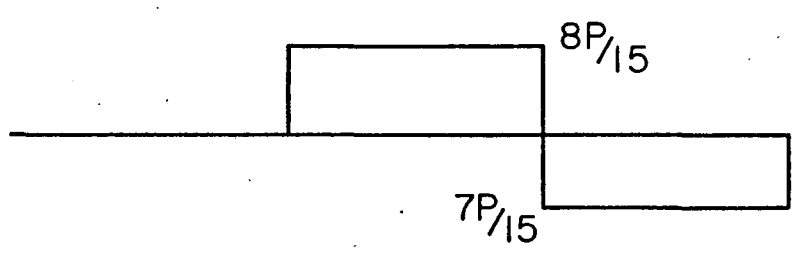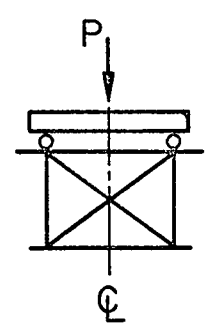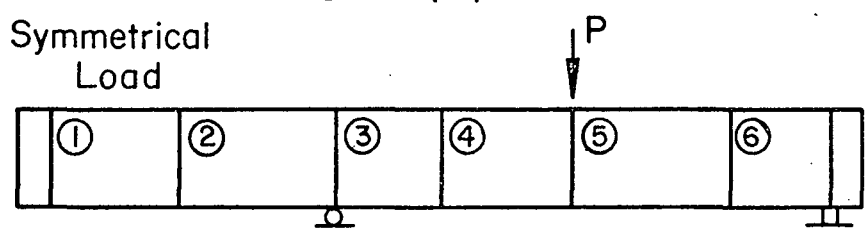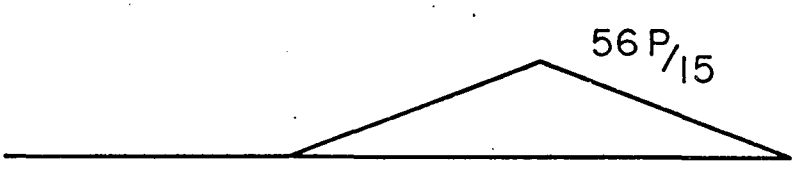
BENDING
MOMENT

(b)

Fig. 2.11   Loading Condition – Specimen M2

(a) NORTH SIDE
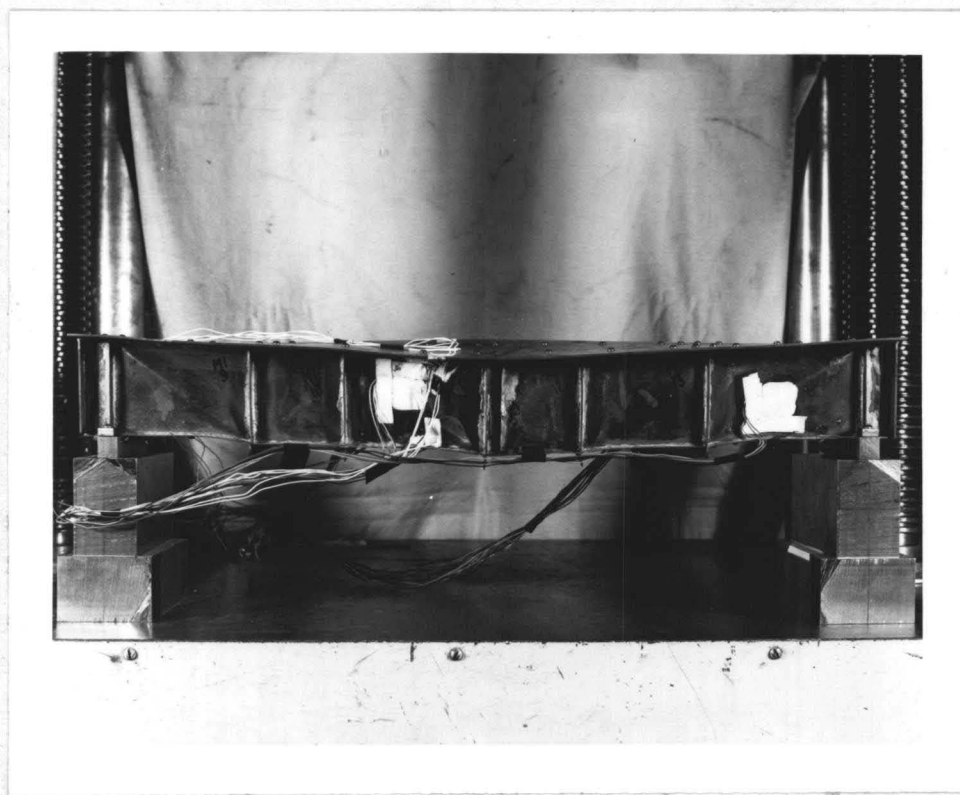
(b) SOUTH SIDE

Fig. 2.12 OVERALL PERMANENT DEFORMATIONS - SPECIMEN M1

(a) PANELS 1S and 2S

(b) PANELS 3S and 4S

Fig. 2.13 PERMANENT WEB PANEL DEFORMATIONS - SPECIMEN M1
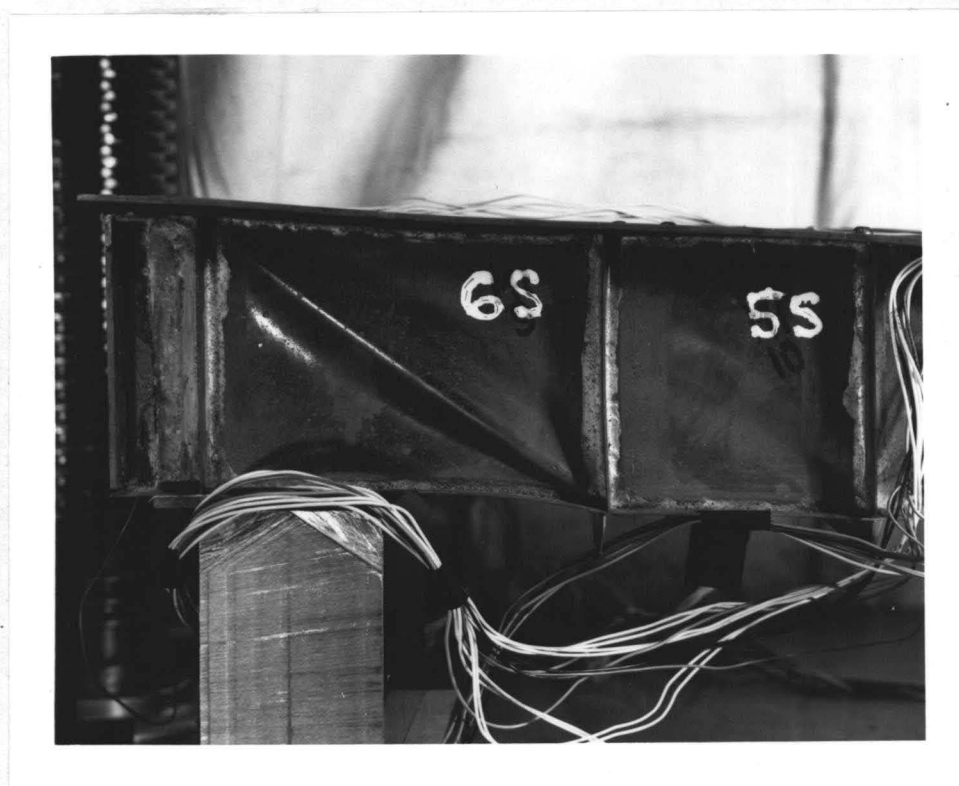
(c) PANELS 5S and 6S

Fig. 2.13 PERMANENT WEB PANEL DEFORMATIONS - SPECIMEN M1
(continued)
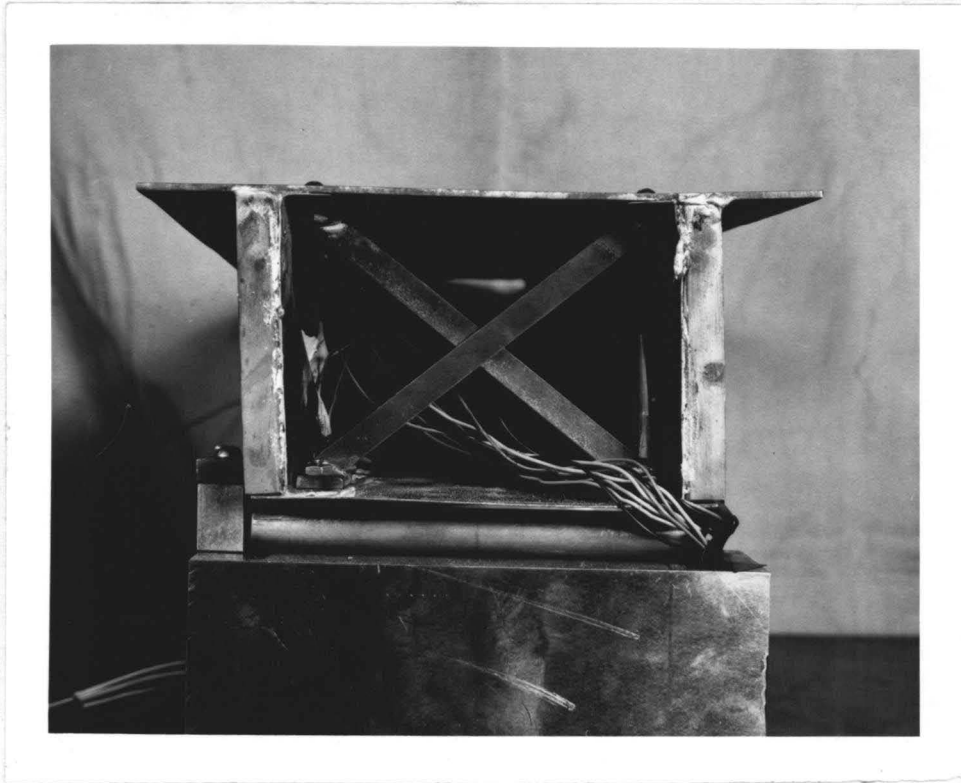
(a) EAST END
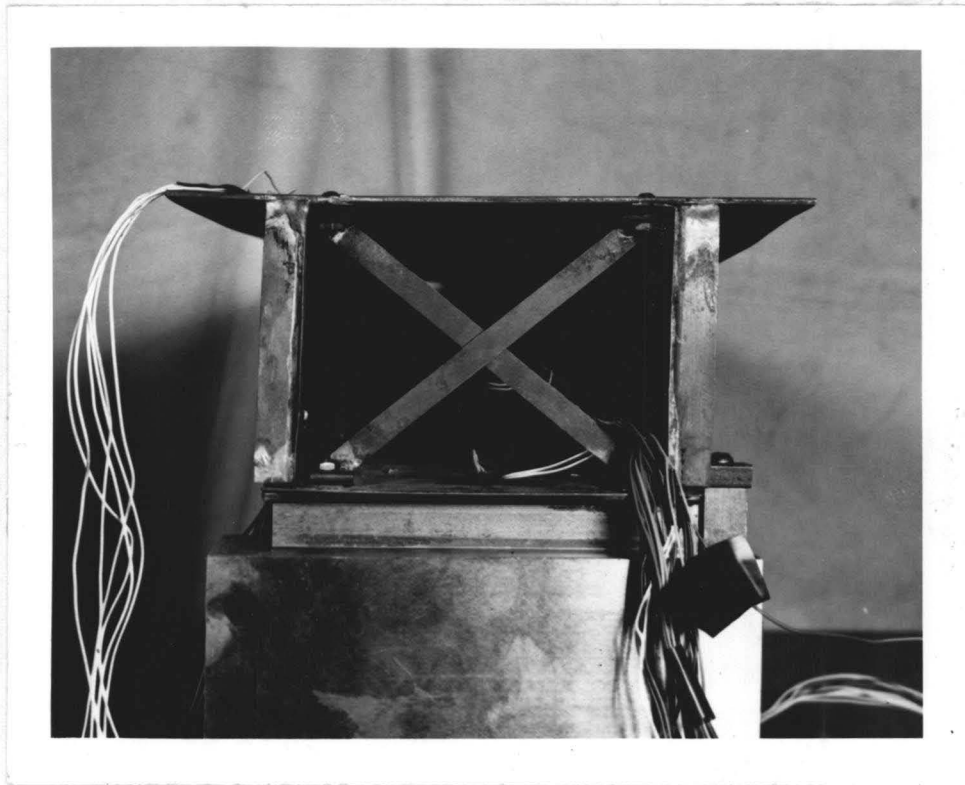
(b) WEST END

Fig. 2.14 VIEW OF END CROSS SECTIONS AFTER TESTING - SPECIMEN M1
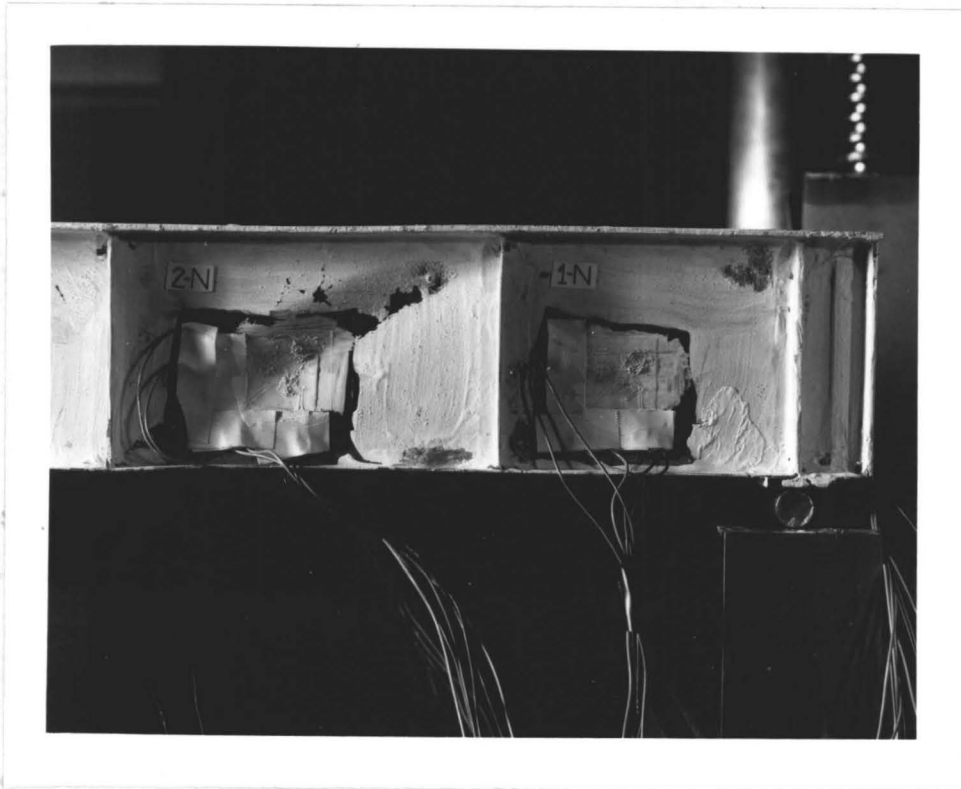
(a)   PANELS 1N and 2N

(b)   PANELS 1S and 2S

Fig. 2.15   PERMANENT WEB PANEL DEFORMATIONS - SPECIMEN M2
(Unsymmetrical Loading)

Fig. 2.16   TEST SETUP FOR SPECIMEN M2
(Symmetrical Loading)
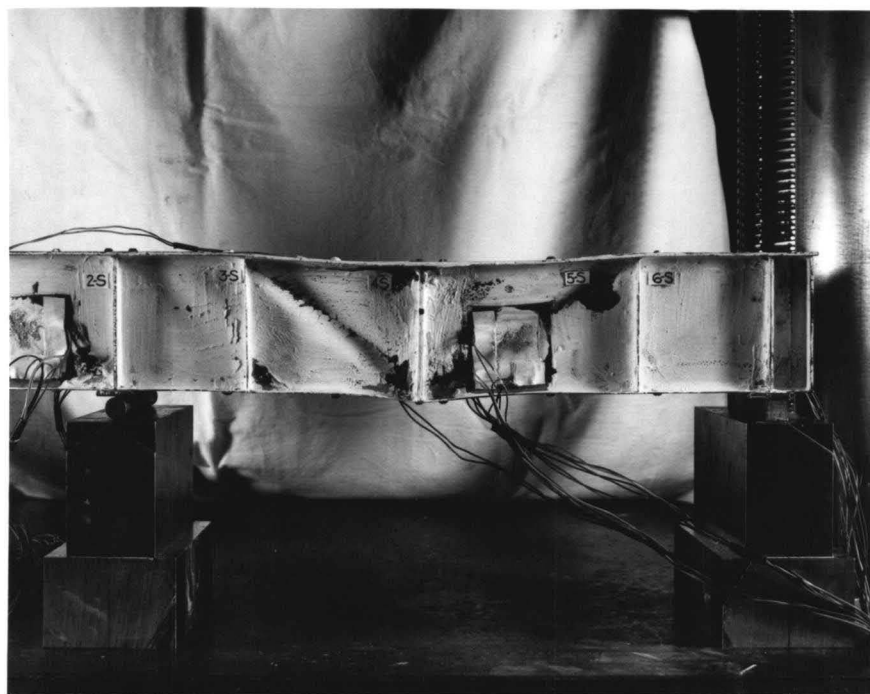
(a) SOUTH SIDE
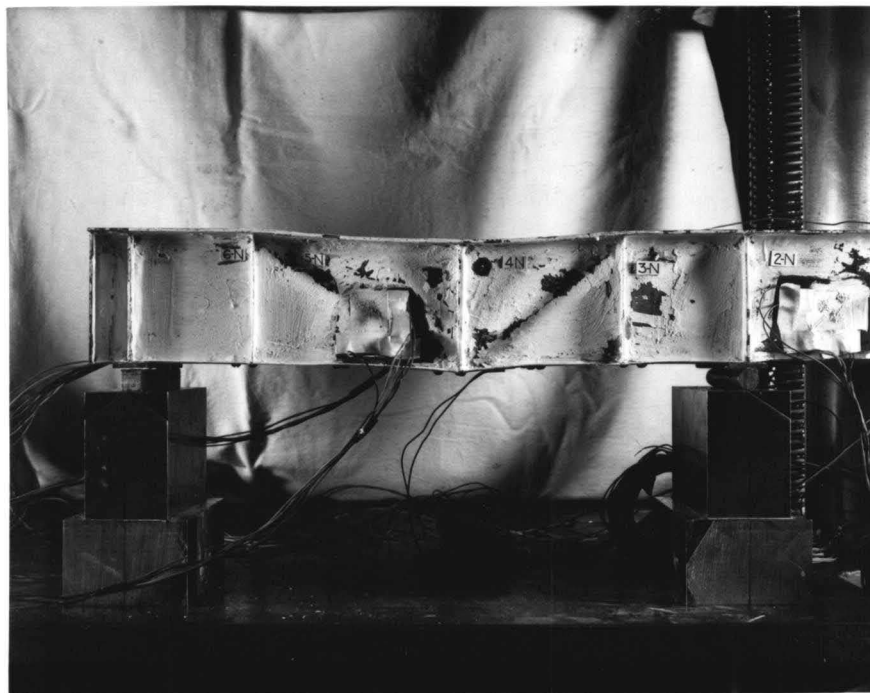
(b) NORTH SIDE

Fig. 2.17 OVERALL PERMANENT DEFORMATIONS - SPECIMEN M2
(Symmetrical Loading)

(a)   PANELS 4S and 5S
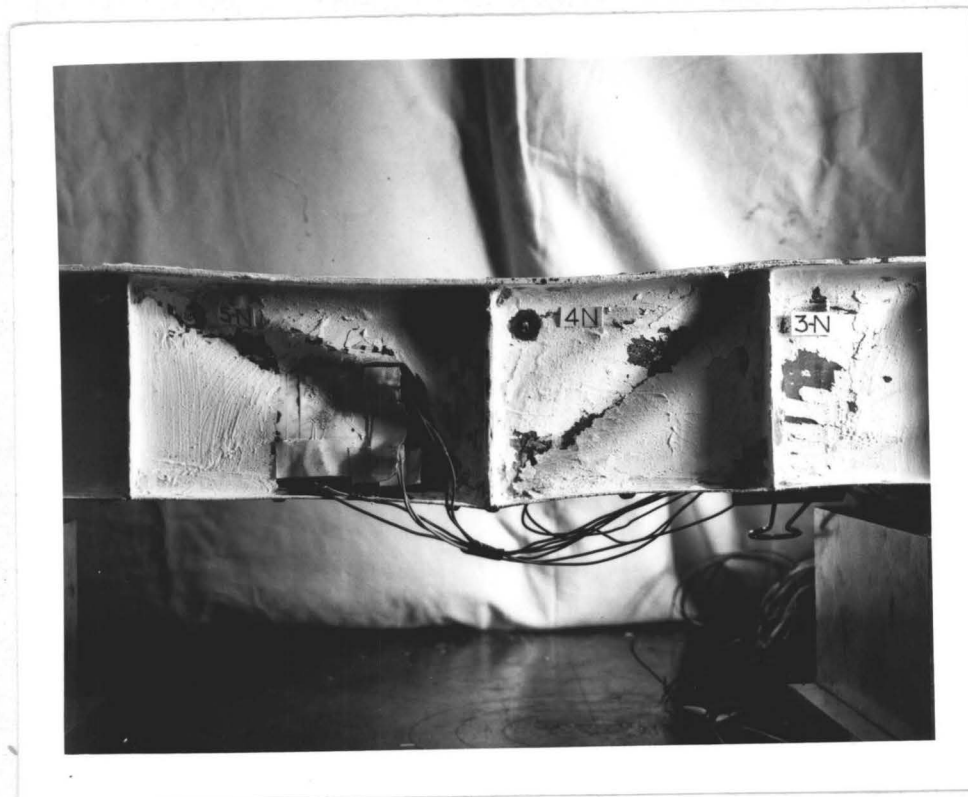
(b)   PANELS 4N and 5N

Fig. 2.18   PERMANENT WEB PANEL DEFORMATIONS - SPECIMEN M2
(Symmetrical Loading)
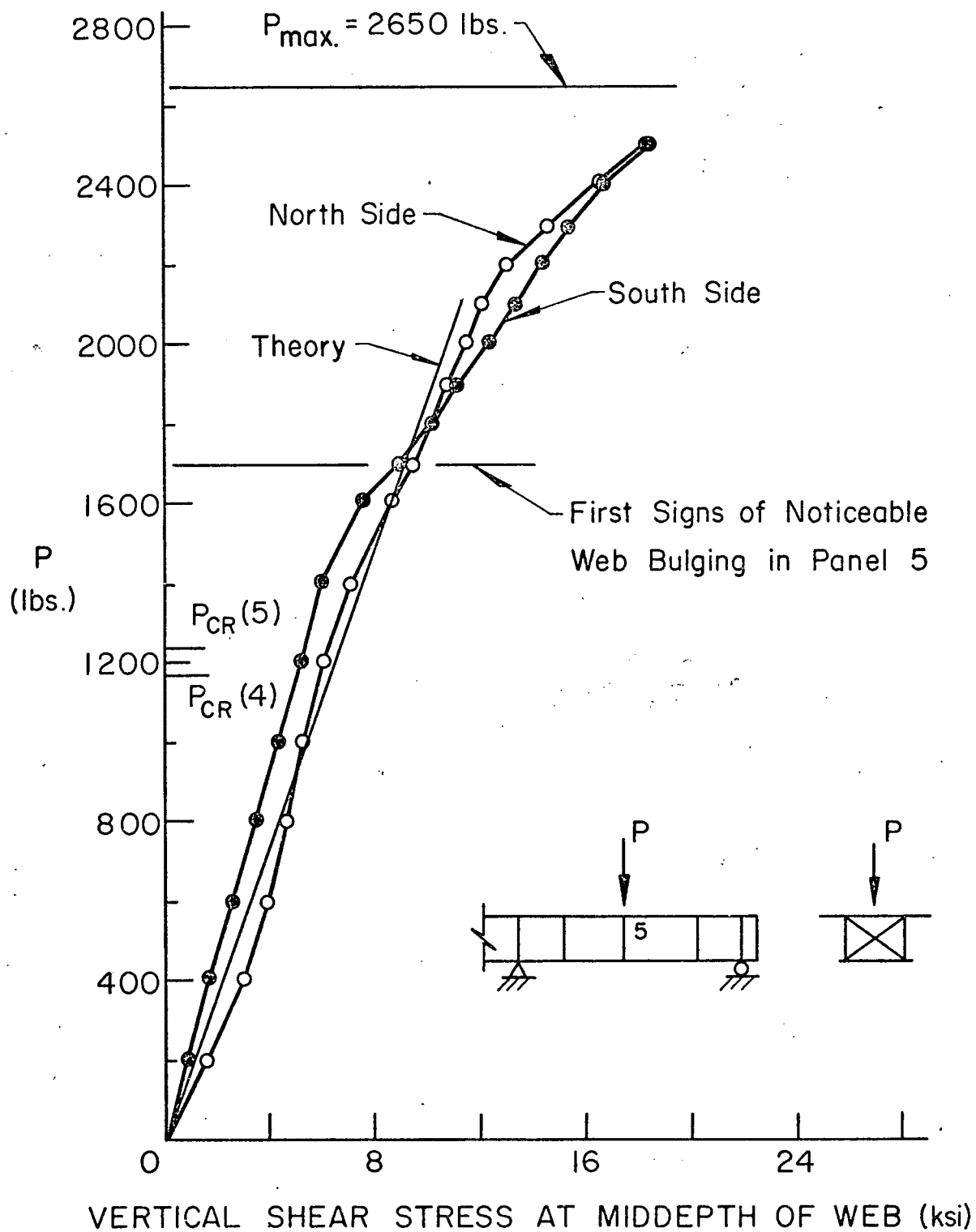
Fig. 2.19   Load vs. Shear Stress at Centerline of Panel 5 -
Specimen M2 (Sym. Load)

Panel 5N

-P = 200#

-P = 1200#

-P = 2400#

Panel 5S

-P = 200#

-P = 1200#

-P = 2400#

PRINCIPAL STRESSES

0   10 ksi
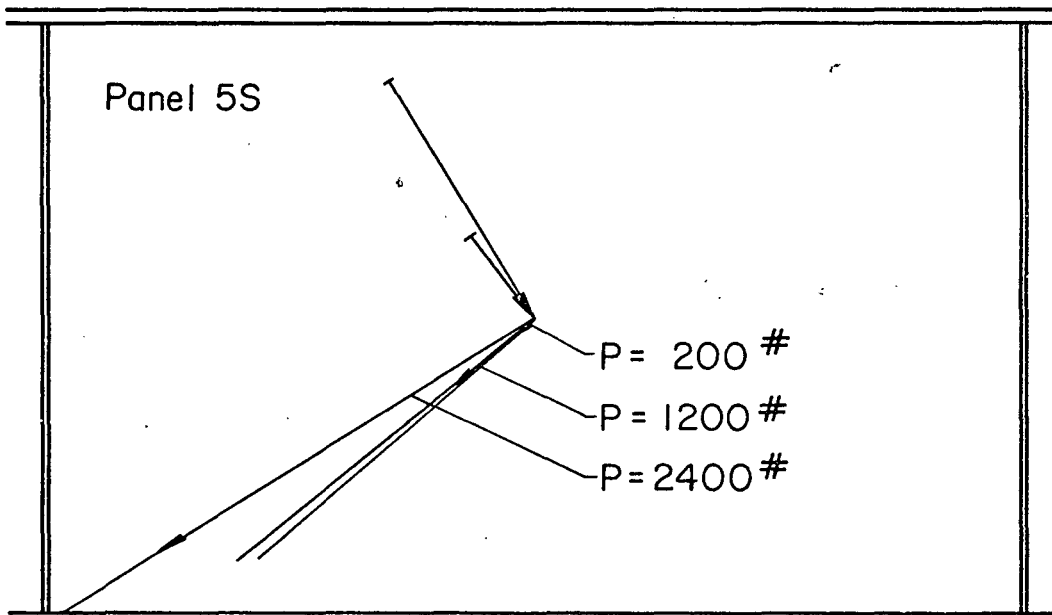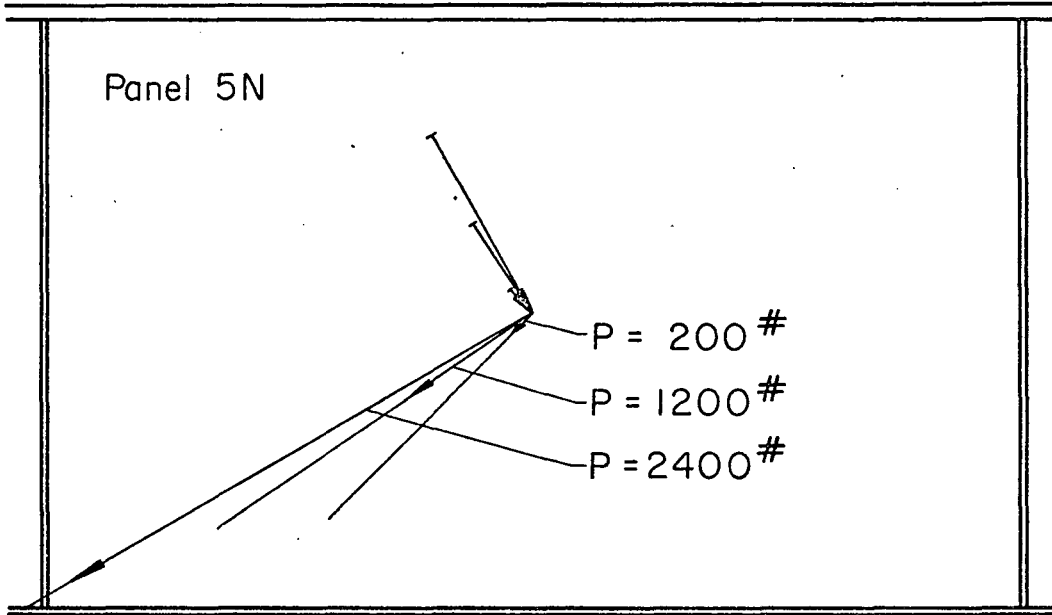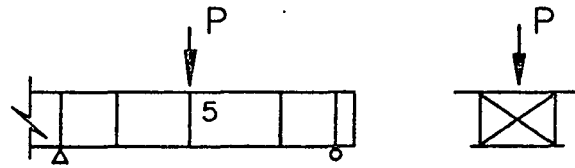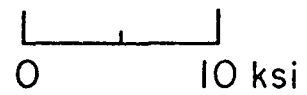
Fig. 2.20   Principal Stresses at Midpoint of Web Panels 5N
            and 5S - Specimen M2 (Sym. Load)
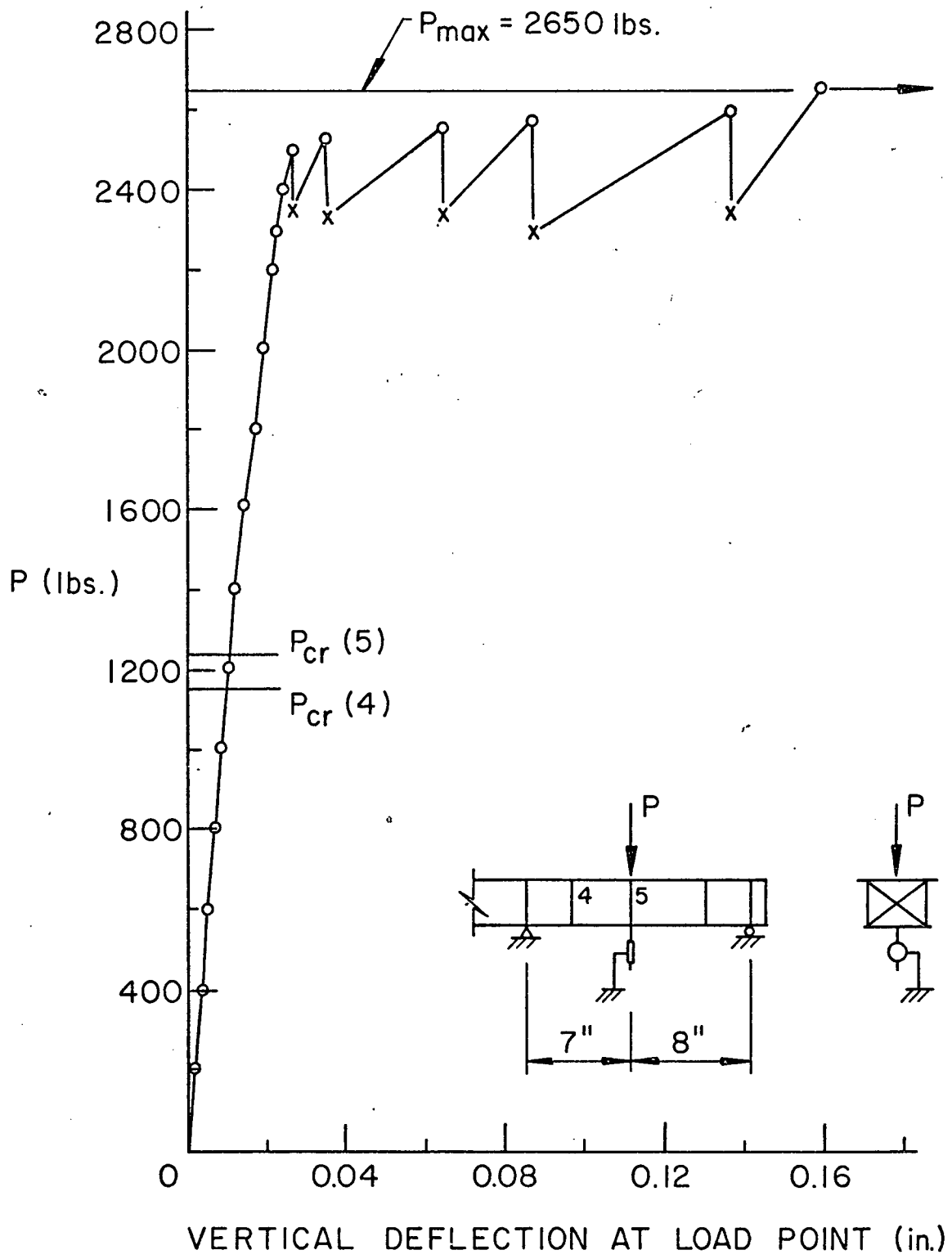
Fig. 2.21   Load vs. Load Point Deflection - Specimen M2
(Sym. Load)
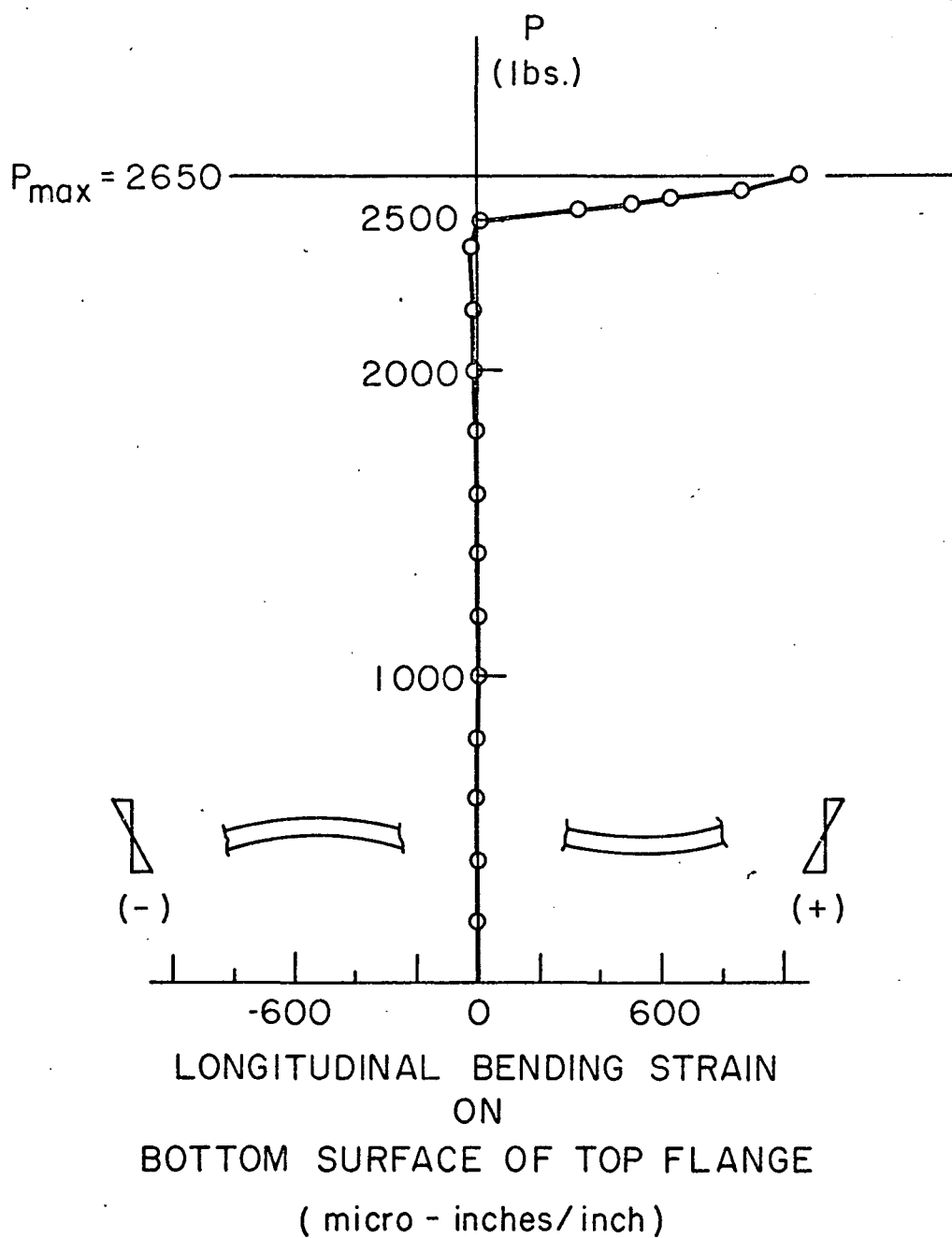
Fig. 2.22   Load vs. Top Flange Bending Strain in Panel 4 - Specimen M2 (Sym. Load)
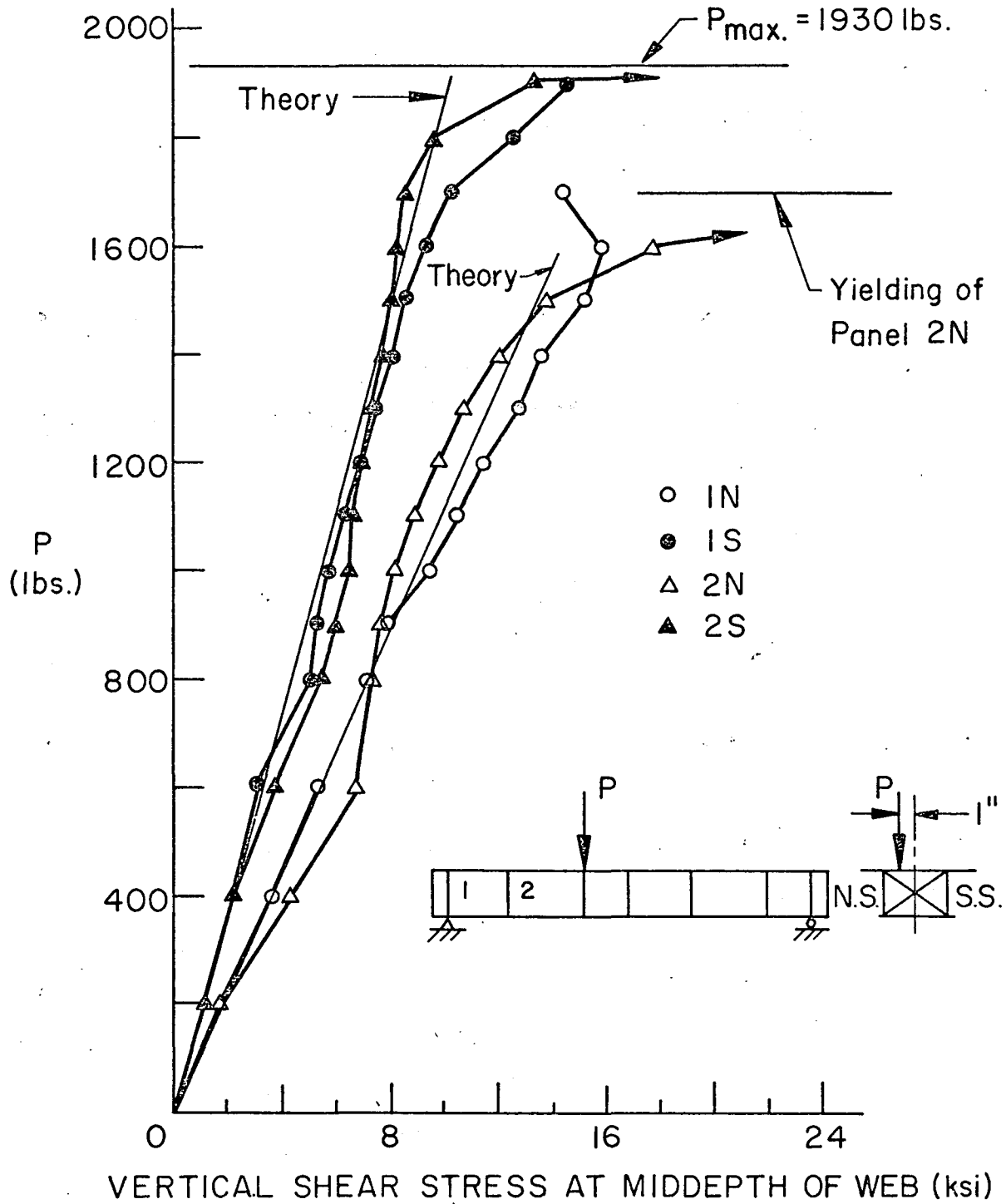
Fig. 2.23   Load vs. Shear Stress at Centerline of Panels 1
and 2 - Specimen M2 (Unsym. Load)
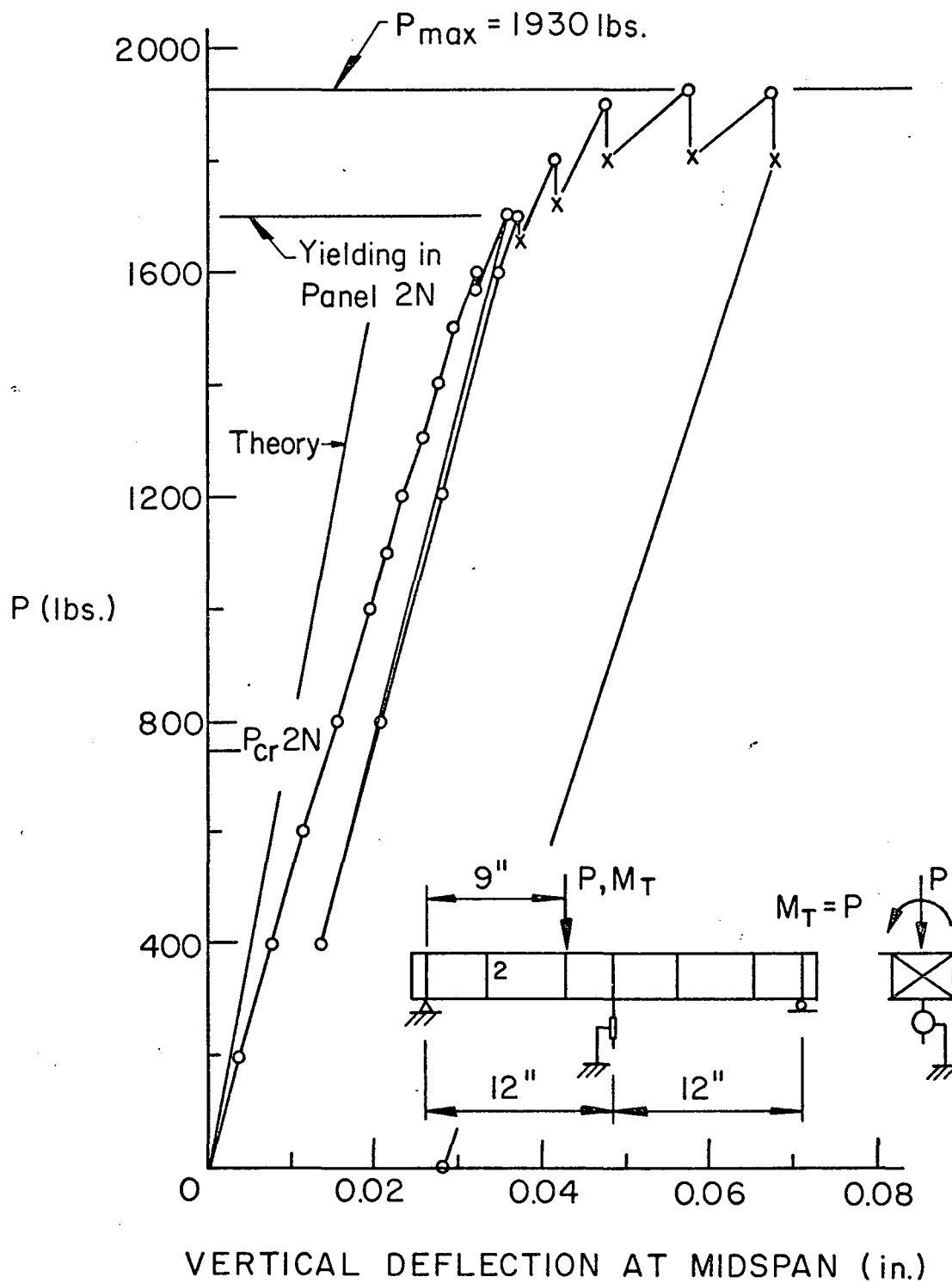
Fig. 2.24 · Load vs. Midspan Deflection - Specimen M2
(Unsym. Load)
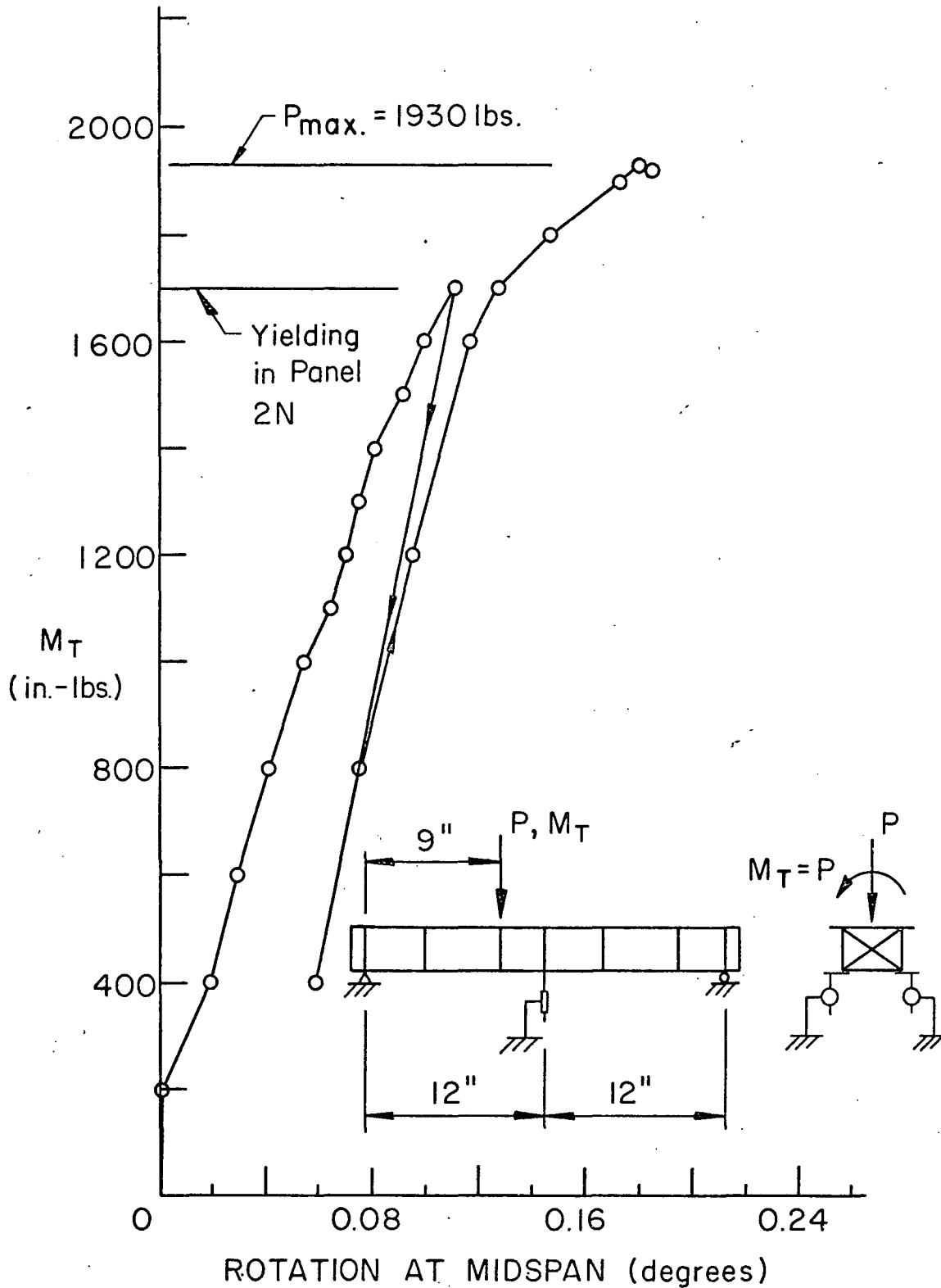
Fig. 2.25   Load vs. Midspan Rotation -
Specimen M2 (Unsym. Load)
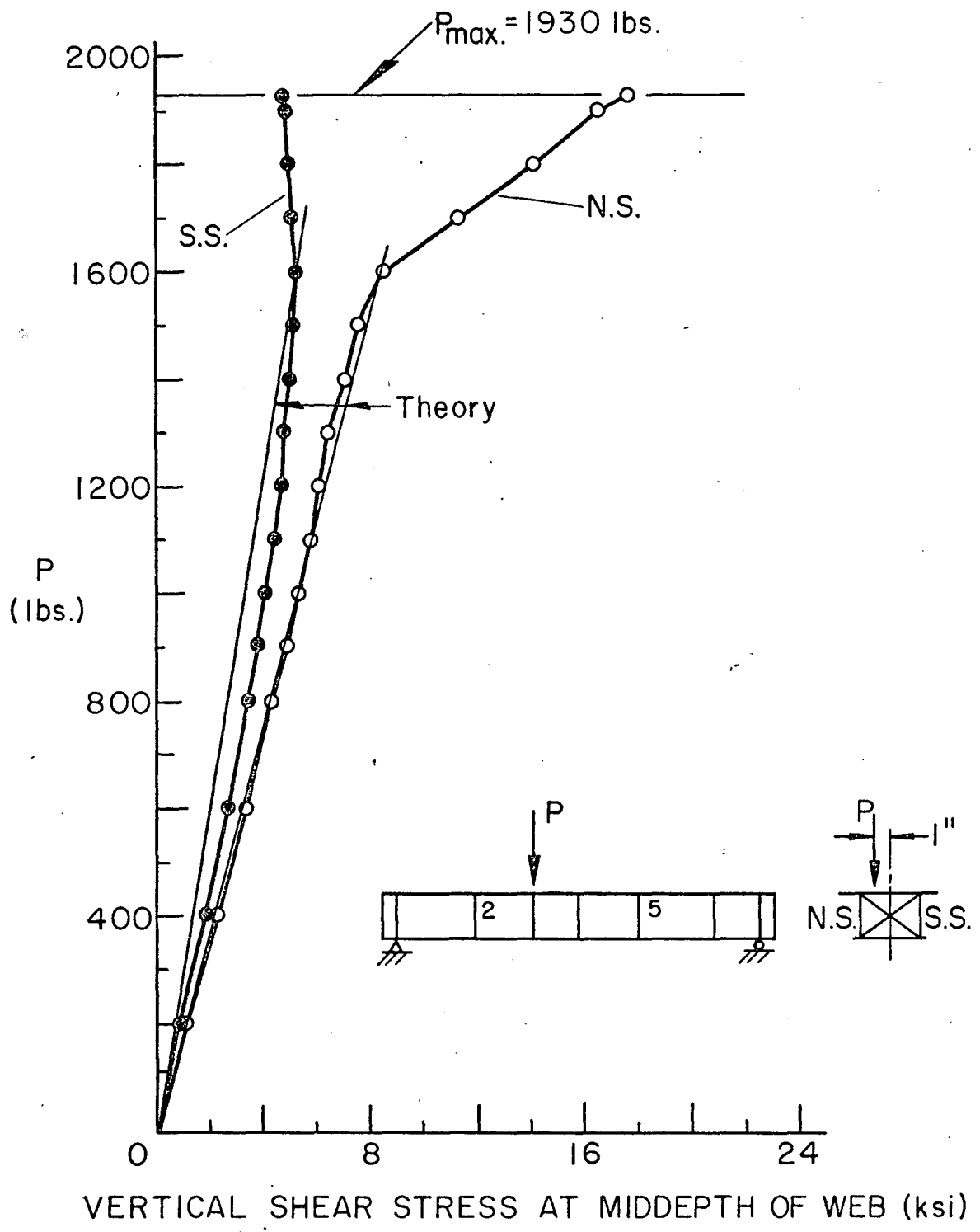
Fig. 2.26   Load vs. Shear Stress at Centerline of Panel 5 -
Specimen M2 (Unsym. Load)
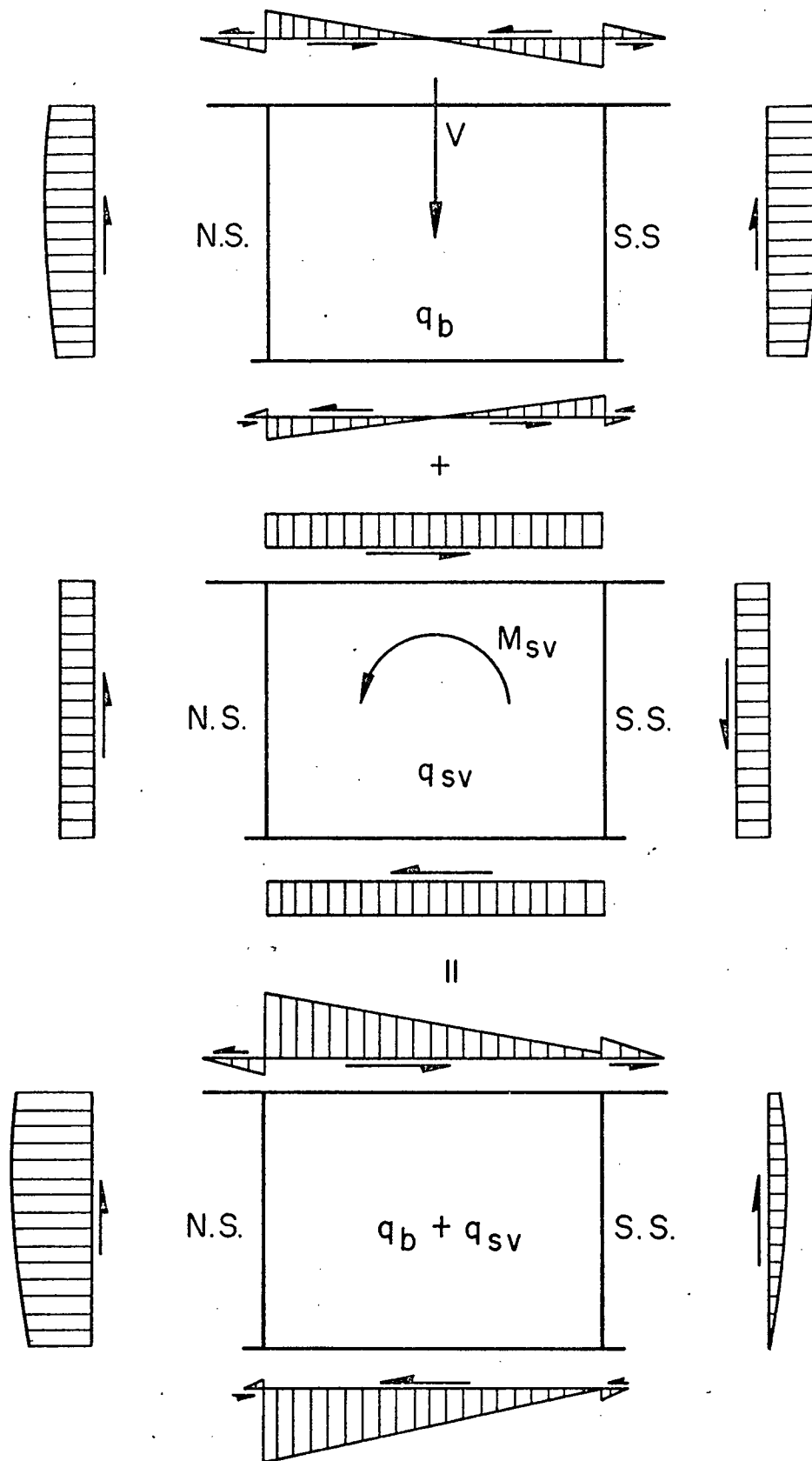
Fig. 2.27   Superposition of Flexural and Torsional Shear Flow
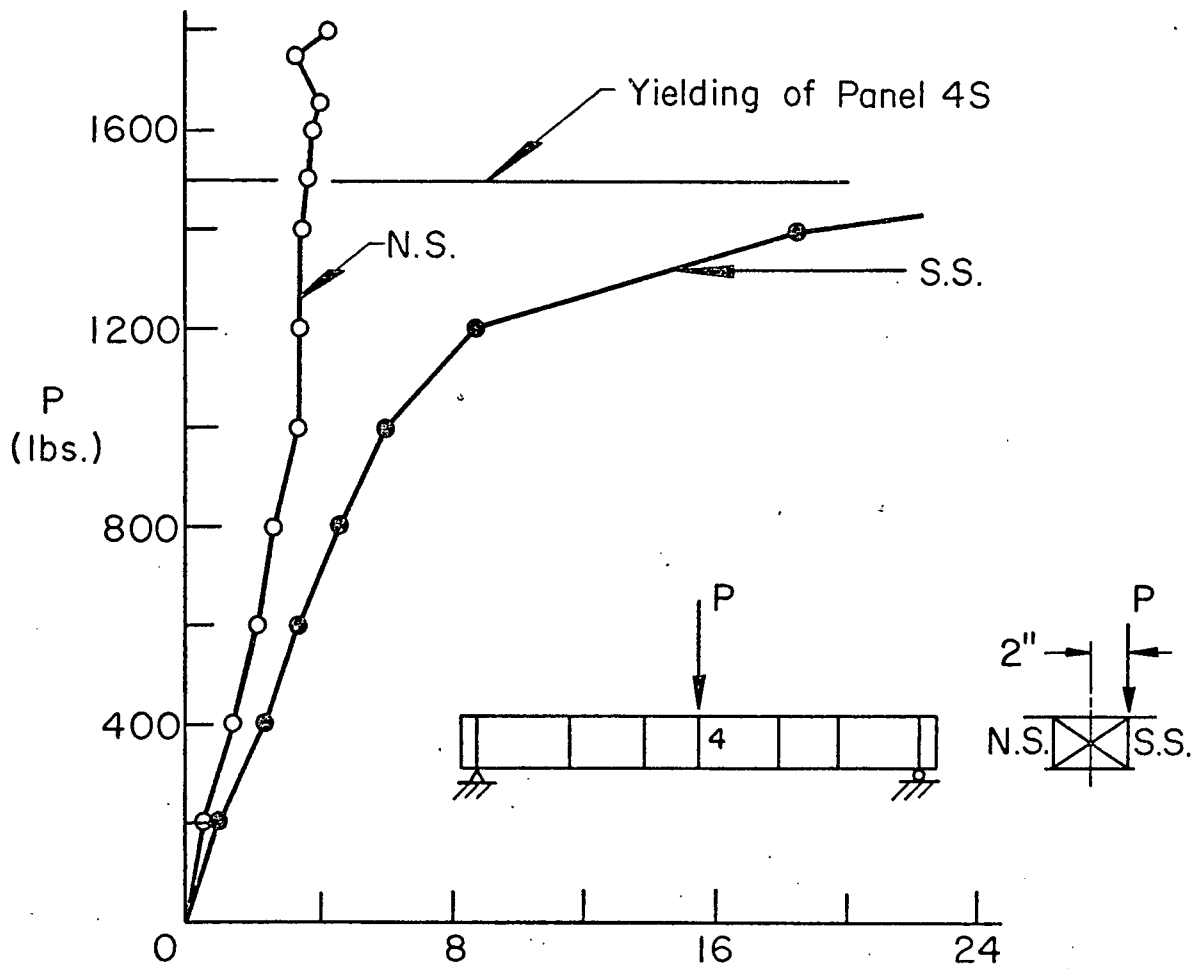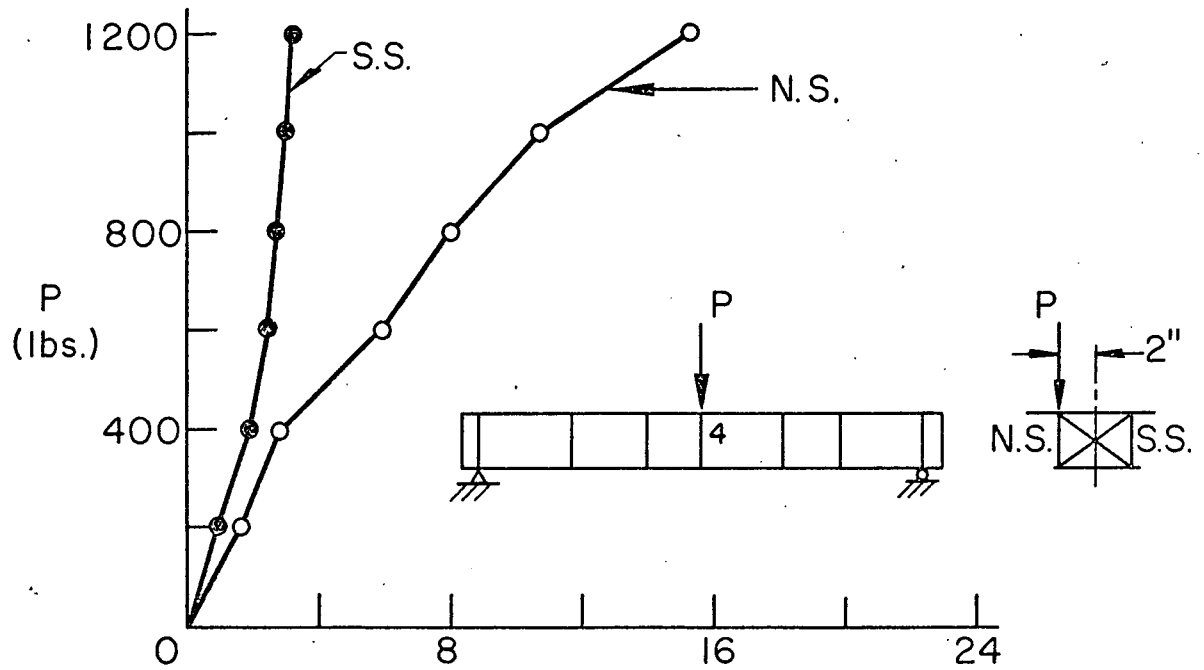
Fig. 2.28   Load vs. Shear Stress at Centerline of Panel 4 -
Specimen M1 (Unsym. Load)
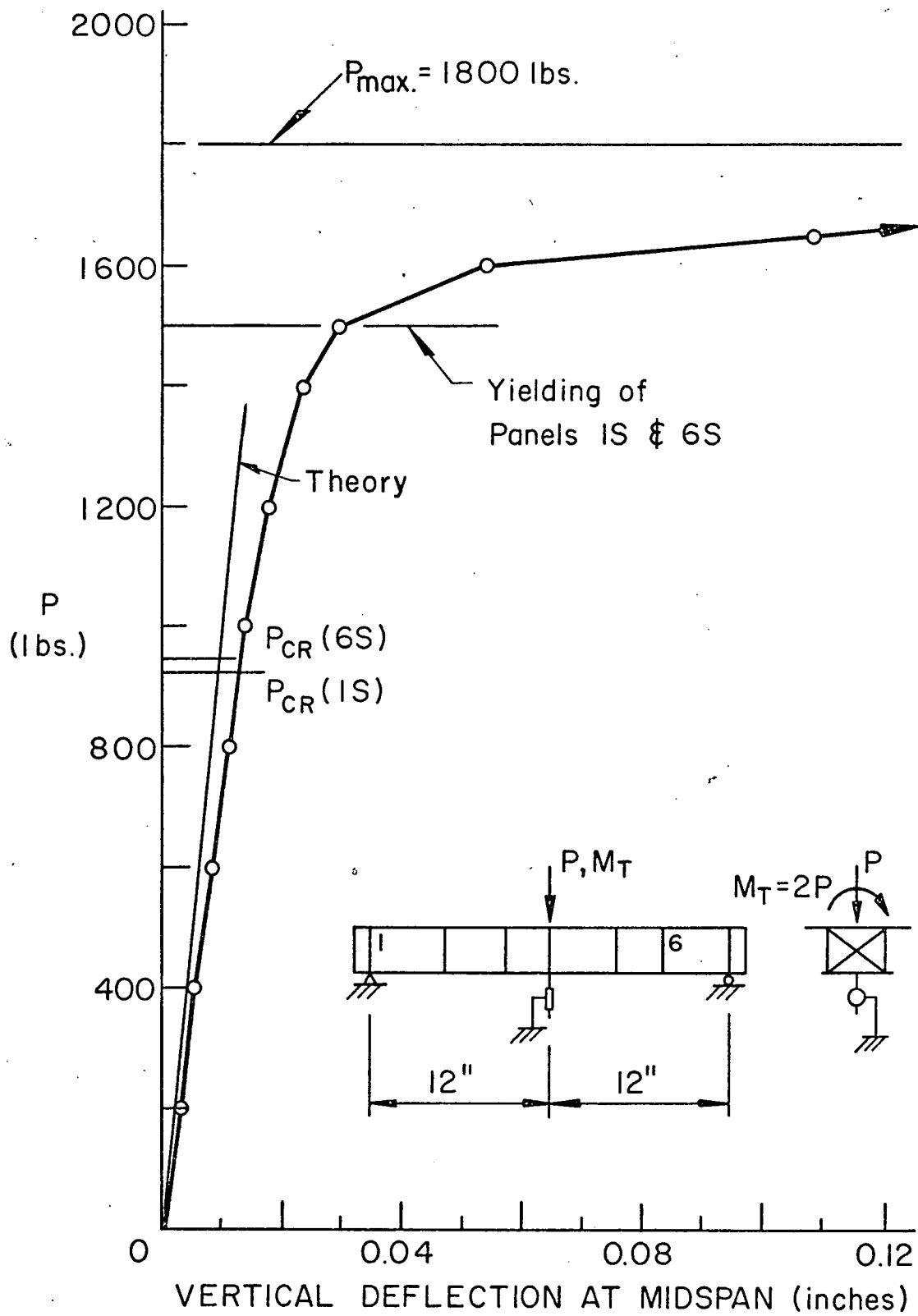
Fig. 2.29   Load vs. Midspan Deflection -
Specimen M1 (Unsym. Load)
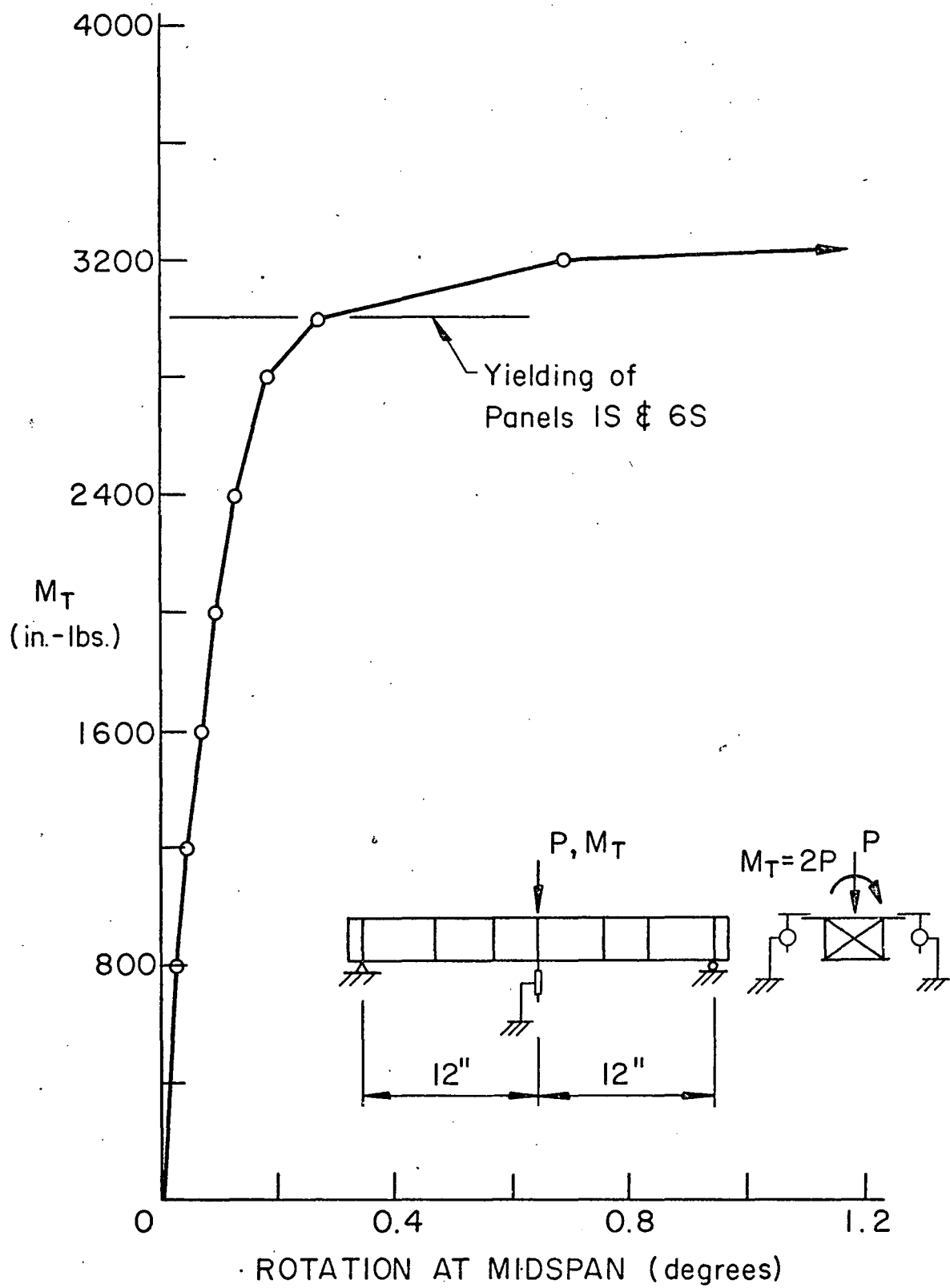
Fig. 2.30 Load vs. Midspan Rotation -
Specimen M1 (Unsym. Load)
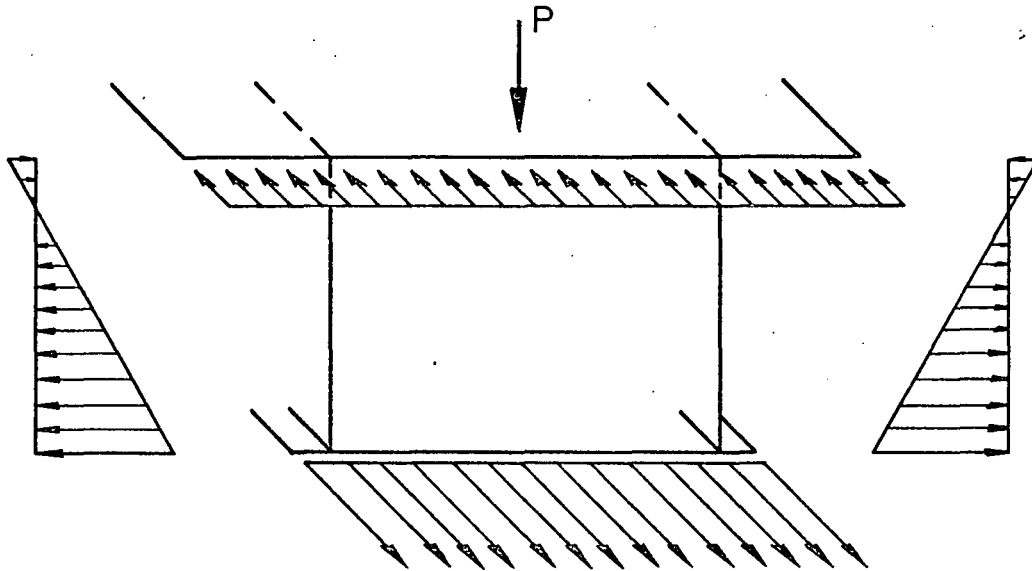
(a) Normal Stress, σ_B
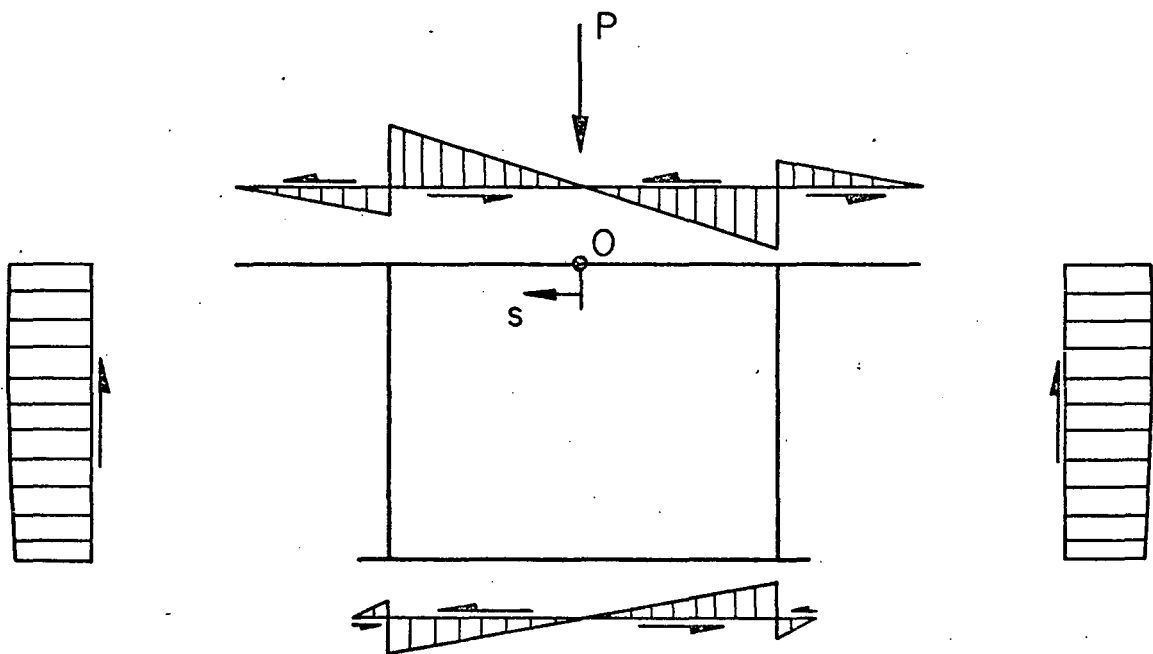
(b) Shear Stress, τ_B

Fig. 3.1 Cross-Sectional Distribution of Theoretical
Flexural Stresses
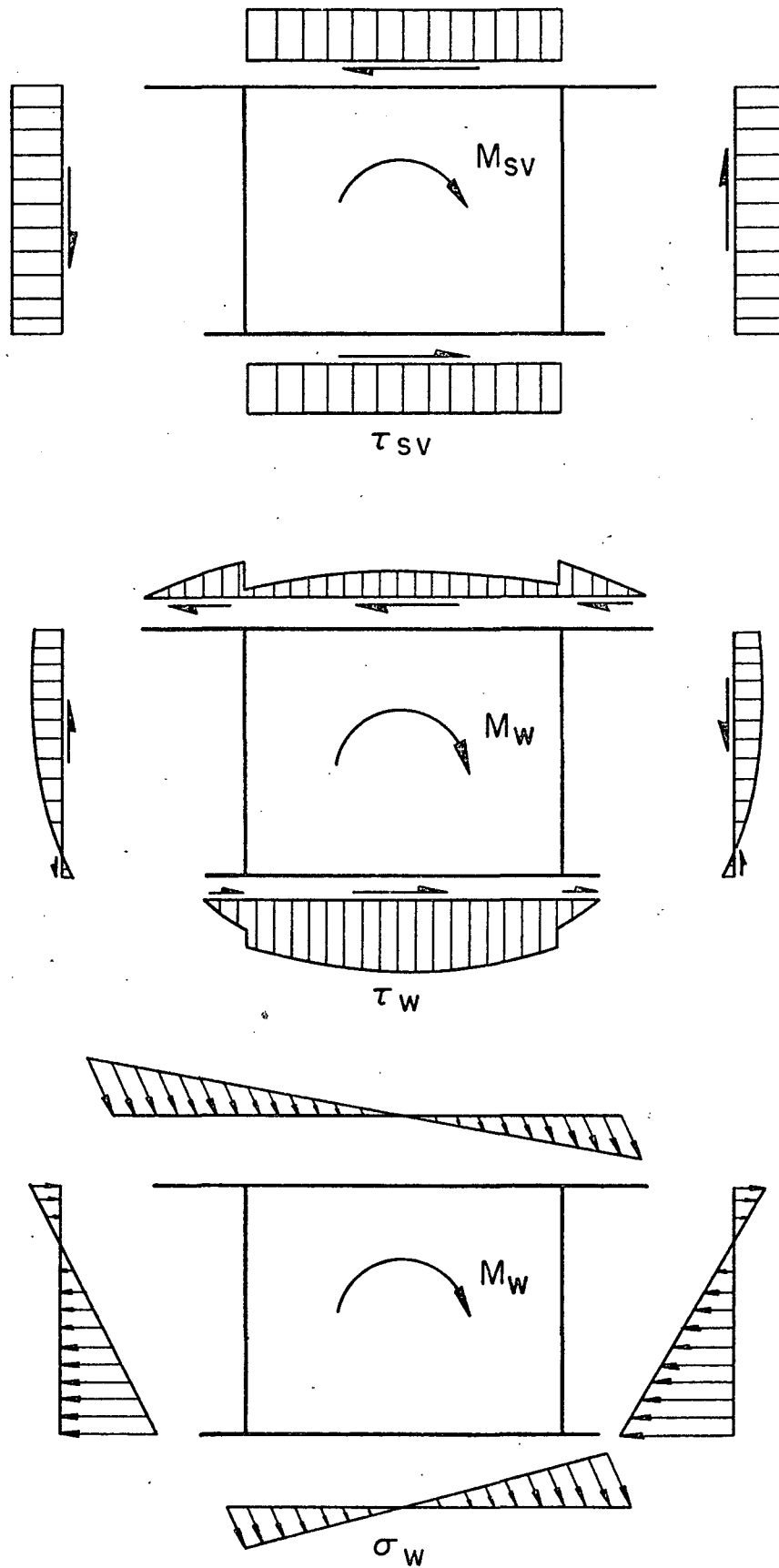
Fig. 3.2   Cross-Sectional Distribution of Theoretical
            Torsional Stresses
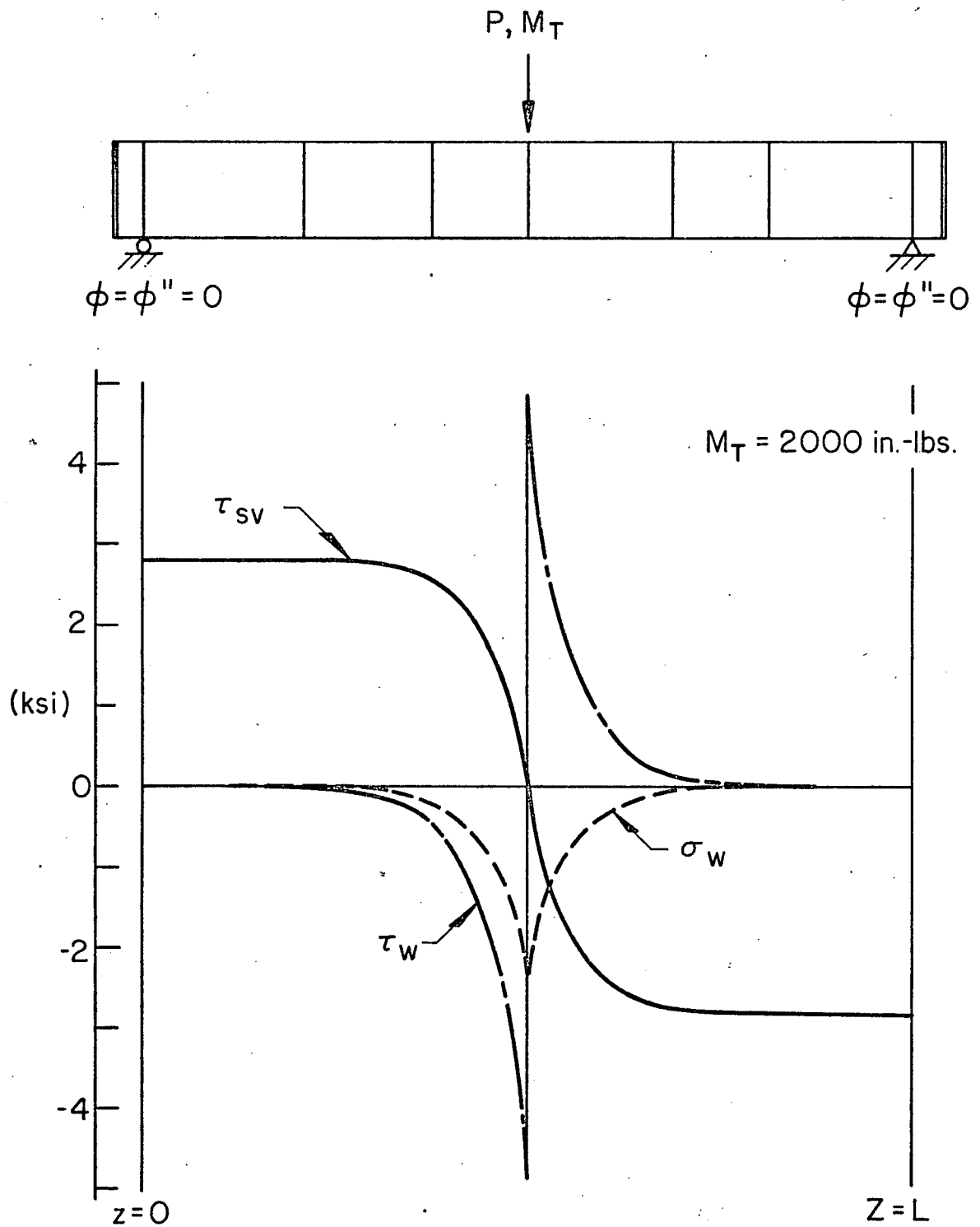
Fig. 3.3   Longitudinal Distribution of Theoretical
Torsional Stresses - Specimen M1
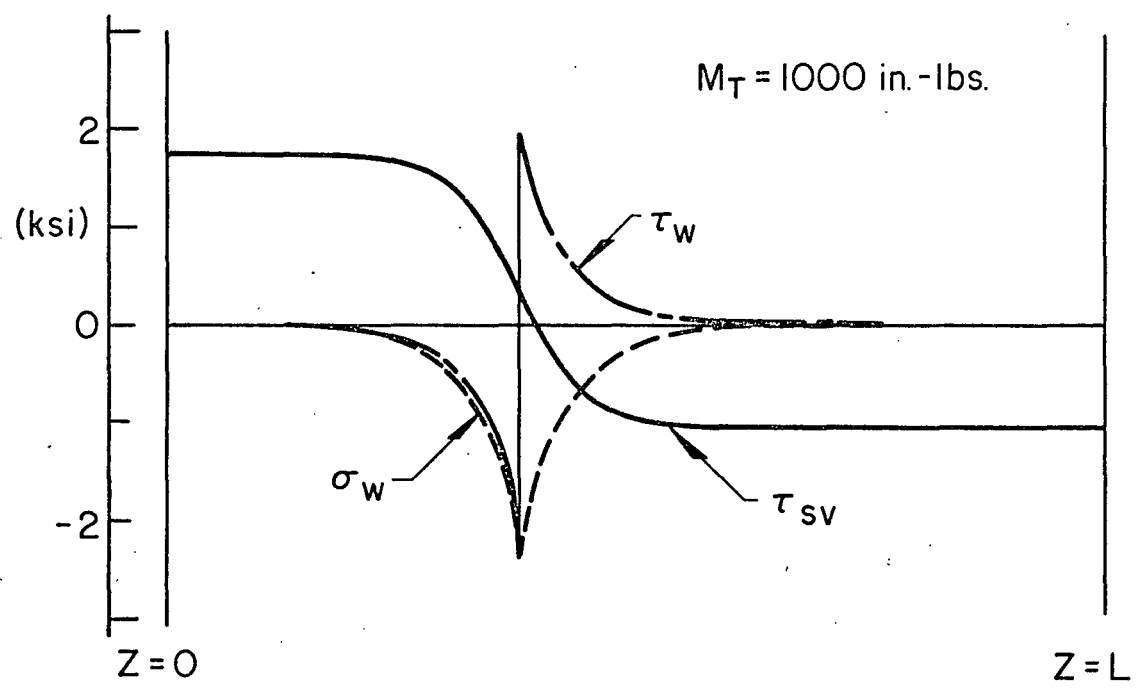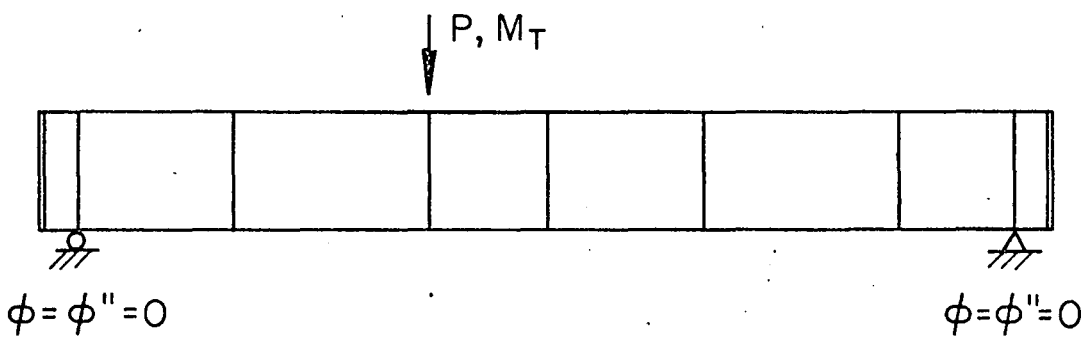
Fig. 3.4   Longitudinal Distribution of Theoretical
Torsional Stresses - Specimen M2
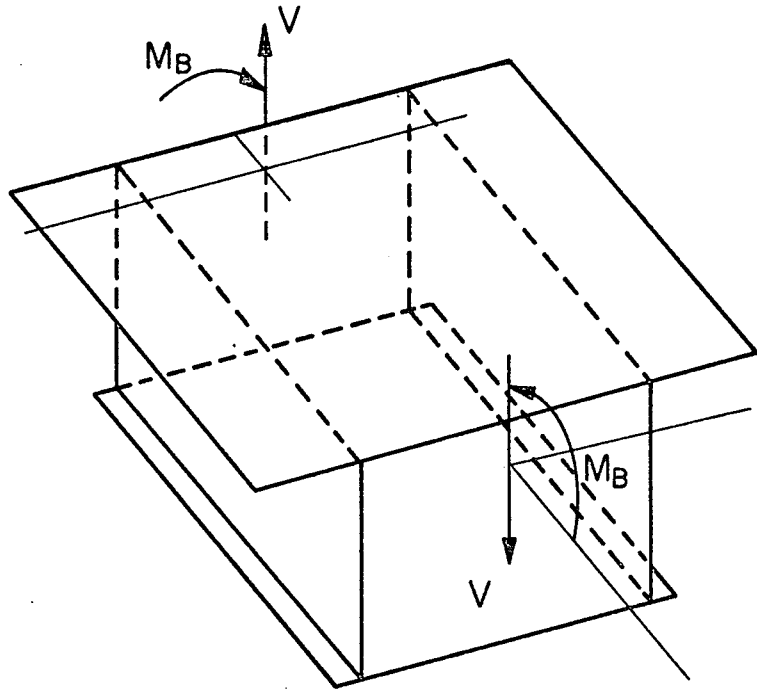
SYMMETRICAL LOADING
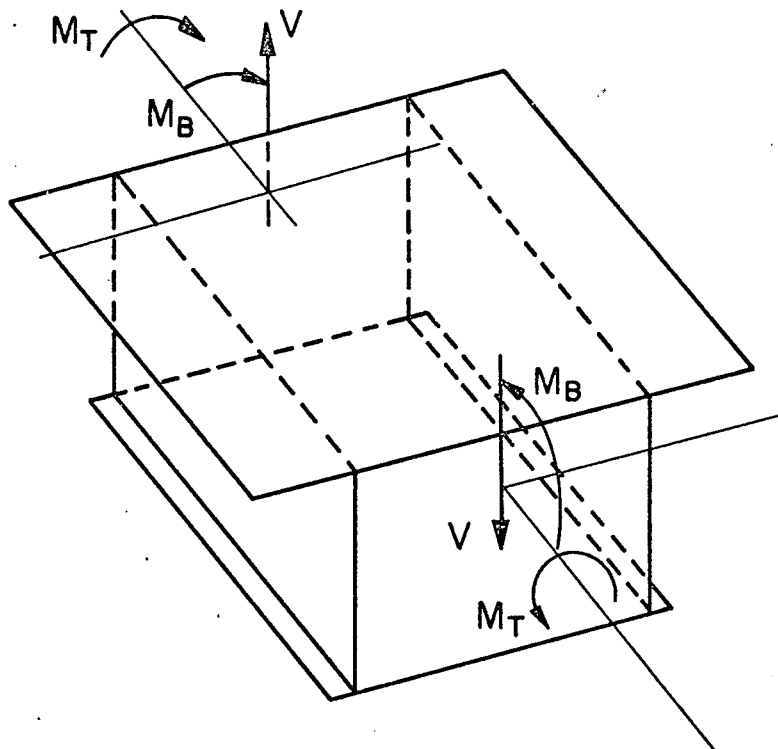
UNSYMMETRICAL LOADING

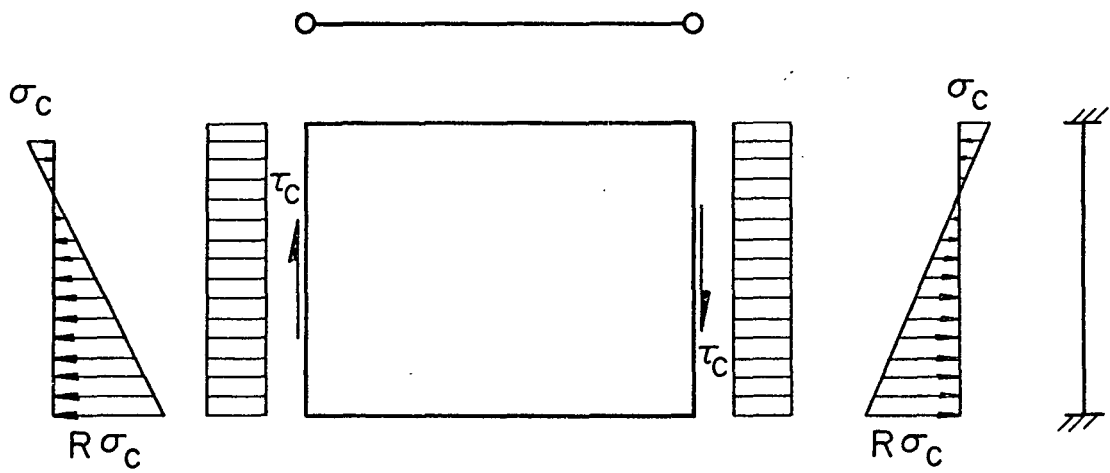Fig. 3.5   Typical Panel Forces for Single-Span Box Girder

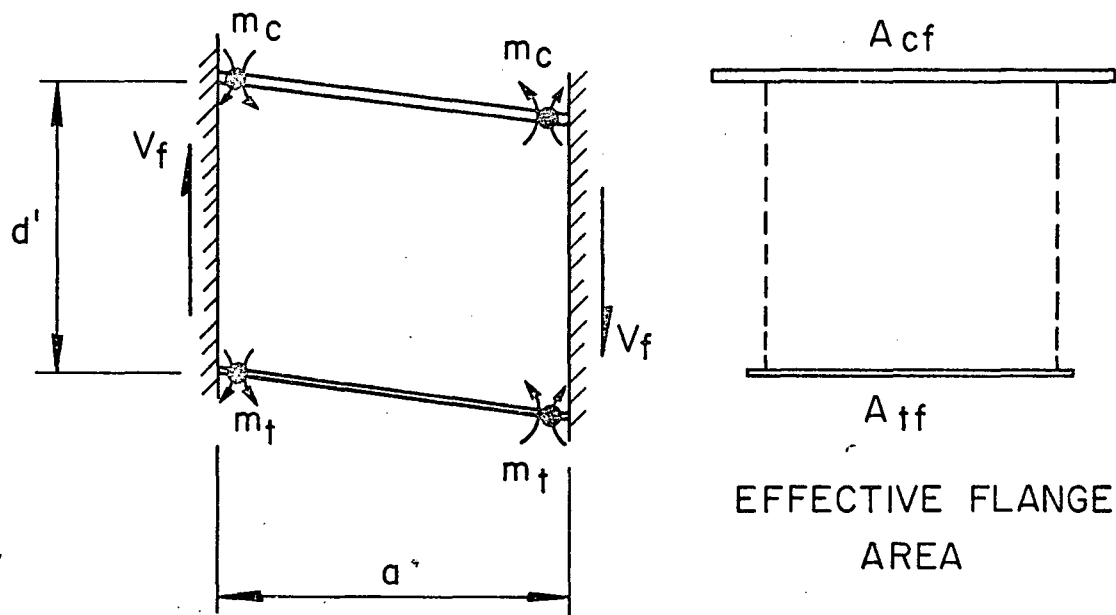Fig. 3.6 Stress and Boundary Conditions for a
Box Girder Web

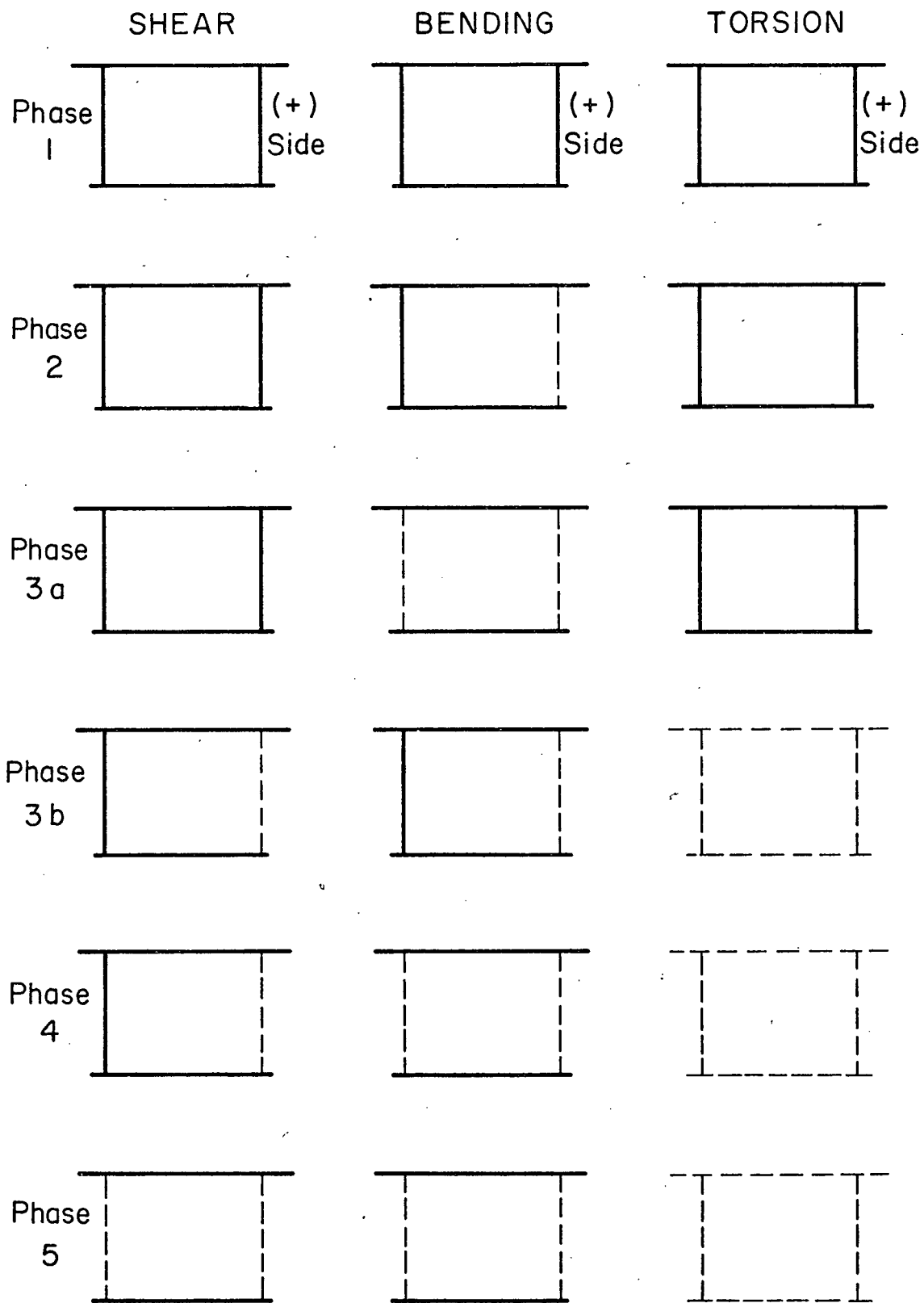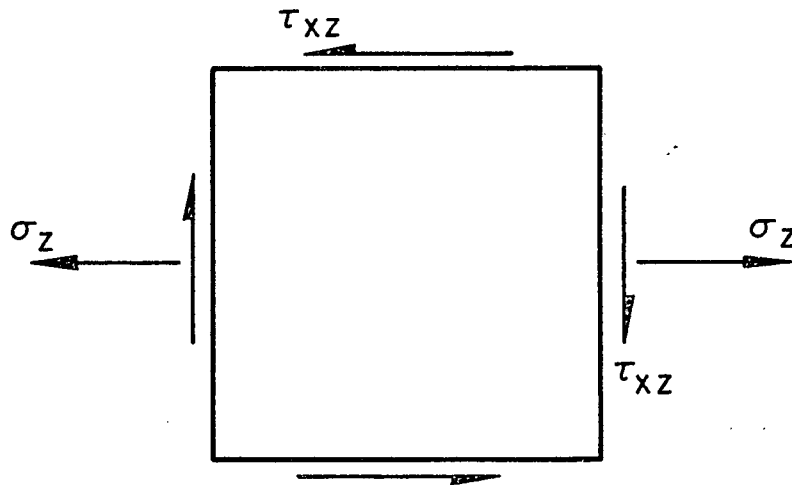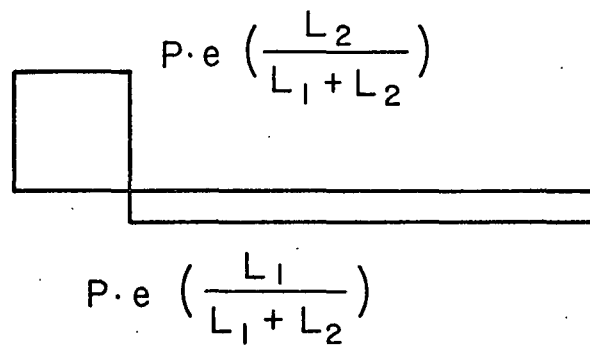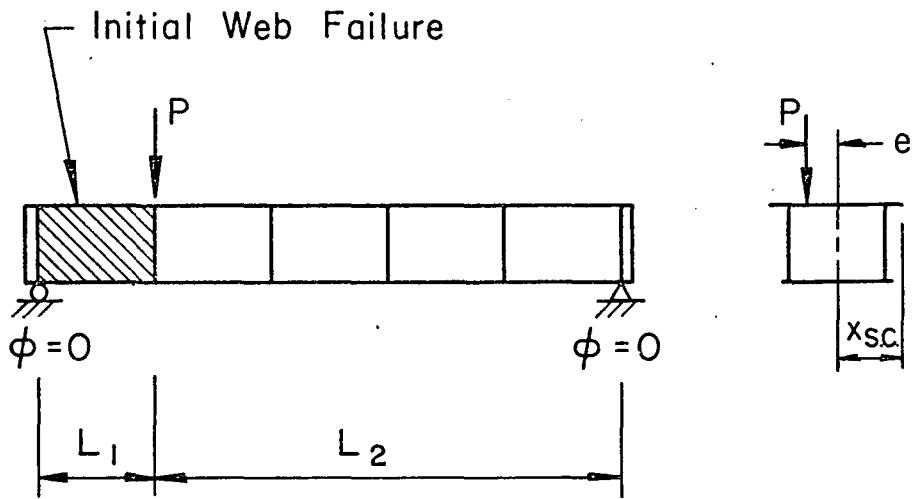Fig. 3.7 Frame Action Failure Mechanism of Box Girder Flanges

Fig. 3.8   Effective Cross Section for Various Phases and
Components of Unsymmetrical Panel Loading

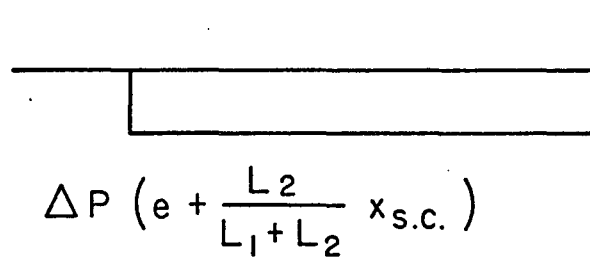σ_Z AND τ_{xz} UNIFORMLY DISTRIBUTED
OVER SIDES AND THICKNESS

Fig. 3.9   State of Stress in Tension Flange
for Unsymmetrical Loading

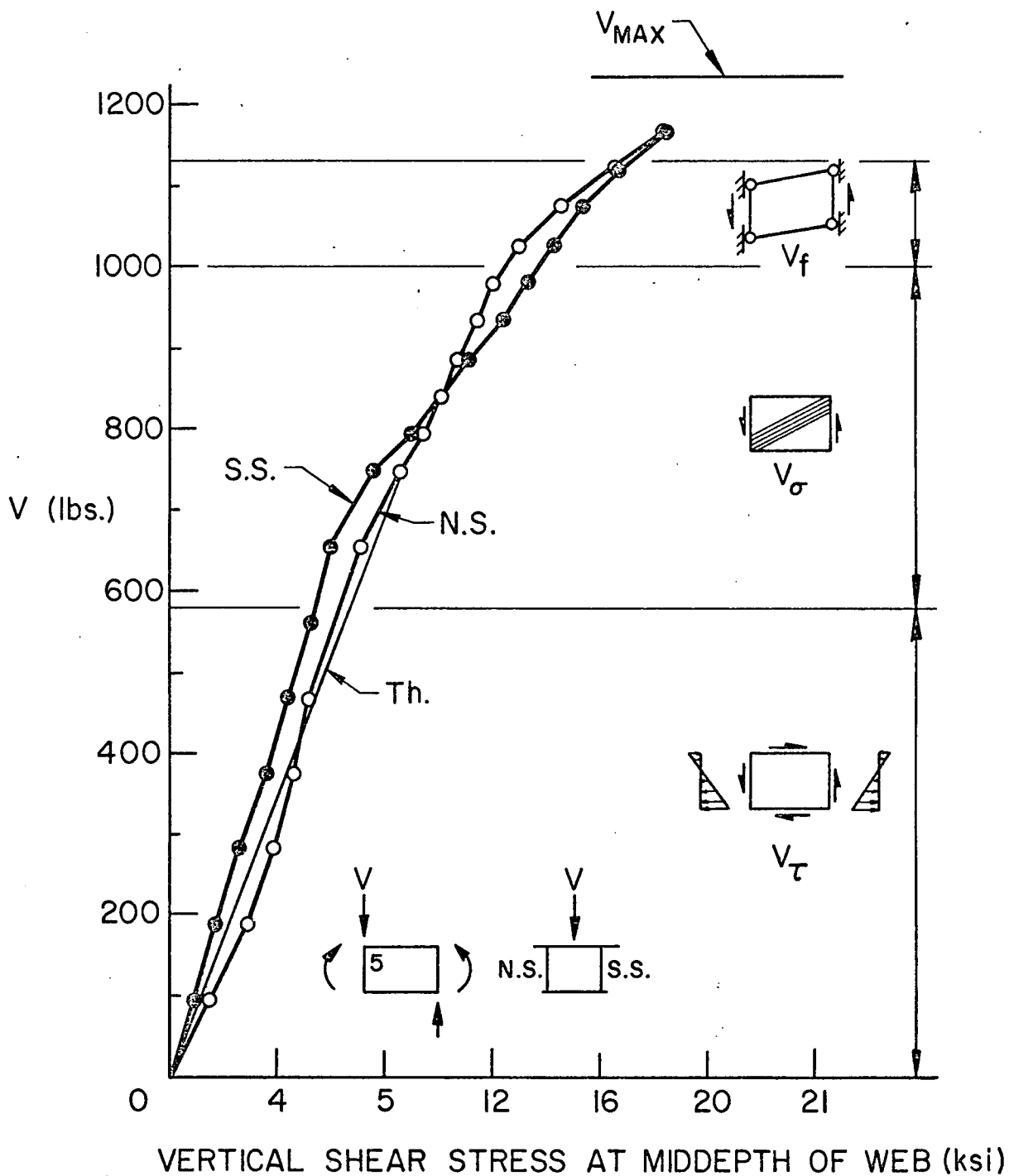Fig. 3.10   Redistribution of Torsional Moment
After Initial Web Failure

Fig. 4.1 Panel Shear vs. Shear Stress at Centerline of Panel 2
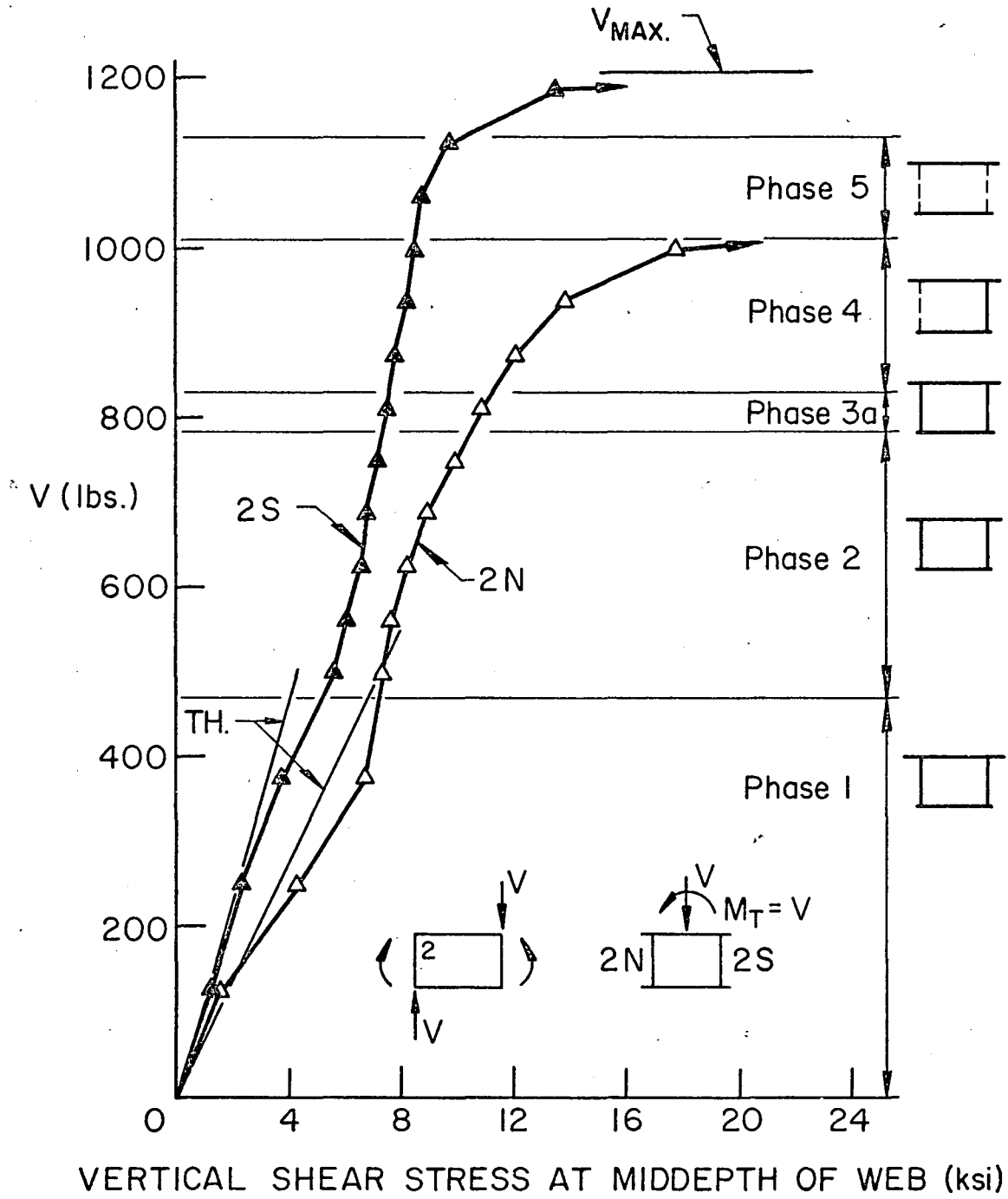Specimen M2 (Unsymmetrical Loading)

Fig. 4.2   Panel Shear vs. Shear Stress at Centerline
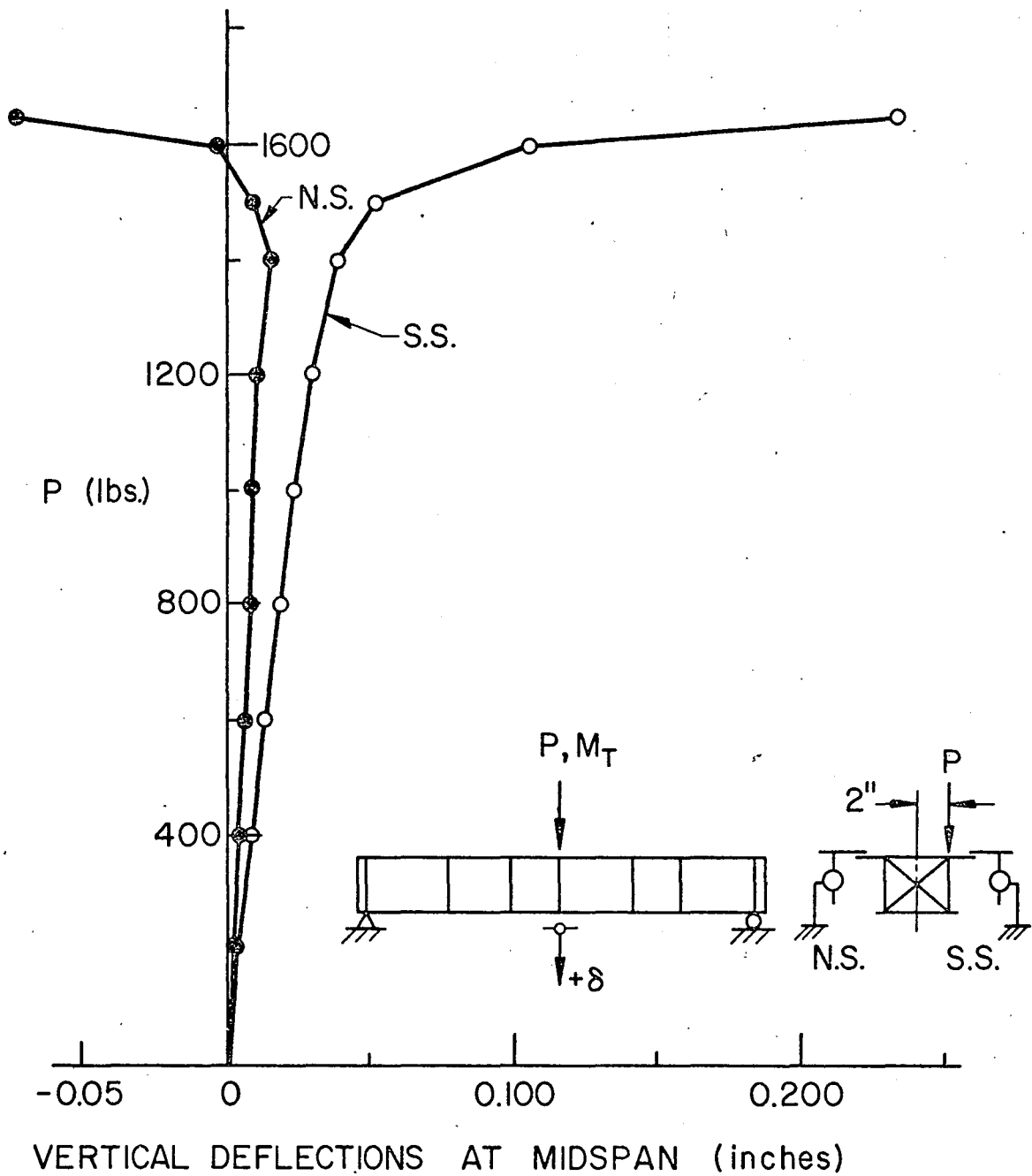of Panel 2 - Specimen M2 (Unsym. Load)

Fig. 4.3 Load vs. Midspan Deflection, N.S. and S.S. of Specimen M1
(Unsymmetrical Loading)

10. <u>REFERENCES</u>

1. ASCE-AASHO Committee on Flexural Members
   TRENDS IN THE DESIGN OF STEEL BOX GIRDER BRIDGES, Progress
   Report, Subcommittee on Box Girder Bridges, Journal of the
   Structural Division, ASCE, Vol. 93, No. ST3, June 1967.

2. Goldberg, J. R. and Leve, H. L.
   THEORY OF PRISTMATIC FOLDED PLATE STRUCTURES, Publications,
   IABSE, Vol. 17, 1957.

3. Vlasov, V. Z.
   THIN-WALLED ELASTIC BEAMS, OTS 61-11400, Office of Technical
   Services, U. S. Department of Commerce, Israel Program for
   Scientific Translations, Catalogue No. 428, Washington, D. C.,
   1959.

4. Wright, R. N., Abdel-Samad, S. R., and Robinson, A. R.
   BEF ANALOGY FOR ANALYSIS OF BOX GIRDERS, Journal of the
   Structural Division, ASCE, Vol. 94, No. ST7, July 1968.

5. Scordelis, A. C.
   ANALYSIS OF CONTINUOUS BOX GIRDER BRIDGES, Report No.
   SESM-67-25, Department of Civil Engineering, University of
   California, Berkeley, 1967.

6. Scordelis, A. C. and David, R. E.
   STRESSES IN CONTINUOUS BOX GIRDER BRIDGES, Proceedings,
   2nd International Symposium of Concrete Bridge Design,
   American Concrete Institute, 1969.

7. Malcom, D. J. and Redwood, R. G.
   SHEAR LAG IN STIFFENED BOX GIRDERS, Journal of the Struc-
   tural Division, ASCE, Vol. 96, No. ST7, July 1970.

8. Parr, D.
   AN ULTIMATE STRENGTH ANALYSIS OF BOX GIRDER HIGHWAY BRIDGES,
   Ph.D. Dissertation, New Mexico State University, May 1968.

9. Basler, K. and Thürlimann, B.
   STRENGTH OF PLATE GIRDERS IN BENDING, Proceedings, ASCE,
   Vol. 87, No. ST6, August 1961.

10. Basler, K.
    STRENGTH OF PLATE GIRDERS IN SHEAR, Proceedings, ASCE, Vol. 87,
    No. ST7, October 1961.

11. Basler, K.
    STRENGTH OF PLATE GIRDERS UNDER COMBINED BENDING AND SHEAR,
    Proceedings, ASCE, Vol. 87, No. ST7, October 1961.

12. AISC SPECIFICATION FOR THE DESIGN, FABRICATION, AND ERECTION OF STRUCTURAL STEEL FOR BUILDINGS.

13. INTERIM SPECIFICATIONS, 1971, American Association of State Highway Officials, 1971.

14. Patterson, P. J., Corrado, J. A., Huang, J. S., and Yen, B. T. FATIGUE AND STATIC TESTS OF TWO WELDED PLATE GIRDERS, WRC Bulletin No. 155, October 1970.

15. Schueller, W. and Ostapenko, A. TESTS ON A TRANSVERSELY STIFFENED AND ON A LONGITUDINALLY STIFFENED UNSYMMETRICAL PLATE GIRDER, WRC Bulletin No. 156, November 1970.

16. Basler, K., Yen, B. T., Mueller, J. A., and Thürlimann, B. WEB BUCKLING TESTS ON WELDED PLATE GIRDERS, WRC Bulletin No. 64, September 1960.

17. Chern, C. and Ostapenko, A. ULTIMATE STRENGTH OF PLATE GIRDERS UNDER SHEAR, Fritz Engineering Laboratory Report No. 328.7, Lehigh University, August 1969.

18. Desai, S. TENSION TESTING PROCEDURE, Fritz Engineering Laboratory Report No. 237.44 - Draft, Lehigh University, February 1969.

19. Maggard, S. P. and Parr, D. H. PRIMARY STRESSES IN THIN-WALLED FLEXURAL MEMBERS, ASCE Structural Engineering Conference, Conference Preprint 485, May 1967.

20. Knittel, G. ZUR BERECHNUNG DES DUNNWANDIGEN KASTENTRAGERS MIT GLEICHBLEIBEN SYMMETRISCHEN QUERSCHNITT, Beton und Stahlbetonbau, Vol. 60, Bulletin 9, Berlin, September 1965.

21. Chern, C. and Ostapenko, A. UNSYMMETRICAL PLATE GIRDERS UNDER SHEAR AND MOMENT, Fritz Engineering Laboratory Report No. 328.9, Lehigh University, October 1970.

22. Galambos, T. V. STRUCTURAL MEMBERS AND FRAMES, Prentice-Hall, Inc., 1968.

23. Heins, C. P., Jr., and Seaburg, P. A. TORSION ANALYSIS OF ROLLED STEEL SECTIONS, Bethlehem Steel Corporation, AIA File No. 13-A-1, 1963.

24. Terrington, J. S.
        COMBINED BENDING AND TORSION OF BEAMS AND GIRDERS, BCSA
        Publication No. 31 (First Part), 1968.

25. Kollbrunner, C. F. and Basler, K.
        TORSION IN STRUCTURES, Springer-Verlag, 1969.

26. Ostapenko, A., Chern, C., and Parsanejad, S.
        STRENGTH FORMULAS FOR DESIGN OF STEEL PLATE GIRDERS, Fritz
        Engineering Laboratory Report No. 328.12, Lehigh University,
        January 1971.

27. Ostapenko, A.
        TORSION OF NON-PRISMATIC MEMBERS WITH STEPPED SHEAR AXIS,
        Lehigh University (Unpublished).

28. Myers, D. E. and Copper. P. B.
        BOX GIRDER MODEL STUDIES, Journal of the Structural Division,
        ASCE, Vol. 95, No. ST12, December 1969.

29. Nelson, H. M., Beveridge, A., and Arthur, P. D.
        TESTS ON A MODEL COMPOSITE BRIDGE GIRDER, International
        Association for Bridge and Structural Engineers, Vol. 23,
        1963.

30. Scordelis, A. C.
        ANALYSIS OF SIMPLY SUPPORTED BOX GIRDER BRIDGES, Department
        of Civil Engineering, Report No. SESM-66-17, University
        of California, Berkeley, Ocrober 1966.

31. Fountain, R. S. and Mattock, A. H.
        COMPOSITE STEEL-CONCRETE MULTI-BOX GIRDER BRIDGES, Pro-
        ceedings of Canadian Structural Engineering Conference,
        Toronto, Canada, February 1960.

32. Skaloud, M.
        ULTIMATE LOAD AND FAILURE MECHANISM OF WEBS OF LARGE WIDTH-
        TO-THICKNESS RATIOS SUBJECTED TO SHEAR AND ATTACHED TO
        FLANGES OF VARIOUS FLEXURAL RIGIDITIES, Institute of The-
        oretical and Applied Mechanics of the Czechoslovakia Academy
        of Science, 1970.

33. Fujii, T.
        ON AN IMPROVED THEORY FOR DR. BASLER'S THEORY, Final Report,
        8th Congress of IABSE, Theme IIC, New York, September 1968.

34. Troitsky, M. S.
        ORTHOTROPIC BRIDGES--THEORY AND DESIGN, The James F. Lincoln
        Arc Welding Foundation, 1967.

35. Kollbrunner, C. F. and Meister, M.
        AUSBEULEN, Springer-Verlag, 1958.

36. Kuhn, P., Peterson, J. P., and Levin, L. R.
A SUMMARY OF DIAGONAL TENSION, PART I - METHODS OF ANALYSIS,
NACA Technical Note 2661, May 1952.

37. United States Steel Corporation
HIGHWAY STRUCTURES DESIGN HANDBOOK, Vol. II, 1965.

38. Richmond, B.
TWISTING OF THIN-WALLED BOX GIRDERS, Proceedings, Insti-
tution of Civil Engineers, Vol. 33, Paper No. 6868, April
1966.

39. ASCE-AASHO Task Committee on Flexural Members
PROGRESS REPORT ON STEEL BOX GIRDERS, Subcommittee on Box
Girders, Journal of the Structural Division, ASCE, Vol. 97,
No. ST4, April 1971.

VITA

The author was born in Hoboken, New Jersey, December 9, 1940, the fourth child of Alphonse and Josephine (Castagnetti) Corrado.

He was graduated from Demarest High School in Hoboken, New Jersey in January 1958. He attended St. Bonaventure University in Olean, New York from September 1958 to June 1960. In September 1960 he enrolled at the University of Detroit, Detroit, Michigan from which he received the degree of Bachelor of Civil Engineering in June 1963. From September 1963 to July 1965 he was a Research Assistant at Fritz Engineering Laboratory, Lehigh University working on a research project on the fatigue strength of welded plate girders. He received the Master of Science Degree from the Civil Engineering Department of Lehigh University in June 1965.

From July 1965 to September 1967 the author was employed as a research engineer with the Electric Boat Division of the General Dynamics Corporation in Groton, Connecticut. He returned to Fritz Engineering Laboratory, Lehigh University to assume a full-time position as Engineer of Tests in September 1967. At that time he enrolled in a Ph.D. program in the Civil Engineering Department and was also involved with research associated with plate girders and box girders.

He is married to the former Arlene Margaret Collins and has two children: Joseph James and Janene Marie.